THE EFFECT OF BORON NITRIDE ON THE RHEOLOGY AND PROCESSABILITY OF MOLTEN POLYMERS

by

Franky Kam Yin Yip

Bachelor of Chemical Engineering, University of Minnesota, 1997

A THESIS SUBMITTED IN PARTIAL FULFILLMENT OF THE REQUIREMENTS FOR THE DEGREE OF MASTER OF APPLIED SCIENCE

in

The Faculty of Graduate Studies
Department of Chemical and Bio-Resource Engineering

We accept this thesis as conforming to the required standard

THE UNIVERSITY OF BRITISH COLUMBIA
Nov 1999

In presenting this thesis in partial fulfilment of the requirements for an advanced degree at the University of British Columbia, I agree that the Library shall make it freely available for reference and study. I further agree that permission for extensive copying of this thesis for scholarly purposes may be granted by the head of my department or by his or her representatives. It is understood that copying or publication of this thesis for financial gain shall not be allowed without my written permission.

Department of Chemical and Biological Engineering

The University of British Columbia
Vancouver, Canada

Date Nov 29th, 1999

Abstract

Experiments were carried out using capillary, sliding plate, and parallel plate rheometer and a blow moulding machine in order to assess the effect of boron nitride (BN) powders on the rheology and processability of a metallocene polyethylene, a Teflon FEP polymer and a polypropylene. In particular, to assess the processability of these resins in the presence of BN or not, the critical conditions for the onset of melt fracture is determined. The influence of the average size of boron nitride particles, its agglomeration if present, its concentration in the resins and the quality of the attained dispersion on the melt fracture of the metallocene polyethylene was particularly investigated. For this a number of boron nitride powders were examined having various characteristics, i.e. agglomeration, different particle size etc. It was found that for BN to be efficient in eliminating surface and gross melt fracture, the particle size should be about 10-20 microns in size, and free of agglomeration. Concentration was also found to be a critical factor, with the optimum value to fall in the range between 200 and 1000ppm. The mechanism by which BN acts to eliminate melt fracture was also investigated. Six different capillary dies with various entrance angles were used to study the entrance effect. A new apparatus was also designed during the course of this study in order to visualize the flow patterns developed at the entrance of the capillary. It was found that BN changes the entrance flow pattern of a PP by eliminating the onset of unstable flow. This is done by providing the condition for a smoother transfer of momentum from a polymer layer to the next. The effect of BN type on two blow molding grade high-density polyethylene was also studied by using a blow moulding machine. It was found that BN can eliminate the surface melt fracture of blow moulding grade HDPE depending on the properties of resins.

List of Figures

List of Tables

Acknowledgements

I wish to express my sincere gratitude and appreciation to my supervisor, Prof. Savvas G. Hatzikiriakos, for his skillful guidance, support, and encouragement during the course of this study. His insights and ideas have greatly contributed to the quality of this work.

I thank Dr. Robert DiRaddo for his collaboration and assistance in studying the effect of boron nitride on blow moulding of high-density polyethylene. Their hospitality while I was performing experiments at NRC-IMI, Boucherville, Quebec is greatly appreciated.

. This work was supported by Carborandum, Amherst, NY, USA. I am also thankful to them for preparing and providing all boron nitride samples.

My colleagues from Rheolab at UBC helped me in various ways. I wish to thank Igor Kazatchkov, Alfonsius Budi Ariawan, and Eugene Rozenbaoum for their helpful discussions and exchange of ideas.

I thank my parents for their love and continuing support. Most of all, I thank my best friend Joyce who has been a source of strength and motivation for success.

1 *Introduction*

Polyethylene (PE) resins have been produced commercially for over fifty years and it is one of the most massively produced commodity polymers. In 1994, the global PE production capacity was 45 million metric tons per year operated at an average rate of 81% to produce almost 37 million metric tons of polyethylene, allocated between high density polyethylene (>40), high pressure-low density polyethylene (<40%) and linear low density polyethylene (20%). North America, Western Europe and Japan were the largest producing areas with almost 70% of the total global capacity: Western Europe was the largest producer of HP-LDPE and the United States was the largest producer of LLDPE and HDPE.

Ziegler-Natta catalysts have been used since the 1950's for the polymerization of ethylene and propylene to produce polyethylene and polypropylene respectively. Before the discovery of Ziegler-Natta catalysts in the 1950's, the methods used for the production of these polymers were not commercially viable and a new technology had to be devised. Ziegler-Natta catalyst was first discovered by the German scientist Karl Ziegler. Later, an Italian scientist, Guilio Natta developed the catalyst further. Out of appreciation of their work, they were both awarded the Nobel prize in 1963. This discovery became a new technology for polymerization in that time.

With Ziegler-Natta catalysts the polymer is produced at much lower pressures than the previous method. The polyethylene produced is also a much less branched polymer than its predecessor. Polymers produced with Ziegler-Natta catalysts have higher melting points than those produced by the old high-pressure method. This makes these polymers much more commercially useful than the previous high pressure ones.

Recently, a new family of catalysts has been discovered, that is metallocenes. The new metallocene catalysts, first used commercially in 1991, are rapidly emerging as the primary driving force for the global polyethylene business. It, metallocene catalysts, represents the next generation of polyethylene manufacturing technology that is becoming the new global benchmark. The discovery of new catalytic systems based on metallocenes began a new era in polyolefins technology. Metallocene-based catalysts in comparison with conventional Ziegler-Natta systems offer higher versatility and flexibility both for the synthesis and control of the structures of polyolefins. High-density polyethylene (HDPE), polypropylene (atatic, isotactic, syndiotactic etc.), polystyrene, ethylene-propylene-diene terpolymers (EPDM) are among the most remarkable products obtained. In rotational molding, for example, metallocene PE (m-PE) grades promise a broader processing window, shorter cycle times, improved flow properties and potentially better warpage control. The metallocene market in 2000 has been estimated to be 6 million tons.

Metallocene polyethylenes exhibit advantages in process and quality over conventional polyethylene products (N.Rohse, P. Bailey, 1997). The metallocene technology allows the synthesis of chemically more homogeneous compounds than that of Ziegler-Natta catalysts. The metallocene product has a narrower molecular weight distribution than that of conventional LLDPE. As a result, it has lower melt elasticity for the same melt index. This leads to lower die swelling in extrusion. Stretch film made from metallocene polyethylene has high tackiness between individual layer and the films adhere well to each other and keep the packaged good firmly together. The low degree of scatter of the strength values permits a higher level of pre-stretching and thus the number of tear decrease. The amount of plastic per packaging unit can be reduced whether through using thinner films or increasing pre-stretching.

Films produced from m-LLDPE also show very good mechanical strength value, in particular puncture toughness and puncture resistance by a factor of 6 (N.Rohse, P. Bailey, 1997). A further advantage of stretch films consists in low relaxation in the stretched state, which leads to a greater packaging stability. The m-LLDPE films are also suitable for medical devices. The toughness of m-LLDPE resins permits thinner, lighter-weight films and the lower density of the films give a higher yield than polyvinyl chloride (PVC) providing more film area per kilogram. Films made from m-LLDPE are very stable under radiation and sterilization and offer good low temperature flexibility.

To process the various PE's in order to make useful products, various processes are used i.e., profile extrusion, film casting, film blowing and blow moulding. For any process to be economically feasible, the rate of production should be high enough. However, it is well known that the rate of production in many polymer processing operations are limited by the onset of flow instabilities (Petrie and Denn, 1976; Larson, 1992). In particular, once the shear rate exceeds the critical value, distortions appear on the surface of the extrudate. As a result of these instabilities, the final product becomes unattractive and commercially unacceptable. This effect can range from loss of gloss of extrudate surface to the appearance of gross distortions. The parameters affecting the degree of extrudate distortion include the process temperature, the flow rate, concentration and type of additive, geometrical dimensions of the die, the chemical nature of the polymer, the entrance geometry to the die and many others. These flow instabilities collectively known as *melt fracture* can manifest themselves in the form of either small amplitude periodic distortions appearing on the surface of extrudates (surface melt fracture or sharkskin) or severe irregular distortions at higher throughput rates (gross melt fracture). Figure

1-1 shows the two different types of melt fracture, namely surface and gross melt fractures, obtained in the capillary extrusion of Teflon® FEP resin.

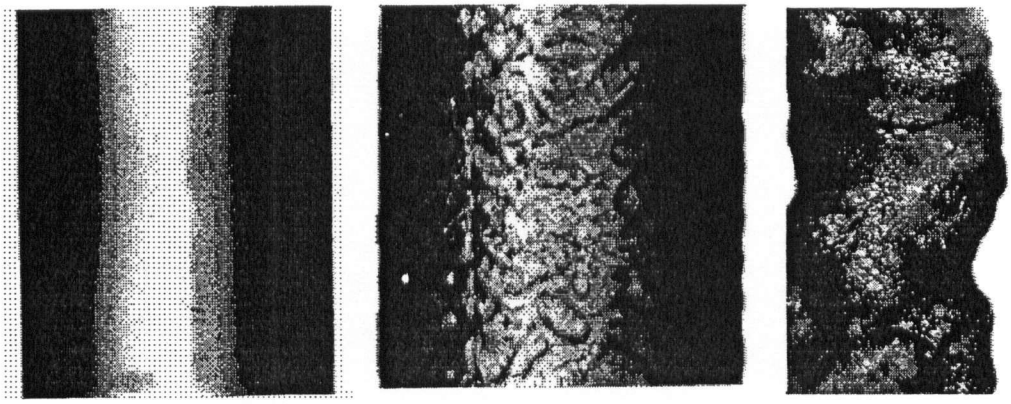

A B C

Figure 1-1: A) smooth extrudate
B) an extrudate showing small amplitude periodic distortions (sharkskin)
C) an extrudate showing gross melt fracture

In order to eliminate the surface melt fracture and increase the rate of production, polymer processing aids (PA's) are used. These processing aids are mainly fluoropolymers that are added into the resin at concentration of a few hundred ppm (typically 1000 ppm). During polymer flow, they diffuse to the wall and slowly coat it with a thin layer. In turn, the polymer slips over this thin layer. As a result, a significant drop in the shear stress and thus pressure drop is obtained, which obviously improves the extrudate appearance. It is noted that these PA's can eliminate sharkskin but not gross melt fracture.

Recently, it was shown that compositions containing fine boron nitride (BN) particles can be successfully used as processing aids to eliminate not only sharkskin melt fracture but also substantially postpone gross melt fracture to significantly higher shear rates, well within the gross melt fracture region in the extrusion of polyolefins and fluoropolymers (Buckmaster, et al.,1997). Boron nitride is a solid lubricant, whose structure resembles that of graphite. In polymer processing, it is used as a foam nucleating agent in most commercial applications for fluoropolymer foams such as heat insulation, foamed tubing, etc. In the presence of a blowing agent, it initiates the nucleation of voids in polymer extrudate.

In this study, BN particles are used without a blowing agent, so that the extruded polymer is unfoamed. During the extrusion of fluoropolymers or polyolefins with BN particles, the maximal shear rate at which the extrudate appears smooth is usually orders-of-magnitude higher than that which can ordinarily be achieved in the absence of this additive. More importantly, this maximal shear rate is usually much higher than that at which the virgin resin exhibits gross melt fracture. This means that BN, unlike fluoropolymers in the extrusion of polyethylene, can eliminate not only surface and stick-slip melt fracture but also significantly delay the onset of gross melt fracture to much higher shear rates (Rosenbaum et al., 1999).

A requirement to observe this unique action of BN in the process is that the extrusion experiments be carried out with a special crosshead die of the type used for wire coating (Rosenbaum et al., 1999). The rheometer used by these authors was a standard Instron piston-driven constant-speed capillary unit. The crosshead was a Nokia Maillefer 4/6 that included dies and tips of various diameters ("tip" is the wire guide) with equal entry cone angles of 60° and the die land length of 7.62 mm. The same equipment was also used to carry out the present work.

In this study, we use several types of boron nitride differing from each other in the particle size and composition. The objective of this thesis is to study the effect of the boron nitride type and concentration on the rheology and processability of molten polymers as they can be assessed by means of a capillary rheometer equipped with the Nokia Maillefer 4/6 crosshead. This particular die mimics the wire coating process. Furthermore, experiments are also carried out using a blow moulding machine at high shear rates for blow moulding grades of HDPE in order to assess the effect of BN as a processing aid in the blow moulding process.

2 *Literature Review*

2.1 Chemical Structure and Physical Properties of Various Polymers

2.1.1 Polyethylene

Polyethylene is probably the polymer one may see most in daily life. It is the most popular plastic in the world. This is the polymer that makes grocery bags, shampoo bottles, children's toys, and even bulletproof vests. For such a versatile material, it has a very simple structure, the simplest of all commercial polymers. A molecule of polyethylene is nothing more than a long chain of carbon atoms, with two hydrogen atoms attached to each carbon atom. It might be easier to draw it like the picture below, only with the chain of carbon atoms being many thousands of atoms long:

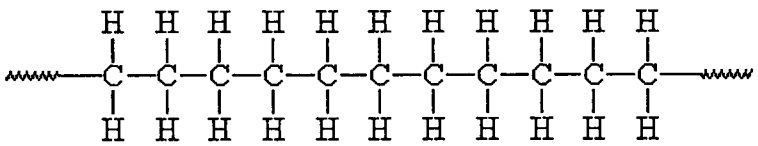

Some of the basic informations about polyethylene are listed below:

Uses:	thermoplastics, fibers
Monomer:	ethylene
Polymerization:	free radical chain polymerization, Zieglar-Natta polymerization and metallocene catalysis polymerization
Morphology:	highly crystalline (linear), highly amorphous (branched)
Melting temperature:	137 °C
Glass transition temperature:	-30 °C

Sometimes its structure is a little more complicated. Some of the carbons, instead of having hydrogens, have long chains of polyethylene attached to them. This is called branched, or low-density polyethylene (LDPE). When there is no branching, it is called linear polyethylene, or HDPE (see schematic below). Linear polyethylene is much stronger than branched polyethylene, but branched polyethylene is cheaper and easier to make.

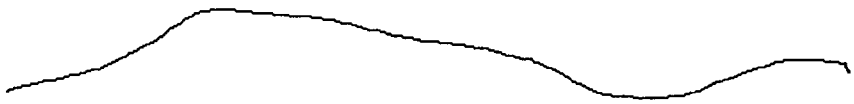

A molecule of linear polyethylene, or HDPE

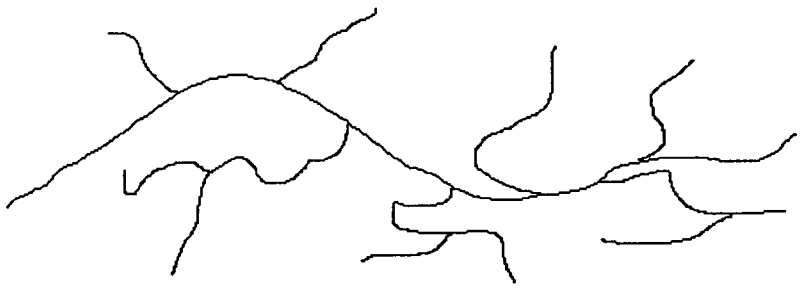

A molecule of branched polyethylene, or LDPE

Figure 2-1: Schematic representation of a linear and a branched polyethylene molecule.

Linear polyethylene is normally produced with molecular weights in the range of 200,000 to 500,000, but it can be made even higher. Polyethylene with molecular weights of three to six million is referred to as ultra-high molecular weight polyethylene, or

UHMWPE. UHMWPE can be used to make fibers, which are so strong that have replaced Kevlar for use in bulletproof vests. Large sheets of it can be used instead of ice for skating rinks.

The new discovery of metallocene technology can be used to produce polymers over the full range of conventional densities. The challenge facing the polymer industry and its converter customer is how this technology can be utilized to obtain a competitive advantage. In the last two years, high-density and linear low-density polyethylene resins produced by metallocene catalysts have become a commercial reality in all regions of the world except Eastern and Central Europe. Polyethylene manufacturers refer to metallocenes as the "next generation catalysts". Technological revolutions in metallocene chemistry have allowed polyolefin producers to molecularly engineer their resins, achieving important results in comonomer amounts (including the addition of a third comonomer), molecular weight, molecular weight distribution, and long chain branching. These systems are compatible with the modern polymerization systems so no major modification costs are required. Now, the yields are similar to those from the current Ziegler-Natta and chromium catalysts and manufacturing costs per pound of polymer approximate those of conventional catalysts. Unlike the linear low-density phenomena of the early 80's, metallocene technology is not restricted by polymerization capacity nor by processing capability. Thus far the market penetration has been specialty areas, but metallocene polyolefins have the potential of penetrating very significantly into the LLDPE and even LDPE markets. Metallocene polyolefins are expected to command 10-20% of the polyolefins market by 2010. Let us look at what metallocene is. Metallocene

is a positively charged metal ion sandwiched between two negatively charged cyclopentdienyl anions. The diagram below shows cyclopentdienyl anions.

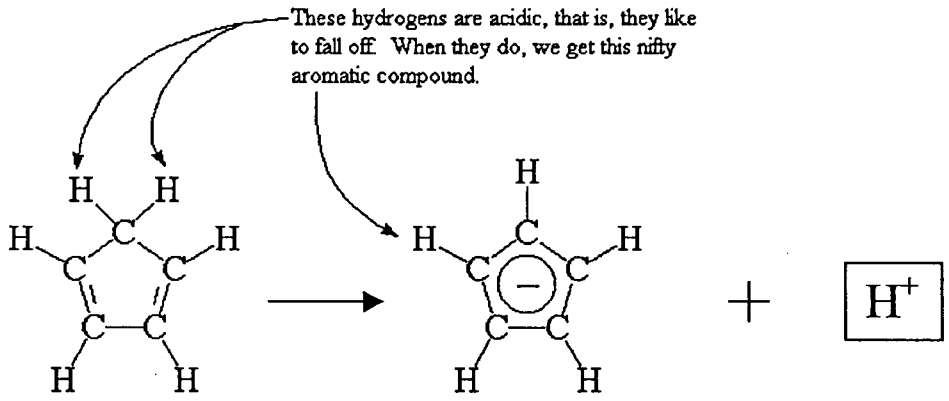

Cyclopentadiene Cyclopentadienide anion

You may notice that one carbon atom with two hydrogens, whereas the rest have one. These two hydrogens are acidic, that is, they can be removed very easily. When this happens, it leaves its bonding electrons behind. So the carbon it left now has an extra pair of electrons. Six electrons in a ring molecule like this will make the ring *aromatic*. It can give a very stable complex. These cyclopentadienide ions have a charge of -1, so when a cation comes along, like Fe with a +2 charge, two of the anions will form an iron sandwich. That iron sandwich is called *ferrocene*. Sometimes a metal with a bigger charge is involved, like zirconium with a +4 charge. To balance the charge, the zirconium will bond to two chloride ions, -1 charge on each, to give a neutral compound.

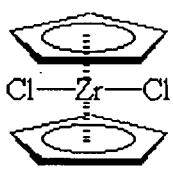

bis-chlorozirconocene

But those chlorines can be removed. When this happens, they take their electrons with them. That zirconium is now lacking electrons. It will take them from wherever it can get them. Good sources of electrons are vinyl monomers. That carbon-carbon double bond is chock full of electrons. So a nearby vinyl monomer, say, ethylene, can come in and donate its electrons to the zirconium. As the process continues, the metallocene polyethylene can be formed.

2.1.2 Fluoropolymer

Fluoropolymer is another class of polymers, which is of interest to the present work. They belong to the class of paraffinic polymers that have some or all of the hydrogen replaced by fluorine. The first known fluoropolymer is Teflon® and it was discovered by DuPont about 50 years ago. Its melting point is very high (about 425°C) and therefore its processing needs special methods such as sintering and pressing. Its structure is shown below:

DuPont discovered that a copolymer of tetrafluoroethylene (TFE) and hexafluoropropylene (HFP) has the good properties of Teflon but it has a much lower melting point that allows for conventional processing. FEP is one of the fluoropolymers. It has

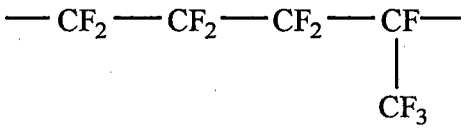

predominantly linear chains and is produced by copolymerization of tetrafluoroethylene (TFE) and hexafluoropropylene (HFP). FEP has a crystalline melting point of about 265°C determined by differential scanning calorimetry (DSC) and density of 2,150 kg/m^3. It is a soft plastic with tensile strength, wear resistance, and creep resistance lower than those of many other engineering plastics. It is chemically inert with a low dielectric constant (about 2) over a wide range of frequencies and temperatures.

2.1.3 Polypropylene

Polypropylene (PP) is a third type of polymer that is of interest to the present work. It has the following structure:

As can be seen, the monomer for PP is propylene. The material mainly produced by the Ziegler-Natta method which discussed in section 2.1.1. Polypropylene has a wide range of applications. It included fiber, filaments to films and extrusion coating. The majority of the polypropylene is in the form of isotactic. The advantages of PP included inertness to water and microorganisms and the cost of the PP is very low (about $0.7 per kg).

2.2 Polymer Processing Aids

As discussed before, processing aids are used together with the resins in order to facilitate extrusion at reduced pressure drops as well as increase rate of production in extrusion operations by eliminating melt fracture phenomena. There are various factors to

determine the performance of a PA. It should be incompatible with the resin (immiscible), have low coefficient of friction with the resin to be processed, coat and adhere to the die surface and it should not react with other additives such as antioxidants and stabilizers that are contained in the polymer to be processed. Processing aids are usually fluoroelastomers that can be added to the resin at concentrations of a few hundred ppm (typically ~ 1000ppm), e.g. at the time of processing or introduced as a masterbatch.

Priester and Stika (1992,1994) suggested that the factors that can affect the performance of the processing aid include the level of additive, dispersion quality and the interaction with other ingredients (antioxidants and stabilizers) in the resin. They have also mentioned that a large number of small particles of the additive can give a better dispersion quality than a small number of large particles. Thus, small particles can do a better job in coating a die. The ideal particle size of the additive should be incompatible with the polymer to be processed, it should have a good affinity for metal surface and should be less than 5 microns. Priester and Stika (1992,1994) have also studied the effect of die composition, surface roughness and surface cleanliness on the appearance of the extrudate. They have found that the higher the percentage of the surface covered with processing aid, the lower the die pressure will be. They reported that there is also a critical surface roughness of the die beyond which the performance of processing aid started decreasing. Moreover, they have examined various methods of die cleaning. The best cleaning method was found to be using high-pressure water (about 20,000 psi). Finally, they reported that a die surface covered with contaminants will require a much higher level of additive than one that is clean in order to achieve the same performance in terms of melt fracture and extrusion pressure.

Rudin (1985) performed experiments for a LLDPE with the addition of Dynamar® as a polymer processing additive. They have found that the presence of Dynamar® at the surface causes the polymer to slip and that the slip velocity increases with increasing the concentration of PA in the resin. They studied the surface of the extrudate samples by using the X-ray photoelectron spectroscopy (ESCA) in order to detect the levels of fluorine. In addition, the extrudate were fractured in liquid nitrogen and the cross section was also analyzed to measure the fluorine concentration. The data indicated that a measurable concentration of fluorine at the surface exists, while the average concentration through the cross section was too low for the ESCA reading. From these data, one may suggest that processing aid such as Dynamar® move to the die/metal interface from the bulk. There the PA functions as a lubricant and as a result reduces the driving pressure of extrusion. They also mentioned that a proper balance of incompatibility and diffusion rate is required to ensure in order for the additive to coat the metal die. This does not affect the efficiency of the extruder. Similar observations have also been reported for other types of processing aids.

Stewart(1992) reported that a masterbatching step was required in order to provide a good quality of dispersion of additives into the resin. Athey and Thamm (1986) reported that there is a rheological change of LLDPE, HDPE, HMWHDPE and PP with the addition of a small quantity of FKM-A (Vinylidene fluoride and hexafluoropropylene). The addition of FKM-A changed the viscosity of the resin, thus reducing the driving pressure during the extrusion at certain shear rate.

In general, processing aids reduce the pressure required to extrude the resin at a particular flow rate and eliminate or postpone melt fracture to higher extrusion rates. Note that these additives can eliminate only sharkskin and the so-called stick-slip (oscillating or cyclic) melt fracture. To the best of our knowledge, they do not appear to have an effect on the extrudate appearance in the gross melt fracture region.

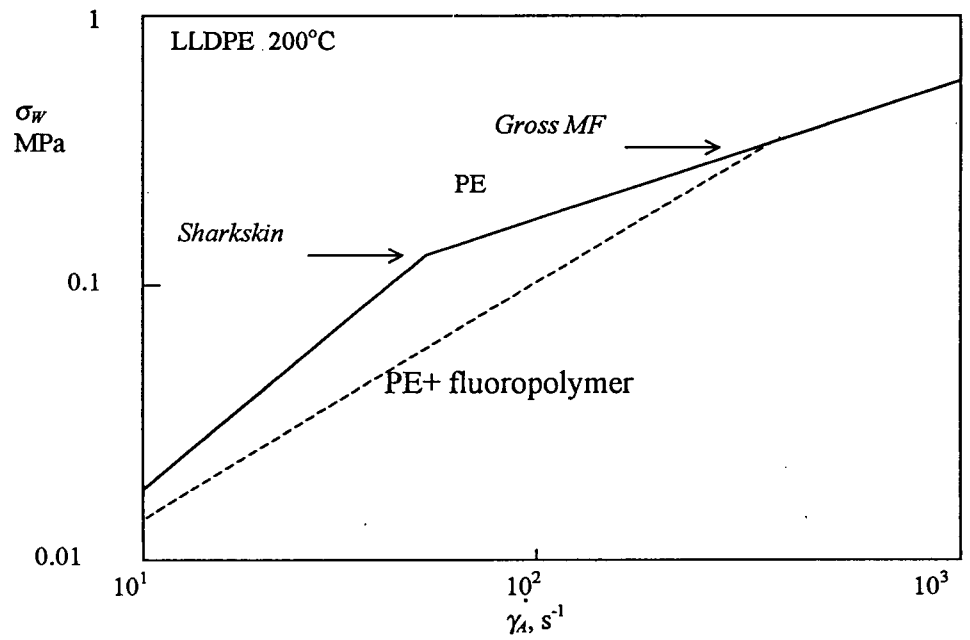

Figure 2-2: The flow curve of a linear low-density polyethylene with and without the addition of 250 ppm fluoropolymer (Stewart et al., 1993).

Typical examples are shown in figure 2-2 and 2-3. Figure 2-2 shows the flow curves of a linear low-density polyethylene with and without the addition of 250 ppm fluoropolymer (Stewart et al., 1993) obtained from an extruder by using an annular die. Figure 2-3 shows the effect of the addition of 0.1% of polyethylene on the flow curve of resin FEP® 4100 at 350 °C (Rosenbaum, and Hatzikiriakos, 1998) obtained by means of a capillary rheometer. Both examples show that the presence of processing aid reduce the

required extrusion pressure before the onset of gross melt fracture region. However, it appears that there is no significant change in pressure in the gross melt fracture region. Sharkskin and stick-slip surface instabilities can be eliminated in both cases. However, these processing aids have no effect on the gross melt fracture regime.

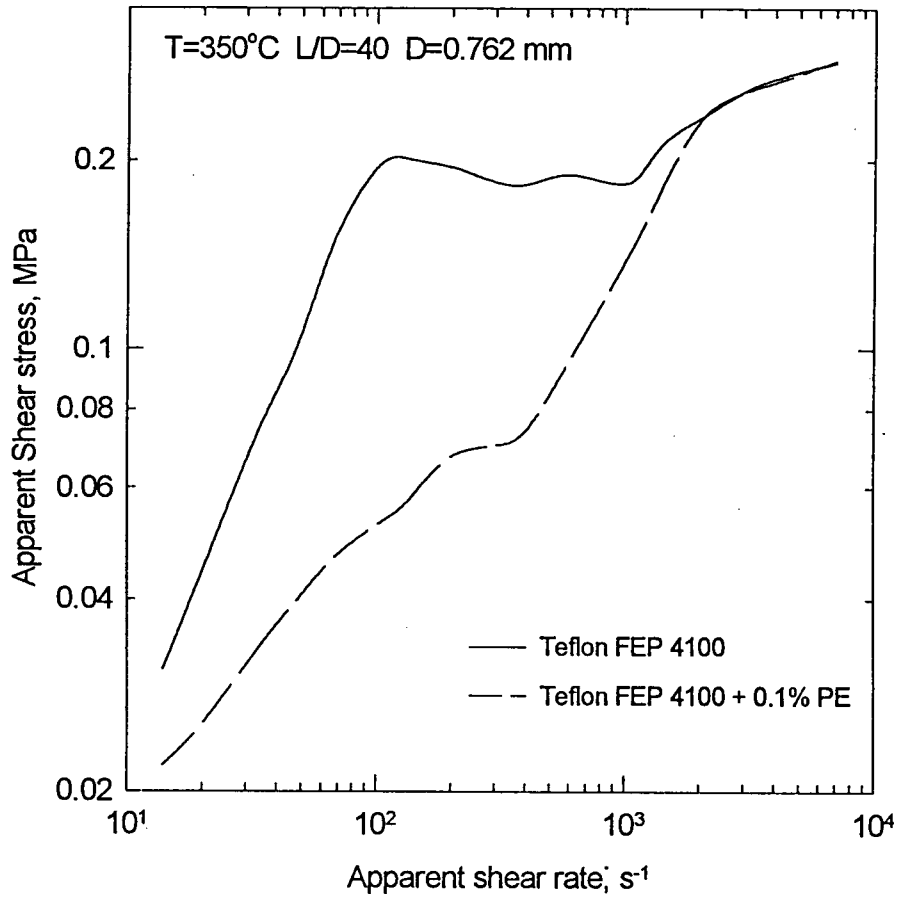

Figure 2-3: The effect of the addition of 0.1% of polyethylene on the flow curve of resin FEP 4100 at 350 °C (E.E Rosenbaum, S.G. Hatzikiriakos, 1998) on a capillary rheometer.

2.3 Equipment Used in this Study

Several pieces of equipment were used to carry out this study. In particular experimental equipment were used to assess the processability of resins in the presence of BN and additionally to characterize rheology of the resins. These pieces of equipment

will be described here together with the equations needed in order to calculate relevant fundamental quantities from the raw data.

2.3.1 Capillary Rheometer

The most widely used type of melt rheometer is the capillary rheometer. The property most frequently measured in a capillary rheometer is viscosity, a quantity very useful from the engineering point of view. A typical capillary rheometer is capable of measuring the viscosity of polymer over the range of shear rates from 5 to 5,000 s^{-1}. Moreover, from such a piece of equipment the processability of the polymers may also be assessed. As the polymer is extruded through a die, a visual inspection of the extrudate surface is possible.

A simple schematic of capillary rheometer is shown in figure 2-4. This apparatus consists of a melt reservoir or barrel ,which is used to melt the polymer. This is accomplished by means of heating elements surrounding the barrel. A piston is used to push the melt flow through the capillary die, having a pre-specified diameter, D, and length, L. The quantities normally measured from this apparatus are the flow rate, Q, which is related to the speed of the piston and the driving pressure, which is related to the force applied on the piston.

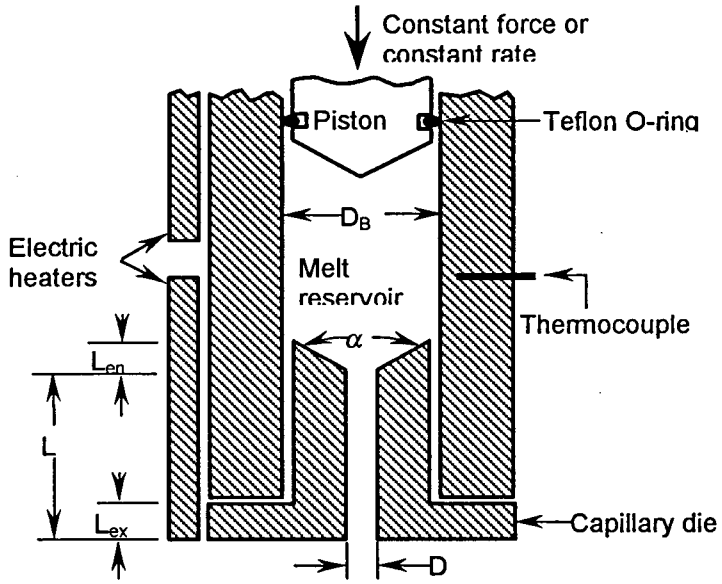

Figure 2-4: A simple schematic of capillary rheometer

For steady-state, fully developed flow of an incompressible Newtonian fluid, the wall shear stress and wall shear rate can be calculated from:

Wall shear stress, $$\sigma_w = \frac{\Delta P D}{4L} \qquad (2\text{-}1)$$

Wall shear rate, $$\dot{\gamma}_w = \frac{32Q}{\pi D^3} \qquad (2\text{-}2)$$

where σ_w is the wall shear stress
ΔP is the pressure drop along the rheometer (see figure 2-5)
D is the diameter of the capillary die
L is the length of the die, and
Q is the volumetric flow rate

For the case of non-Newtonian fluids, the quantity defined by Eq. 2-2, is only the apparent shear rate, $\dot{\gamma}_A$, defined as

Apparent shear rate, $$\dot{\gamma}_A = \frac{32Q}{\pi D^3} \quad (2\text{-}3)$$

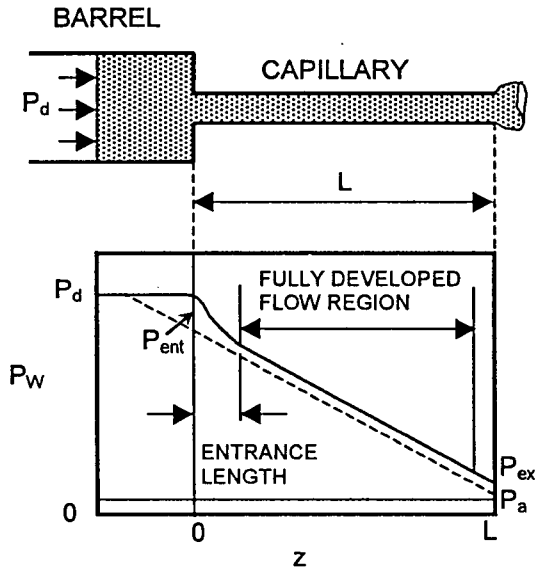

Figure 2-5: Wall pressure distribution for capillary flow (Dealy, 1982)

It can also be shown that the true wall shear rate and the apparent shear rate are related through a correction factor, known as the Rabinowitsch correction. This can be expressed as (Dealy and Wissbrun, 1990):

$$\dot{\gamma}_w = \left(\frac{3+b}{4}\right)\dot{\gamma}_A \quad (2\text{-}4)$$

where $$b = \frac{d(\log \dot{\gamma}_A)}{d(\log \sigma_w)} \quad (2\text{-}5)$$

For a power law fluid, the shear stress is related to the shear rate through:

$$\sigma = K\dot{\gamma}^n \quad (2\text{-}6)$$

where K is the consistency index, σ is the shear stress and n is the power law exponent. For such a power law fluid, it can be shown that the wall shear rate can be expressed as:

$$\dot{\gamma}_w = \left(\frac{3+1/n}{4}\right)\dot{\gamma}_A \qquad (2\text{-}7)$$

It can be seen that, the Rabinowitsch correction ,b, is equal to 1/n for a power law fluid and equal to unity for a Newtonian fluid.

The schematic diagram for the pressure drop in capillary flow of a molten polymer is shown in figure 2-5. First, there is a large pressure drops associated with the entrance region, ΔP_{ent}. There also appears a small pressure drop at the exit of the capillary known as the exit pressure, ΔP_{ex}. The summation of these two pressures (entrance and exit) are known as, ΔP_{end}, the end pressure.

$$\Delta P_{end} = \Delta P_{ex} + \Delta P_{ent} \qquad (2\text{-}8)$$

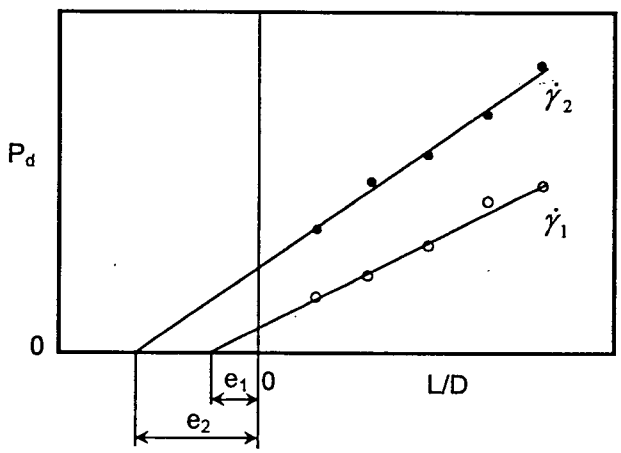

Figure 2-6: The schematic diagram for Bagley plot.

The end pressure can be determined by using a well known technique called Bagley technique (1931). According to this procedure, the driving pressure, P_d, is measured using a variety of capillaries with different L/D ratio at various flow rates. For each flow rate, the driving pressure is plotted as a function of L/D ratio, and extrapolating the lines to L/D=0. The end pressure can be obtained as the intercept on the pressure axis or as an end correction on the intercept on the L/D axis. The schematic diagram for a typical Bagley plot is shown in figure 2-6. Using the Bagley correction, the true wall shear stress can now be calculated as:

$$\sigma_w = \frac{P_d}{4(L/D+e)} \qquad (2\text{-}9)$$

Cogswell (1981) has suggested that the use of an orifice die(L/D=0) is a shortcut method to determine with reasonable accuracy for ΔP_{end}. In this case, the wall shear stress can be calculated by,

$$\sigma_w = \frac{(P_d - \Delta P_{end})}{4(L/D)} \qquad (2\text{-}10)$$

The capillary rheometer is capable of providing much of the data that are necessary for the study of melt processability. The capillary rheometer mimics reasonably well the practical flow in moulds and dies and also provides extrudate on which a subjective assessment of quality may be made.

Besides the capillary die, a crosshead die was also applied to assess the processability of the various resins. The crosshead was a Nokia Maillefer 4/6 that included dies and tips of various diameters ("tip" is the wire guide) with equal entry cone

angles of 60° and the die land length of 7.62 mm. The schematic of the crosshead is shown in Figure 2-7.

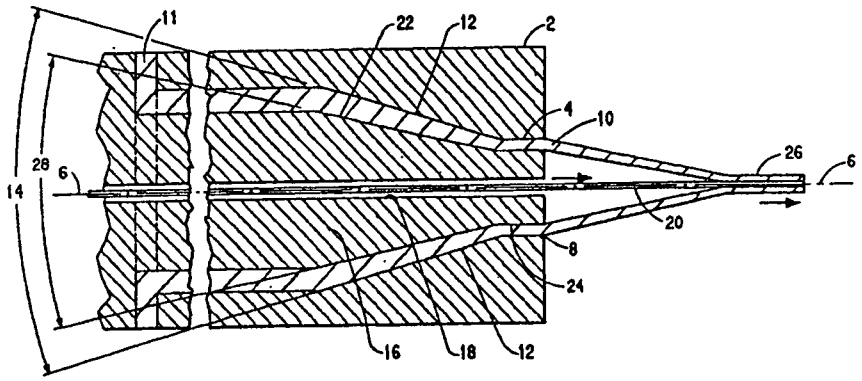

Figure 2-7: Crosshead die for wire coating (from Buckmaster *et al.*, 1997)

The molten polymer enter the port 11 to the die 2. Then the polymer is guided through to orifice 8 by the wire guide 16. The interior and the exterior surface of the wire tubular shape is formed by the passage 24 and 4 respectively. The wire guide provides a channel as a mandrel to produce the tubular shape extrudate (10). The speed of wire reached the orifice 8 and draw down to a thinner cross-section. It makes a thinner polymer coating 26 on the wire. By using this crosshead, wire was not used in our study. Therefore, a hollow shape extrudate was obtained during the experiment. The apparent shear rate was calculated by using the formula applied for slit dies having a large aspect ratio (Bird et. al, 1987):

$$\dot{\gamma}_A = \frac{6Q}{0.25(D-d)^2 0.5\pi(D+d)} \qquad (2\text{-}11a)$$

where Q is the volumetric flow rate, d and D are the tip and die diameters, correspondingly. The apparent wall shear stress was estimated as the average of the shear stress at the inner and outer walls by using the following formula which is based on the

assumption of a power-law fluid (Bird, R.B et al., 1987). The general formula for the shear stress distribution is:

$$\tau_{rz} = \frac{\Delta P D}{4L}\left(\frac{2r}{D} - \beta^2 \frac{D}{2r}\right) \qquad (2\text{-}11b)$$

where τ_{rz} is the shear stress at radius r, ΔP is the pressure drop, L is the length of the die land, and β is the parameter depending on the geometry and the power law index.

2.3.2 Parallel Plate Rheometer

The parallel plate rheometer is used primarily for the measurement of linear viscoelastic properties. The subjection of a material to a sinusoidal shear history and measurement of the stress response is well established as a very useful tool in order to obtain information about the rheological behavior of this material. In this work, a Rheometrics System IV parallel-plate rheometer was used to characterize the linear viscoelastic behavior of the materials. The upper and lower plate are mounted on the same axis of symmetry. The upper plate is rotated with a certain angular speed ω(t), and as a result, the sample is subject to shear. The type of deformation used is small amplitude oscillatory shear. The strain as a function of time is given by:

$$\gamma(t) = \gamma_0 \sin(\omega t) \qquad (2\text{-}12a)$$

where γ_0 is the strain amplitude and ω is the frequency.

This small amplitude oscillatory shear test experiment is essentially used to determine the linear viscoelastic properties of polymeric material. If the strain amplitude is too small, then the shear stress is sinusoidal in time and independent of the magnitude of strain. Thus it can be written as:

$$\sigma(t) = \sigma_0 \sin(\omega t + \delta) \qquad (2\text{-}12b)$$

where σ_0 is the stress amplitude and δ is the phase shift, or the mechanical loss angle.

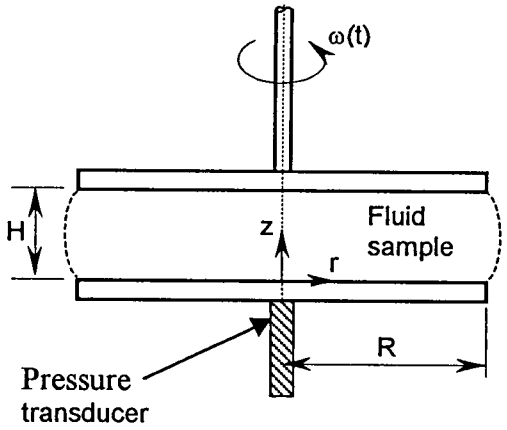

Figure 2-8: Parallel plate rheometer

By using the trigonometric identity, the shear stress can be written as:

$$\sigma(t) = \gamma_0 [G'(\omega)\sin(\omega t) + G''(\omega)\cos(\omega t)] \qquad (2\text{-}13)$$

where the quantity $G'(\omega)$ is the storage modulus and $G''(\omega)$ is the loss modulus. These two quantities can be calculated from the amplitude ratio and phase shift.

$$G' = G_d \cos(\delta) \qquad (2\text{-}14)$$

$$G'' = G_d \sin(\delta) \qquad (2\text{-}15)$$

where $G_d = \sigma_0/\gamma_0$ is the amplitude ratio . From the storage and the loss modulus, one can calculate the complex modulus, $G^*(\omega)$, which is given as:

$$G^*(\omega) = G'(\omega) + iG''(\omega) \qquad (2\text{-}16)$$

Also, the shear stress can be expressed as follow:

$$\sigma(t) = \dot{\gamma}_0[\eta'(\omega)\cos(\omega t) + \eta''(\omega)\sin(\omega t)] \quad (2\text{-}17)$$

where the complex viscosity can be expressed as:

$$\eta^*(\omega) = \eta'(\omega) - i\eta''(\omega) \quad (2\text{-}18)$$

$$\eta' = G''/\omega \quad (2\text{-}19)$$

$$\eta'' = G'/\omega \quad (2\text{-}20)$$

where η' is the dynamic viscosity, η'' is the in-phase component of the complex viscosity. From the above equation, the tangent of the mechanical loss or phase shift can be calculated as:

$$\tan\delta = G''/G' = \eta'/\eta'' \quad (2\text{-}21)$$

2.3.3 Sliding Plate Rheometer

The sliding plate rheometer generates shear deformations by the linear motion of one flat plate relative to another. It has certain advantages over the use of rotational flows. Edge failure is a less problem in this geometry so that higher shear rates can be reached for polymer melts. The type of flow generated by such rheometer is called simple shear. A thin layer of fluid is placed between the two flat plates, where the upper plate is translated over the lower by a constant velocity. A simple schematic of this is shown in Figure 2-9.

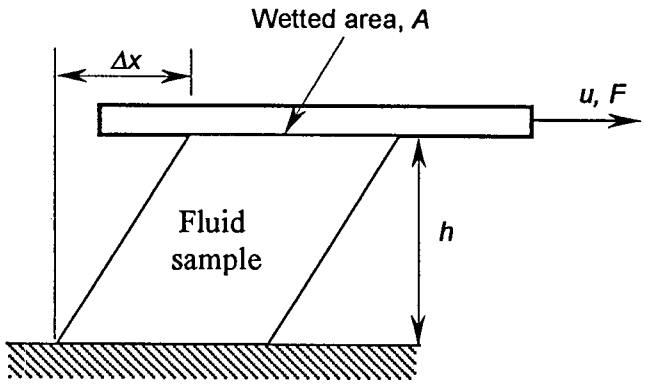

Figure 2-9: Simple schematic of simple shear flow utilized by a sliding plate rheometer.

When the upper plate is translated by a certain displacement Δx, the shear strain can be defined by:

$$\gamma = \Delta x / h \qquad (2\text{-}22)$$

where h is the gap spacing between the two plates

By differentiating this with respect to time and defining d(Δx)/dt as u, the velocity of the upper place, then one can define the nominal shear rate, $\dot{\gamma}_n$, as equal to u/h. The shear stress can also be calculated, if one measures the force required to shear the upper plate, as $\sigma = F/A$ where F is the pulling force and A is the wetted area.

If one assumes that the no-slip boundary assumption is valid, then the actual shear rate, $\dot{\gamma}$, is equal to the nominal shear rate , $\dot{\gamma}_n$. When slip is present, the actual shear rate is less than the nominal shear rate and these two cases are shown schematically in figure 2-10.

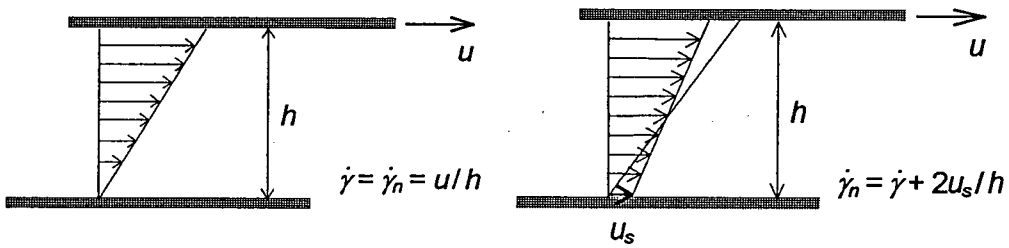

Figure 2-10: a) Simple shear flow without slip. b) and with slip occurs.

In fact $\dot{\gamma}$ and $\dot{\gamma}_n$ under slip condition are related through the following expression

$$\dot{\gamma}_n = \dot{\gamma} + 2u_s / h \qquad (2\text{-}23)$$

where u_s is the slip velocity.

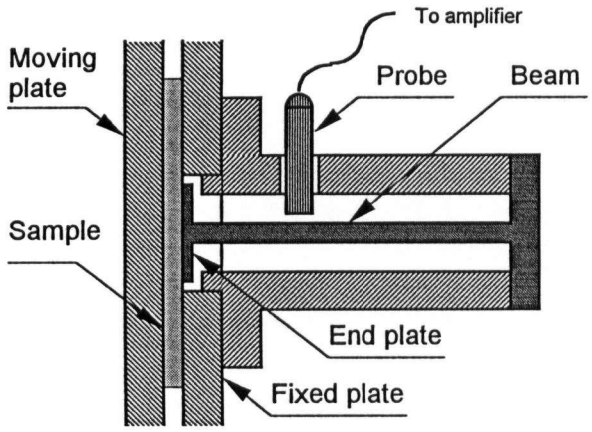

Figure 2-11: Sliding plate rheometer with a flush-mounted shear stress transducer.

For this work a commercial sliding plate rheometer with a flush-mounted shear stress transducer was used (Interlaken). The basic features of the transducer are shown in figure 2-11. An end plate is acted on by the shear stress generated by the fluid and transmits the resulting moment to the cantilever beam. To avoid melt penetration into the gap around the end plate, the deflection of the latter must be limited to very small levels. That is why a capacitance system was used, where a capacitor is formed by the probe acting as one of the plates, and the beam as the second plate. The shear stress is measured by means of calibrating the transducer by hanging known weight and measuring the displacement. Thus, in real experiments beam deflection is transformed directly into stress.

2.3.4 Flow Visualization

A new apparatus was designed during the course of this study to visualize the flow patterns developed at the entrance of the capillary i.e. going from a large reservior to a fine capillary die. Figure 2-12 shows a schematic diagram of the flow visualization experiment.

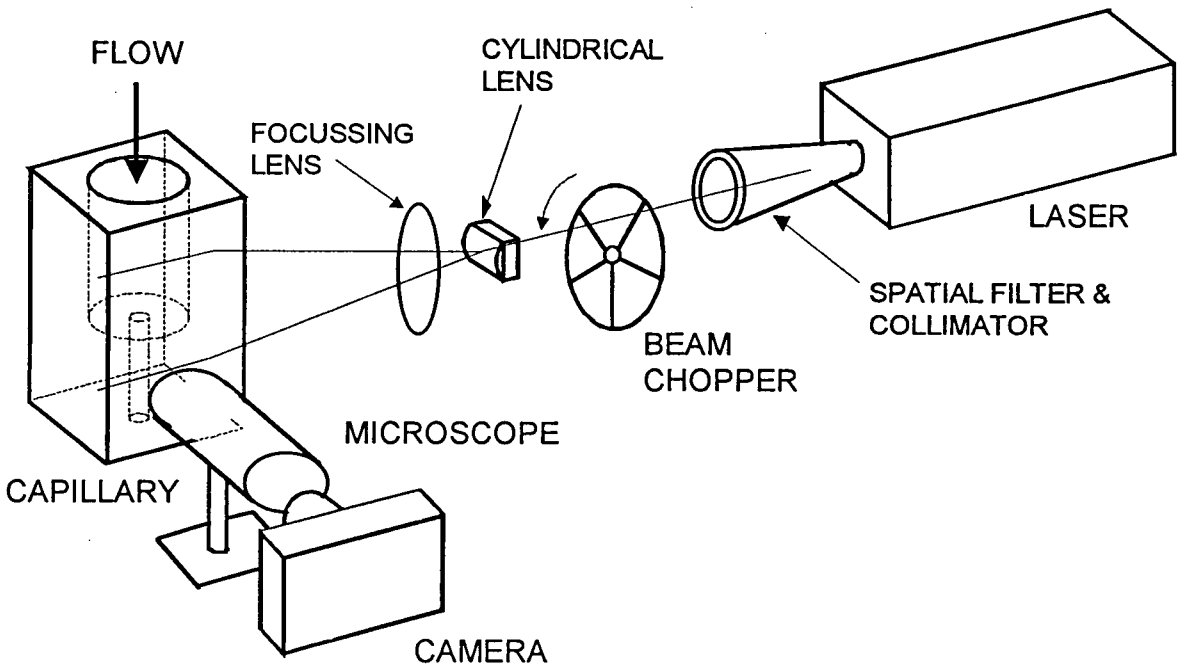

Figure 2-12: The schematic diagram of the flow visualization set up.

This new apparatus consists of the following parts:

- Helium-Neon laser having output power 10 mW, with a spatial filter and collimator with a focal length of 200 mm;
- Laser beam chopper, a DC motor with a plastic disc having 5 segments;
- Cylindrical lens, focal length 150 mm;
- Spherical focusing lens, focal length 600 mm.

- Quartz capillary, 1.5 mm diameter, encased in a steel holder, surrounded by 4 radiation heaters;
- Microscope (Nikon SMZ-2T) and a Nikon FM-2 photographic camera.

Figure 2-13 also shows the equipment set-up for the laser and a beam forming system. The total length of the metal optical support rail is 2 meters. The collimated laser beam is spread into a plane by means of a cylindrical lens and subsequently focused by a spherical lens onto the center axis of the capillary. The resulting thickness of the laser sheet crossing the capillary did not exceed 0.1 mm.

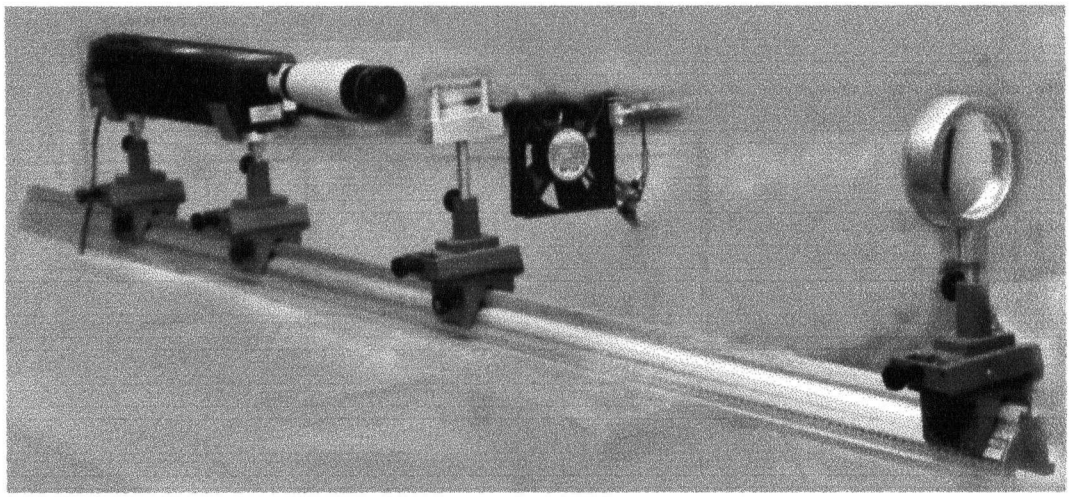

Figure 2-13: The laser and a beam forming system.

Figure 2-14 shows the position of quartz capillary die surrounded by four radiation heaters. Figure 2-15 shows the lower part of the rheometer, microscope and camera.

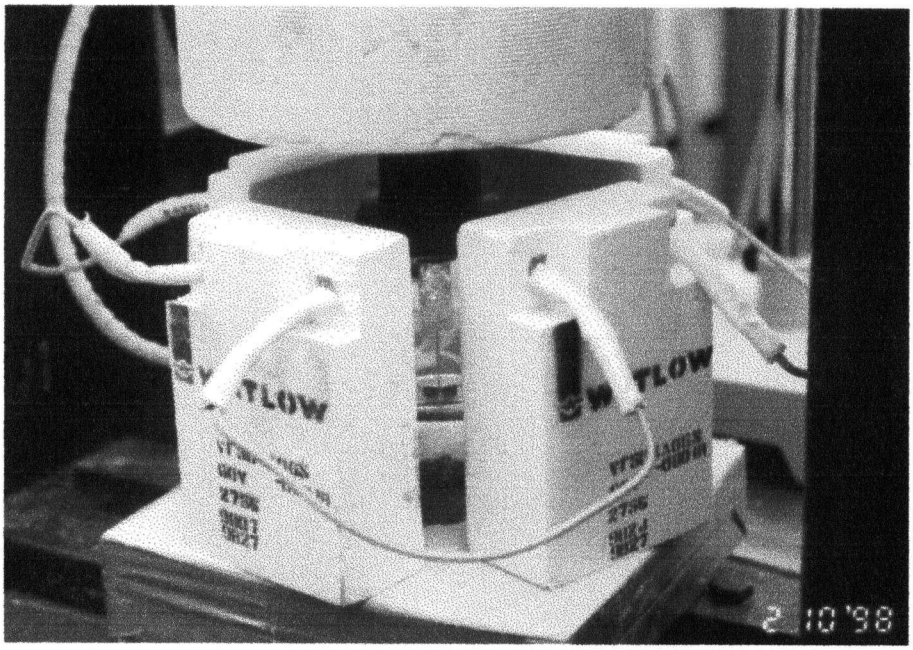

Figure 2-14: Photograph of the quartz capillary and four radiation heaters surrounding the die.

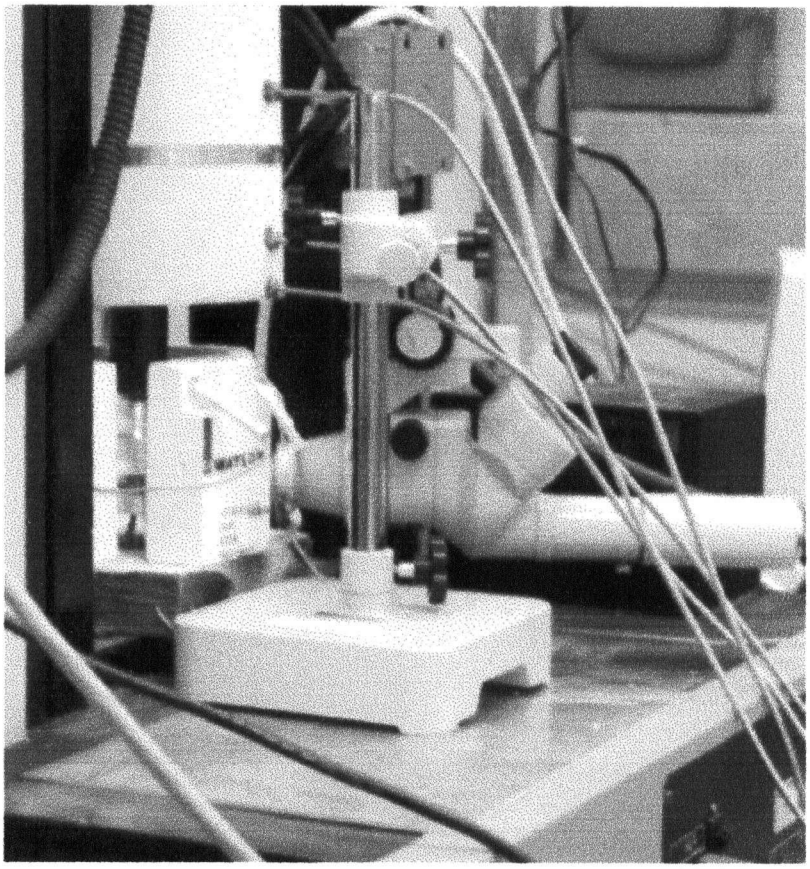

Figure 2-15: Photograph of the rheometer, microscope and the camera.

The heaters were insulated in all sides except the side facing the quartz die. There was also a thermocouple attached to the bottom of the quartz capillary die to control the temperature. Figure 2-15, it shows the combination of the capillary with the microscope. The laser beam should be turned on at all times during video recording and picturing.

The quartz die was made by Precision Glass Products and the schematic diagram is shown in figure 2-16. The diameter of the capillary is 1.5 mm and the L/D ratio is 7.5. This quartz capillary die allows observation of the flow at the shear stresses up to 0.4 MPa and temperatures up to 250 °C

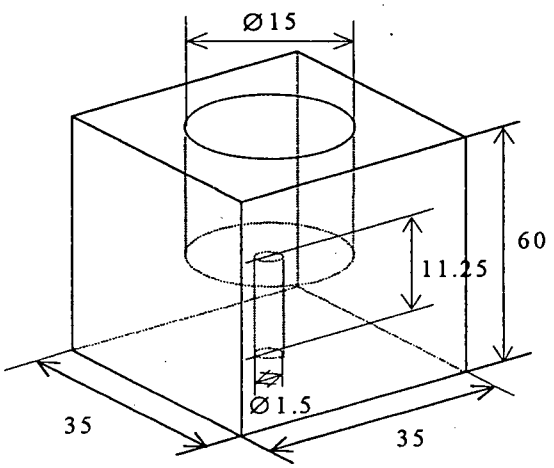

Figure 2-16: The schematic diagram of the quartz capillary die.

2.3.5 Blow Molding Machine

Extrusion blow moulding is one of the main processes in the plastic industry. The Battenfeld/Fisher 50 mm extrusion blow moulding machine was employed in our experiments in order to examine the effect of BN on the processability of blow moulding

high-density polyethylene. It mainly consists of an extruder and blow moulder parts. The processing step can be simply summarized as follows:

- The extruder plasticises and homogenizes the raw plastic material.
- The parison head shapes the plasticised material into a perform (parison) that must be suitable for the end product.
- The blow moulder receives a parison by the mould and form the article.
- The post operating unit trims the article from flash and release the product completely finished orientated out of the machine.

The blow moulding machine forms hollow parts and containers from plastic. The formation of a hollow tube, so called "Parison" and the mold itself is a hollow cavity in the shape of the part. Extrusion of the parison is controlled by a heated hollowed barrel in which a rotating screw conveys solid feed material, compresses and melts it, and finally pumps the melt through the tubing die to form a parison. The actual screw shape is dependent on the rheological characteristics of the plastic melt. Air is introduced into the parison by the blow pin and blow the parison into the hollow cavity mold. Figure 2-17 shows a schematic diagram for the extrusion blow moulding machine.

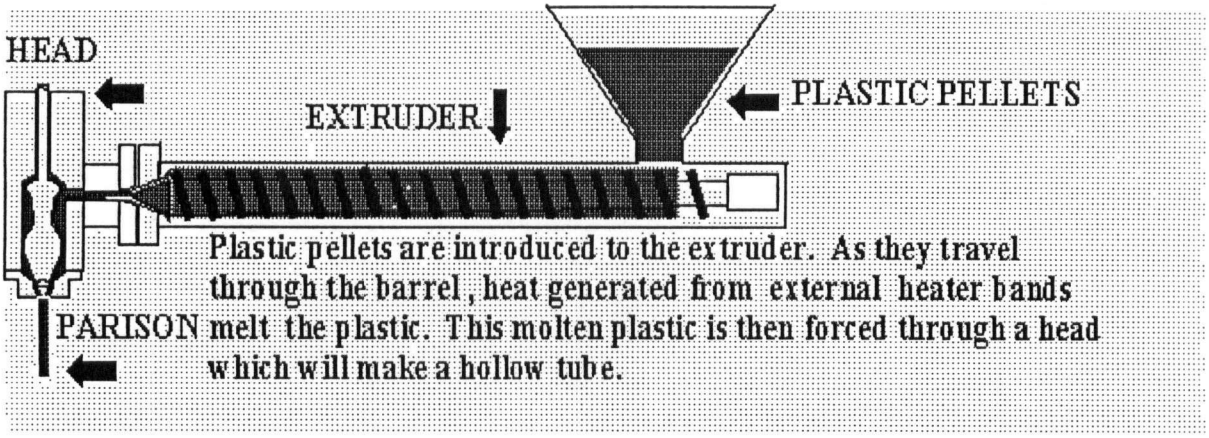

Figure 2-17: A schematic diagram of an extrusion blow moulding machine.

The material feed section has deep conical grooves on the inside circumference of the barrel. The grooves are getting shallower toward the feed section of the screw. The extrusion screw transports the polymer from the extruder feed zone through the diehead. Extrusion screws is most important part of the extruder. It have three basic sections.

1. feed section.

2. transition section.

3. metering section.

In the feed section, the material is taken in and compacted in conjunction with the feeding grooves at the rear of the extruder barrel. It supplies the compression section with a constant polymer flow. In the transition, friction heat is generated. The material is molten and plasticized. Any entrapped air from the feed zone will escape backwards. The metering section mixes and homogenizes the polymer. At the screw tip, the material should be completely homogeneous and ready for the next processing step in the diehead.

The thickness of the blow molded part is determined by the thickness of the parison, which , in turn, is determined by the length of the die opening and the extrusion speed.

After the material passes through the diverging die, it forms a parison and the final desired product can be made. The procedure to produce the final desired blow mould product in the blow molder part can be summarized in figure 2-18.

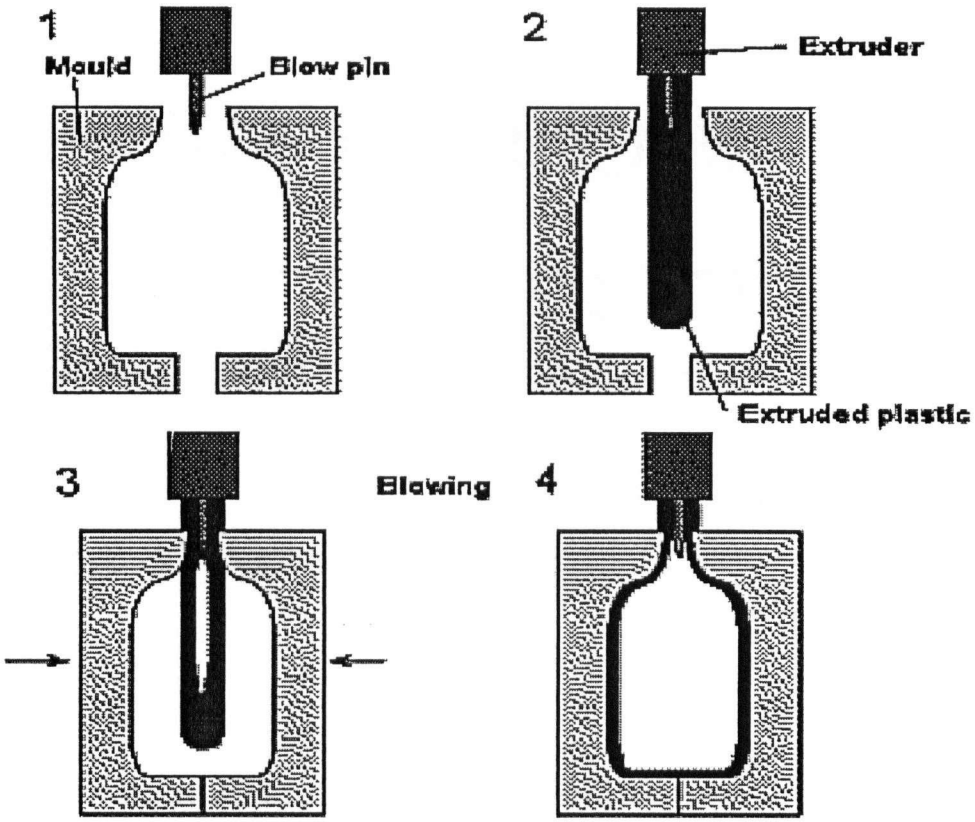

Figure 2-18 : The procedure to produce the final desired blow mould product

- step 1 : The mould and the blow pin are in the original form.
- step 2 : The parison comes out from the extruder.

- step 3 : The mould close and the swing knife move at a high speed in order to cut the parison. The mould is cooled by water and this assist the plastic to hold the shape of the mould.
- step 4 : The parison is blowed by injection of air through the blow pin. The plastic is released until the bottle shape was formed.

Figure 2-18b shows the diagram of annular geometry die and mandrel of the blow moulding unit. The inside diameter of the die is 3.8 cm and the diameter of the mandrel is 3.5cm.

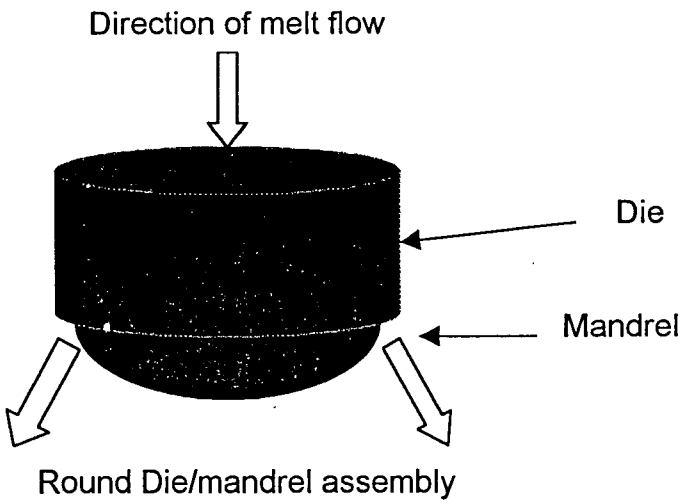

Figure 2-18b: The diagram of die and mandrel of the blow moulding unit.

Figure 2-18c shows the front view of the cross section of blow moulding die and mandrel. The dimension of the die and mandrel are shown in the figure.

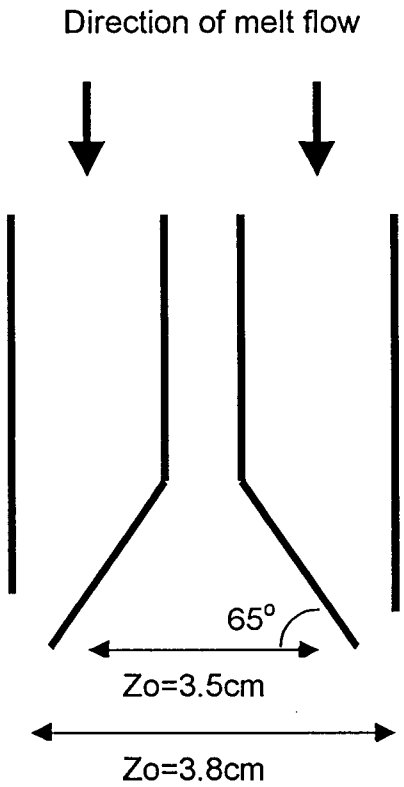

Figure 2-18c: The diagram of the cross section of blow moulding die and mandrel.

In blow moulding extrusion, a die having an L/D ratio of 20 is used as a standard . If one wishes to increase the output rate, a 24:1 ratio can also be employed. The L/D ratio is the screw length divided by its diameter. Screws to process different materials have also different compression ratios. The compression ratio is generally referred to as the depth of the feeding zone flight compared to the depth of the metering zone flight. Blow moulding is an effective way to process hollow parts, and it involves relatively low tooling costs. However, the process requires long cycle times, secondary trimming, and requires high start-up cost.

2.4 Melt Fracture and the Flow Curve of Polymers

Melt fracture is a major problem in the extrusion of polyolefins and many other polymeric materials. As originally proposed by Tordella, the transition from a smooth laminar flow to the melt fracture region involves the rupture of streamlines and this is how the term "melt fracture" was originated. Melt fracture depends on several operational and geometric factors. These include the die geometry, the polymer structure and its molecular characteristic, the temperature, and the types and concentration of additives. Melt fracture always appears in extrusion, when the flow rate or shear stress exceeds a critical value [Ramamurty (1986)]. The melt fracture behavior of most commercially significant polymers has been widely investigated by researchers. However, most of the literature is biased towards the polyethylene. This is expectable, since PE exhibits all related phenomena, ranging from loss of gloss to gross melt fracture. Other polymers either show fewer types of distortions or do not show melt fracture at all during processing. For LLDPE, the first appearance of surface roughness known as sharkskin or surface melt fracture is followed by the occurrence of gross melt fracture at the wall shear stress of about 0.3-0.4 MPa.

The flow instabilities of polymeric liquids through capillary, slit and annular dies generally known as melt fracture, can also be reflected in the apparent flow curve. Such a curve can typically be determined by means of a capillary rheometer. It is essentially a log-log plot of the wall shear stress, σ_w, as a function of the apparent shear rate, $\dot{\gamma}_A$.

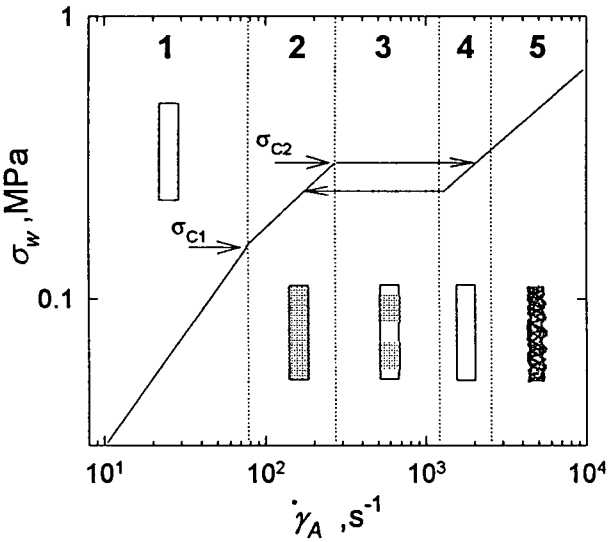

Figure 2-19: A typical flow curve for linear polymer

A typical flow curve for a linear polymer such as high-density polyethylene and linear low-density polyethylene is shown in figure 2-19. Similar flow curves have been determined in the capillary extrusion of many linear polymers such as high-density and linear low-density polyethylene (Kalika and Denn, 1987), polytetrafluoroethylene (Tordella, 1969), polybutadiene (Vinogradov *et al.*, 1972b), and others. In the first region, the shear stress is directly proportional to the shear rate to some power n (Eq. 2-6). The viscosity of the polymer follows such a relation in this region. The extrudate is smooth and the no-slip boundary condition can be assumed to be valid. When the wall shear stress exceeds a critical shear stress value, σ_{c1}, (region 2) small amplitude periodic distortions appear on the surface of the extrudate. This phenomenon is known as "sharkskin" or surface melt fracture. Consequently, when the wall shear stress exceeds the second critical point, σ_{c2}, (region 3) the flow ceases to be stable. Instead, pressure drop along the die fluctuates between two extreme values. In other words, the flow curve in this region is never stable. The appearance of the extrudate in this flow region is

referred to as "stick-slip" or oscillating melt fracture. It consists of smooth and melt fracture parts that alternate periodically. The smooth portion of the extrudate corresponds to the descending part of the flow curve and the melt fractured portion corresponds to the ascending one. At higher throughput value (region 4) or wall shear stress values, there is sometimes a transition to a second stable flow regime, in which the extrudate becomes again smooth. This is known as the *superextrusion* region although not in all polymers such a flow region has been observed to exist. Finally, at even higher shear rate values, there is a transition to a wavy chaotic distortion (*gross melt fracture*), which gradually becomes more severe with increase of the apparent shear rate, $\dot{\gamma}_A$ (region 5).

2.4.1 Surface Melt Fracture

Many researchers reported the critical wall shear stress value at the onset of surface distortion (surface melt fracture). Table 2-1 summarizes representative results:

Table 2-1: Critical wall shear stress values at the onset of surface melt fracture of various types of polymer.

Authors	σ_c(MPa)	Polymer	Temperature (°C)
Herranen and Savolaninen	0.35	LLDPE	237 and 267
Ramamurthy	0.14	LLDPE	160 and 260
Tordella	0.15	HDPE	150
Kalika and Denn	0.26	LLDPE	215
Hatzikiriakos and Dealy	0.09	HDPE	180
Bartos	0.08	PP	200-260
Bartos	0.07-0.11	LDPE	125-225
Vinogradov et al	0.03-0.097	PP	180-240
Rosenbaum	0.18	TFE-HFP	300-350

Surface melt fracture has been reported to be affected by various parameters. Some of the main parameters are discussed below and are classified as operational, geometrical, surface and chemical structure parameters.

Operational Parameters:

Kurtz (1992) has reported that the distortion severity increases with increase of the shear rate. The amplitude of the distortion increases linearly with the wall shear stress. Moreover, he reported that both sharkskin frequency and period increase with increase of the flow rate. Furthermore, the severity of distortion decrease and the onset of surface melt fracture is delayed with increase of temperature.

Geometrical parameters:

In general, the length to diameter ratio of the die is found to be independent of the critical wall shear stress. However, Moynihan (1990) has shown that the critical flow rate decreases with decrease of the die length. Venet (1996) also reported that the surface distortion is more intense in longer dies. Constantin (1984) has found that the wall shear stress is independent of the diameter of the die for LLDPE, but increases with increase of die diameter for HDPE. Dennison (1967) and Kurtz (1984) have shown that there is no effect of the die entry angle on the onset and development of surface distortion. Piau et al (1990) reported that there is a possible die exit shape effect on the critical condition for the onset of surface melt fracture.

Surface parameter

Ramamurty (1986) and Kurtz (1992) have reported that there is a significant influence of die composition (die material) both on the onset and development of surface melt fracture. However, some researchers have found no influence. The difference may

be due to the insufficient duration of the flow (induction time). In general, one can say that the extrusion process must be long enough for the equilibrium of chemical exchanges between wall and polymer to be established. Kissi and Piau (1995) promoted polymer slip at the wall by addition of small amounts of fluoropolymers into the resins.

Chemical structure of polymer

Many researchers have reported that the number and the length of branches of the polymer molecules have strong effects on the development of the instability. For example, the surface distortion of LLDPE is stronger than those of HDPE and PP at certain flow rates. The critical shear stress for the onset of surface distortion for LLDPE is lower than those of HDPE. Karbashewski (1995) found that an increase in the number of short branches (comonomer content) in a linear polymer reduces the degree of sharkskin. Moreover, comonomer type and composition also affect the flow curve and the melt fracture behavior. Venet (1996) found that polymers, which exhibit less strain hardening, result in sharkskin at smaller wall shear values.

2.4.2 Gross melt fracture

Table 2-2 summarizes some of the finding reported by various researchers for critical shear stress values for the onset of gross melt fracture.

Gross melt fracture is also affected by various parameters. Some of the main ones are discussed below and are classified again as operational, geometrical and surface parameters.

Table 2-2: Critical wall shear stress for the onset of gross melt fracture.

Authors	σ_c(MPa)	Molecular characteristic	Polymer	T (°C)
Utracki and Gendron	0.75	MW=126k	HDPE	190
Ramamurthy	0.435	MFI = 1 MW=114,000	LLDPE	220
El Kissi and Piau	0.25	MW=143,000	LLDPE	190
El Kissi and Piau	0.06	MW=835,000	PDMS	23
El Kissi and Piau	0.06	MW=1,840,000	PDMS	23
Vinogradov et al	0.36	MW=102,000 to 580,000	PB	22

Operational parameters:

Uhland (1979) reported that an increase of the temperature reduces the spurt flow rate range for HDPE. Ramamurthy (1986) has also concluded that for LLDPE in the temperature range between 160°C and 260°C, the critical shear stress is constant.

Geometrical parameters:

Ballenger and Chen (1971) have reported that the spurt zone depends heavily on the die geometry. They have also suggested that the spurt flow rate range increases with increase of the L/D ratio. An orifice die, therefore, makes it totally disappear. Tordella (1963) found that the die entry angle has no effect on the spurt flow for LDPE. Also, the frequency of the volume distortion was three times as high for conical entry dies (60°)

compared to the flat entry die. Although the amplitude is reduced, the critical shear rate does not change.

Surface parameter

Ramamurthy (1986) noticed that the die material has an effect on the critical shear stress for the volume distortion. For LLDPE, the shear stress varies between 0.39 MPa for aluminum to 0.43 for carbon steel and bronze. Lim (1970), Piau and Kissi (1995) have reported that coating the die with PTFE makes the spurt oscillations disappear.

Chemical structure of polymer

The flow curve discontinuity can be reduced by reducing the molecular weight of the polymer or boarding the MWD. A lower Mw shifts the spurt zone to higher flow rates. Before the oscillation zone, the flow curve is sensitive to the molecular parameter. The pressure levels decrease with decrease of the Mw. In the gross melt fracture region, the flow curve is insensitive to the Mw and MWD.

2.5 Explanation of Melt Fracture Phenomena

Several theories have been proposed to explain the melt fracture phenomenon in the literature. In spite of this, no single satisfactory theory exists that provides a reasonable explanation for all observed phenomena. In this section, a summary of some of these theories will be presented. It should be noted that theories which are most relevant to the present work will only be discussed.

2.5.1 Die Exit Effect: Sharkskin Melt Fracture

Surface distortions occur under stable flow conditions. There is no measurable barrel instability and the polymer flow is laminar in the die. High tensile stress may created at the exit of the die. The surface of the melt accelerates from velocity zero inside the die to the extrusion velocity outside as shown in figure 2-20. If the developed elongational stress exceeds a critical value, rupture occurs. As a result, a loss of gloss of extrudate (sharkskin) or its more severe form of small amplitude periodic distortion will appear on its surface. This phenomenon could be avoided if the material is able of responding elastically so that the skin can stretch and the stress relax becoming less than the critical value for rupture. Therefore, a low elastic modulus and low viscosity material can promote the stress relaxation. Such materials are low molecular weight polymer or polymers with long branches in their backbone. In these types of polymers, sharkskin is never observed.

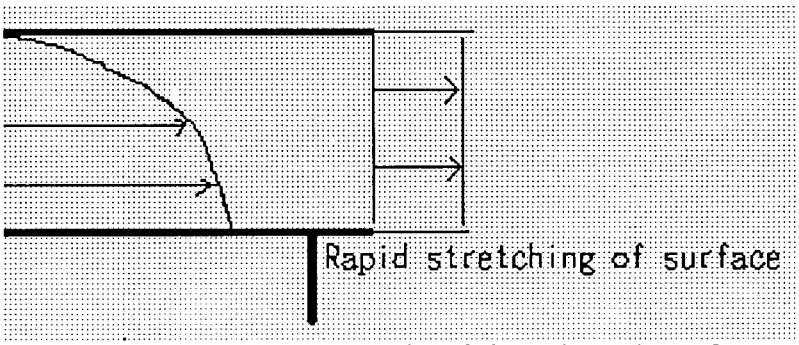

Figure 2-20: The surface velocity of the melt accelerate from zero inside the die to the extrusion velocity outside

2.5.2 Flow instability in the die land: sharkskin

Weill (1980) has explained the surface and gross distortions with relaxation oscillation. In the case of surface distortion, the relaxation oscillation is initiated at the die

entrance and propagate towards the exit where the crack on the extrudate skin appears. There is no variation of pressure in the entrance of the die during the surface melt fracture. Tordella (1963) observed the instability in the die wall but not the converging entrance part during the surface melt fracture region by using the birefringence technique. He suggested that this observation is a rupture of streamlines by strong elongation (limit of elastic deformation and entanglement of molecules at the wall) and local slip. In spite of the experimental observation, it is still not clear how to relate the flow instability to the surface melt fracture. Therefore, use of the concept of flow instability in relation to melt fracture should be considered with great care.

2.5.3 Die Entrance Effect: Gross melt fracture

Many researchers have reported that there is some relation between the converging flow at the die entry and flow instabilities that manifest itself as gross distortion on the surface of extrudates (Leonov and Prokunin, 1994). They suggested that the region upstream of the contraction is the site of initiation of gross melt fracture type of instability. Vinogradov and Malkin (1980) used the flow birefringence technique for observing and investigating the flow of polymer. They investigated the appearance of the melt fracture before and after the critical regime. Bagley and Schreiber (1961) gave out an explanation that the melt fracture of polymer melts is due to the elongational stresses in the entry region of the die. However, White (1973) gave out a different explanation. He suggested that the hydrodynamic instability was initiated in the form of a spiral flow when the critical Weissenberg number ($We=\lambda v/\delta$, where λ is the characteristic relaxation time, v is the relative velocity, δ is the spacing) was reached.

The melt fracture mechanism is not completely understood yet and it seems to depend on various parameters, such as the polymer rheology, thermal effect and the die entry geometry. Piau et al (1990) used a visualization technique and Tordella (1969) used a birefringence technique to confirm that above a certain extrusion rate, the flow upstream of the contraction becomes unstable. These instabilities occur in the form of sudden pulsations before the flow entering the contraction. They have shown that the instabilities start along the upstream flow axis due to the high elongation stresses that are developed in this area.

2.5.4 Wall slip

It has been commonly observed that the melt loses its adhesion to the wall once the wall shear stress exceeds a critical value, σ_c. At such high shear stress values, the no-slip boundary condition is no longer valid. Wall slip of molten polymer has been reported by many researchers. Mooney and Black (1952) were the first to study the slip phenomenon. They used capillaries with various radii to determine the flow curve of raw rubber. They found that the slope of the flow curve depends on the radii once shear stress exceeds the critical value as shown in figure 2-21.

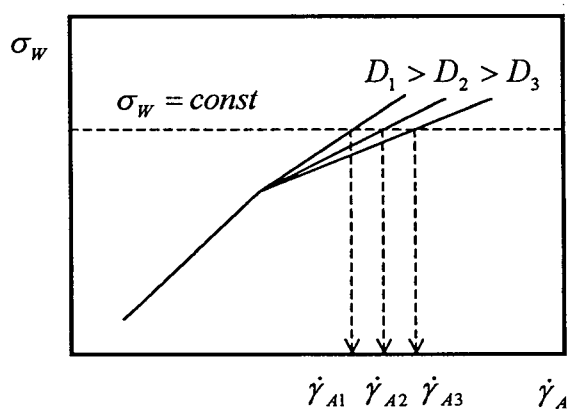

Figure 2-21: The flow curve of polymers and rubbers depends on the radii once the wall shear stress exceeds the critical condition.

Moreover, Lim and Schowalter(1989) have studied the slip behavior of polybutadiene melts by using a probe to measure heat transfer from the melt to the wall under slip and no slip conditions. Kalika and Denn (1987) reported that the flow curve obtained for various polyethylenes is discontinuous and that the slope of the flow curve changes beyond a critical wall shear stress value. This change of slope has been reported to correspond to the occurrence of the surface melt fracture and therefore it has been related to the onset of slip. Ramamurty (1986) observed that the onset of slip also depends on the material of the capillary die and that improving adhesion to the wall (decrease slip) improves extrudate distortion. Many other authors have proposed the relation between sharkskin and wall slip.

However, Rudin et al (1985) has reported that the addition of a fluoropolymer to the resin eliminates the surface melt fracture by promoting slip. Hatzikiriakos and Dealy (1992a,b) also measured the effect of two fluoropolymer on the slip velocity of HDPE. One of the fluoropolymers increased the slip velocity, while the other was decreased it, although both eliminated the occurrence of surface defects. Therefore, it can be shown that wall slip is not the only contributor to the cause of surface melt fracture.

Mooney (1931) has derived an expression for determining the slip velocity as a function of wall shear stress. He has assumed that the slip velocity, wall shear stress and pressure gradient are all constant along the length of capillary die. The expression for the case of circular channels is as follows:

$$\dot{\gamma}_A = \dot{\gamma}_{A,s} + 8\frac{u_s}{D} \qquad (2\text{-}24)$$

where $\dot{\gamma}_A$ is the apparent shear rate, $\dot{\gamma}_{A,s}$ is the apparent shear rate corrected for the effect of slip and u_s is the slip velocity. For a given shear stress, the apparent shear rate is linearly proportional to 1/D with a slope equal to $8u_s$. Ramamurthy (1986) has reported a set of such lines for linear low-density polyethylene for different wall shear stress values. The slope of each line was set equal to $8u_s$. Therefore, by using capillary dies having different radii, slip velocity can be determined as a function of wall shear stress. However, this Mooney technique to measure the slip velocity is indirect and does not account for the viscous heating effects that can be significant. (Rosenbaum et al., 1998)

2.6 Factors Affecting Polymer Flow

There are many factors affecting polymer flow. Some of the most significant ones will be discussed in this section.

2.6.1 Time Temperature Superposition: Temperature Effect

The rheological properties of molten polymer are highly depended on temperature. Therefore, experiments must be carried out at several temperatures in order to get a complete picture of their rheological behavior. A single master curve can be obtained by shifting the data taken at several temperatures together. This greatly simplifies the description of the temperature effect. Besides, the single master curve can cover a broader range of frequency or time scales compared to the range covered by data obtained at a single temperature.

A shift factor, a_T, can be calculated in order to superpose the data from different temperatures at a reference one. The amount of shifting on each curve represents the shift factor at that particular temperature. When the temperature, T, is much higher than the

glass transition temperature, T_g, usually T_g +100 K, the shift factors can be represented by an Arrhenius equation, as follows

$$a_T = \exp\left[\frac{E_a}{R}\left(\frac{1}{T}-\frac{1}{T_{ref}}\right)\right] \qquad (2\text{-}25)$$

where E_a is the activation energy of flow, T_{ref} is the reference temperature and R is the universal gas constant. If the activation energy increases, then the viscosity becomes more temperature dependent, as one approaches T_g. As mentioned, the above equation is only valid for temperatures at least 100 K above T_g. If the temperature is close to glass transition temperature, then the WLF equation should be used:

$$Log(a_T) = \frac{-C1(T-To)}{[C2+(T-To)]} \qquad (2\text{-}26)$$

where C_1 and C_2 are the universal constants and can be determined at T_o for each polymeric material.

2.6.2 Pressure Effect

The presence of large pressure gradients are typical in the processing of molten polymers. The compressibility of these materials in a molten state is not negligible, and the effect of pressure on the viscosity and other rheological material functions cannot be neglected. Rauwendaal and Fernandez (1985) and Kalika and Denn (1987) reported that the apparent flow curves do not superpose for capillaries of different *L/D* ratios. The apparent flow curves shift to higher values of the wall shear stress, pressure, with increase of the *L/D* ratio. The pressure dependence of viscosity can be written as follow:

$$\eta = \eta^0 \exp(\alpha P) \qquad (2\text{-}27)$$

where α is the pressure coefficient of viscosity, η^0 is the viscosity at ambient pressure, and P is the absolute pressure.

It has also been proven that pressure has an effect on the slip velocity. Hatzikiriakos and Dealy (1992a) studied the slip behavior of several high-density polyethylene blends at various pressures and temperatures. They have found that the slip velocity decreases with increase in pressure and this effect saturates at very high pressure values. Therefore, as the pressure drops along the capillary, the slip velocity increases and the fluid accelerates towards the exit of the capillary. This gives rise to a high extensional rate, which may be the primary cause of the surface melt fracture [Hatzikiriakos, 1994].

2.6.3 Viscous heating

Most polymer processing operations give rise to the generation of high deformation rates. Viscous heating cannot be neglected for such high shear rates. Due to the low thermal conductivity of polymer, temperature increases are considerable non-uniform within a flowing polymer melt.

Shidara and Denn (1993) have discussed the effect of viscous heating for a molten polystyrene in slit extrusion. To explain their results they assessed this effect to be significant. They pointed out that a numerical solution of the full field in capillary/slit flow incorporating pressure and temperature effects is needed. Cox and Macosco (1974) observed large temperature rises in capillary extrusion of acrylonitrile butadiene styrene (ABS), which can be as high as 70 K for certain apparent shear rates.

In order to assess viscous heating effects, it is necessary to assume appropriate boundary conditions at the wall of the capillary. Two limiting cases are usually considered. In the isothermal case, the wall is assumed to be at a uniform temperature. In the adiabatic case, it is assumed that there is no heat transfer to the wall. In the isothermal case, the temperature profile asymptotically reaches a fully developed profile, while in the adiabatic case a continuous, infinite temperature rise is predicted for a infinitely long capillary. The real condition is between these limiting cases. It is also important to note that, according to these solutions, the temperature rise is higher for longer capillaries and for those having a larger diameter. Thus, length and height of slits or length and diameter of capillaries are important parameters. If one suspects that viscous heating effects are important, then correction factors should be used. For this, see Rosenbaum and Hatzikiriakos (1995) and references therein to appropriately assess the viscous heating effects.

3 *Objectives*

The primary objective of this work is a comprehensive study of the effect of boron nitride (BN) type and concentration on the rheology and processability of molten polymers. In particular, the following goals are targeted and these can be summarized as follows:

- To conduct a thorough rheological characterization of a metallocene linear-low density polyethylene (m-LLDPE) and a Teflon FEP® 4100 resin with and without the addition of boron nitride as a function of temperature, pressure, boron nitride type and composition.
- To determine the critical condition for the onset of melt fracture of the m-LLDPE with addition of BN as a function of temperature, additive type and composition.
- To study the processability of the m-LLDPE with the use of various boron nitride powders in extrusion using a crosshead die that mimics the wire coating process.
- To study the effect of presence of BN on the processability of two blow moulding HDPE grades in the blow molding operation.
- To understand the mechanism by which BN eliminates gross melt fracture. To this direction the visualization experiments and the imaging of the flow pattern development in the die entrance will be very helpful.

4 *Materials and Blending Methods*

The objective of this chapter is to present the characteristics of the various types of polymers and BN powders used to carry out the work. The different preparation methods of the polymer blends are also discussed.

4.1 Polymers Studied

Three resins were studied in this work in order to assess the effect of various BN powders in their processability in continuous extrusion. These are the metallocene catalyzed polyethylene Exact® 3128 (Exxon), a polypropylene resin and a DuPont fluoro-copolymer of tetrafluoroethylene/hexafluoropropylene (Teflon® FEP 4100). The chemical structure of polyethylene, polypropylene and Teflon® FEP 4100 are shown in figure 4-1 to 4-3.

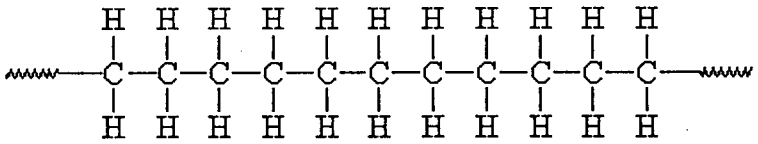

Figure 4.1 polyethylene

Figure 4.2 Polypropylene

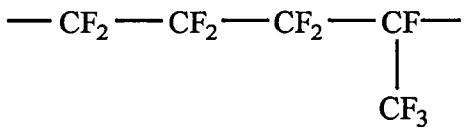

Figure 4.3 DuPont fluoro-copolymer of tetrafluoroethylene/hexafluoropropylene (Teflon® FEP)

Besides these three resins, two types of high density polyethylene resins were also empolyed in our studies to assess the effect of BN in the extrusion blow moulding. These are labeled as Resin A and Resin B, which are produced by Pétromont company, Montreal, Quebec. Some of the chemical and physical properties of resins A and B are listed below in Table 4.1.

Table 4.1 : The chemical and physical properties of Resin A and Resin B.

Properties	**Typical values, Resin A**	**Typical values, Resin B**
melt index	0.08 dg/min	0.35 dg/min
flow index	10 dg/min	35 dg/min
density	0.948 g/cm^3	0.953 g/cm^3
processing temperature	190 °C	185 °C
tensile strength at yield	24.1 MPa	26.9 MPa
melting point	140 °C	130 °C

Resin A is a high molecular weight high density polyethylene resin with a broad molecular weight distribution produced using the Union Carbide's UNIPOL® process. This resin is designed for use in the blow moulding of large parts such as shipping containers in sizes from 5 to 50 gallons. It is also used in automotive fuel tanks, jerrycans, floating docks, etc.

Resin B is a high density polyethylene resin with an intermediate molecular weight distribution that is also produced using Union Carbide's UNIPOL® process. This resin is intended primarily for use in intermittent high shear rate blow moulding equipment designed for high speed production of blow moulded containers.

4.2 Types of Boron Nitride

Boron nitride is a white solid lubricant. It has a high thermal conductivity, low dielectric loss modulus, low thermal expansion and high lubricity over a wide temperature range. To the best of the author's knowledge, BN has the highest thermal conductivity of any commercial electrical insulator in the polymer system. Boron nitride powder has been shown to be an excellent additive for coatings and release agents, as well as for oils, potting compounds, friction plates, etc. Also, the powder is white, clean, and safe-to-use directly as a high-temperature lubricant and release agent. The product typically enhances lubricity, chemical resistance, and thermal conductivity. Table 4-2 shows the comparison of boron nitride powder to other common fillers.

Table 4-2: Comparison of boron nitride to common fillers

	BN	AL_2O_3	ALN
Thermal Conductivity (W/m/K)	~ 300	40	50-170
Dielectric Constant	4	9	9

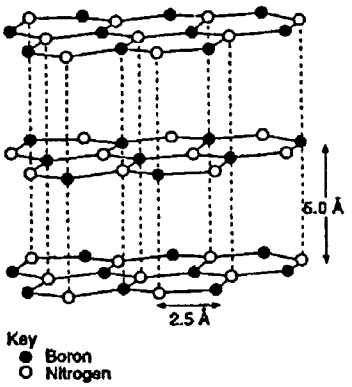

Figure 4-4: The structure of boron nitride

Figure 4-4 shows a typical structure for BN. Each boron atom is connected to four nitrogen atoms, and each nitrogen atom is connected to four boron atoms. The structure of BN is similar to that of graphite. In this study, we have examined eight types of BN. The average particle size and its state of agglomeration of each type are summarized in table 4-3. These include BN type CTF5 with particle size of 5-10 μm, CTL40 which is essentially an agglomerated version of CTF5 with particle size of more than 40 μm, and CTUF which contains a fair amount of B_2O_3 compared to CTF5. Among all BN used, only CTUF, BN427 and BN 429 exhibit agglomeration. On the other hand BN 428, BN 431 and CTF5 have the smallest particle size and are free of any agglomerated particles. Pictures taken under microscope to determine the degree of dispersion of CTF5 and CTL40 into the m-PE

are shown in figure 4-5. SEM pictures were also taken for each type of BN as shown in figure 4-6. These pictures allow us to get useful information on the average particle size and whether or not agglomerated particles are present.

Table 4-3: The average particle sizes and states of agglomeration properties of various boron nitride powder.

	particle size from SEM, approx. (μm)	agglomerated	agglomerated size (μm)
Ctl40	40	no	
ctf5	10	no	
ctuf	3	yes	>50
427	4	yes	>180
428	1.5	no	
429	3	yes	>300
430	20	no	
431	5	no	

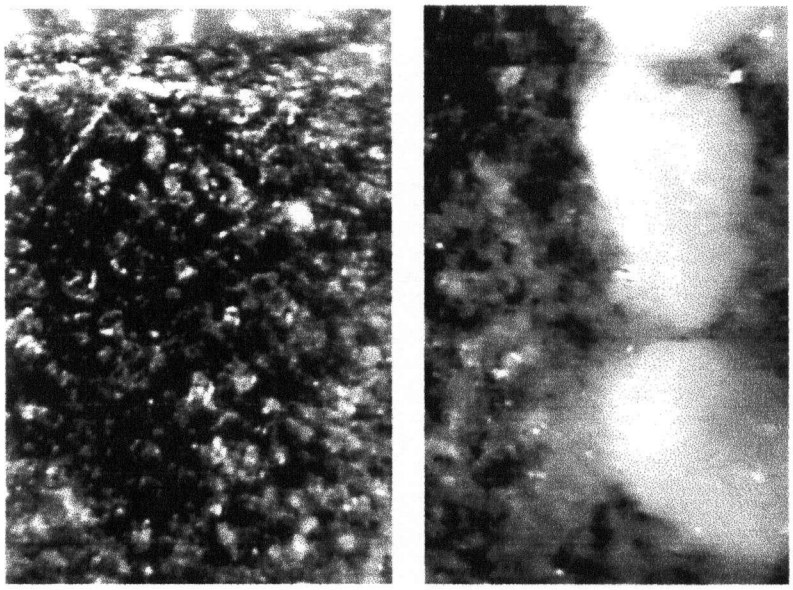

a) Good dispersion of CTF5 into m-PE b) Poor dispersion of CTL40 into m-PE

Figure 4-5: Photos of the BN particles (white) dispersed into PE (black). The magnification is 320 times in these pictures. The particle size is 5-10 μm for CTF5 and more than 40 μm for CTL40. It can also be seen that CTF5 is well dispersed (a) as opposed to the CTL40 that exhibits a certain degree of agglomeration (b).

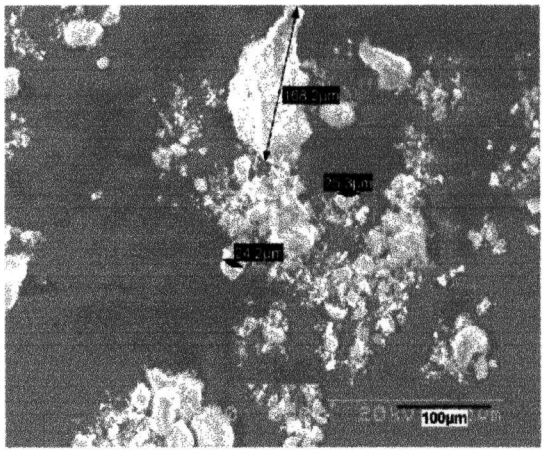

427-200

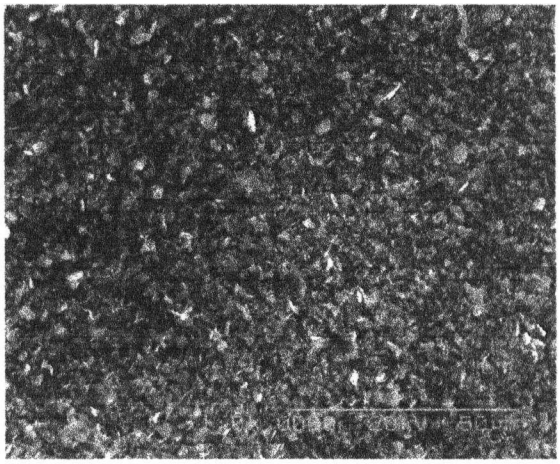

428-1k

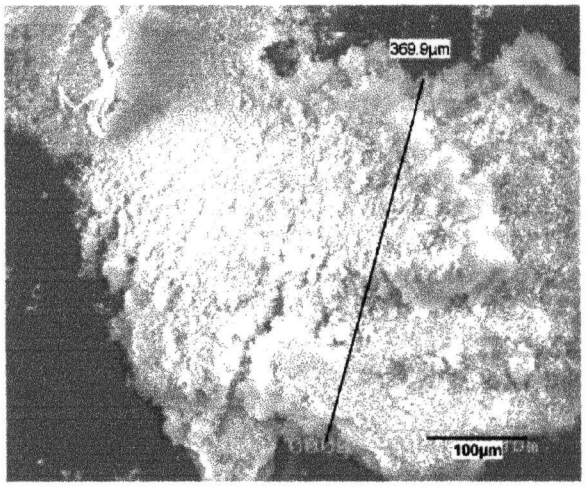

429-200

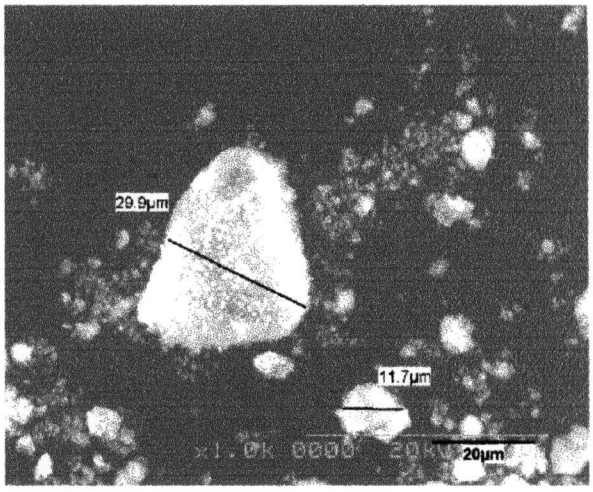

430-1k

Figure 4-6: SEM picture of various BN powders (200 = 200 times magnification, 1k = 1000 times and 6k = 6000 times). It can be seen that 428 is a uniform powder having no agglomerated particle. On the other hand, agglomerated particles of BN 429 can be as large as 370 µm.

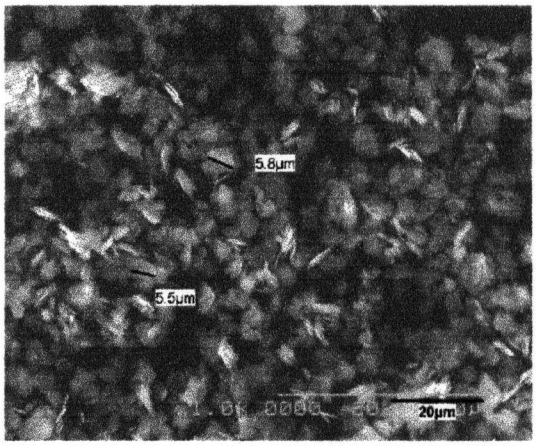

431-1k

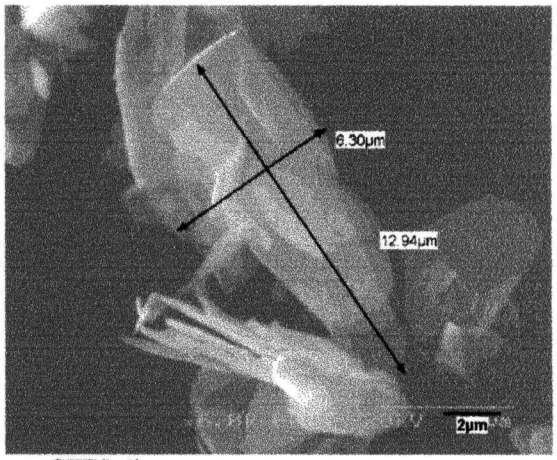

CTF5-6k

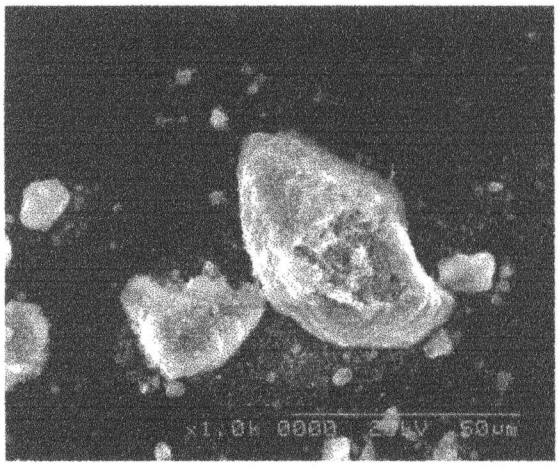

CTUF-1k

Figure 4-6 (continued): SEM picture of various BN (200 = 200 times magnification, 1k = 1000 times and 6k = 6000 times). It can be seen that 431 & CTF5 have uniform particle sizes including no agglomerated particle as opposed to CTUF.

4.3 Polymer Blends

Three techniques were used to introduce BN into the resins. According to the first technique, the BN particles in a finely divided state were thoroughly dry-mixed with the resin pellets at appropriate concentrations without using any extrusion equipment. According to the second technique, the pure resin pellets were first ground into a fine powder form by using a grinder. Then, a masterbatch of 10 wt % BN with ground m-LLDPE was prepared by using a preparation mixer. A desired final concentration of materials were obtained by mixing the pure ground m-LLDPE with the masterbatch by means of a ¾" single screw extruder equipped with a cooling system. The final material was chopped and collected in the pelletized form by using a 2" pelletizer. According to the third technique, a masterbatch of 10% BN with ground m-LLDPE was also prepared. However, a twin screw extruder was used to blend the BN with metallocene catalyzed polyethylene Exact® 3128 instead of the single screw extruder this time. Using these techniques mentioned above, one can obtain various levels of BN dispersion into the polymer matrix. The blends which were prepared and studied in this work are listed in Table 4-4 along with their composition..

Table 4-4: Summary of the various blends prepared together with the blending methods used.

Blend (at 200, 500 and 1000ppm)	Dry-mixed	10% Masterbatch + single screw extruder	10% Masterbatch + twin screw extruder
m-PE + CTUF	√	√	
m-PE + CTL40	√	√	
m-PE + CTF5	√	√	
m-PE + 427 to 431			√
Resins A and B + CTF5			√

5 Results and Discussion

5.1 Introduction

It is well known that the rate of production of many polymer processing operations including fiber spinning, film blowing, extrusion, and various coating flows, is limited by the onset of flow instabilities (Petrie and Denn, 1976; Larson, 1992). In particular in extrusion processes when the throughput exceeds a critical value, small amplitude periodic distortions appear on the surface of extrudates (surface melt fracture or sharkskin) and at higher throughput rates these take a more severe form of larger irregular distortions (gross melt fracture) (Tordella, 1969).

To increase the rate of production by eliminating or postponing the melt fracture phenomena to higher shear rates, processing additives/aids must be used. These are mainly fluoropolymers that are widely used in the processing of polyolefins (HDPE, LLDPE) and other commodity polymers. They are added to the base polymer at low concentrations (approximately 0.1%), and they essentially act as die lubricants, modifying the properties of the polymer-wall interface (increasing slip of the molten polymers). As a result of this lubrication effect, the onset of instabilities is postponed to much higher output rates and the power requirement for extrusion is significantly reduced. Note that these additives can eliminate only sharkskin and the so-called stick-slip (oscillating or cyclic) melt fracture. To the best of author's knowledge, they do not appear to have an effect on the extrudate appearance in the gross melt fracture region.

In this chapter, the effect of boron nitride (BN) based compositions as a processing aid in the continuous extrusion of a number of resins is examined. Its effect on the rheology of these resins is also tested. It has shown previously that compositions

containing BN can be successfully used as processing aids to eliminate not only sharkskin melt fracture but also substantially postpone gross melt fracture to significantly higher shear rates well within the gross melt fracture region in the extrusion of polyolefins and fluoropolymers (Buckmaster *et al.*, 1997). In this work, we first try to determine the characteristics of the BN powders that point out this unique action and secondly to determine the mechanism by which BN eliminates melt fracture. Finally the use of the boron nitride additives in commercially blow moulding extrusion processes is also demonstrated.

5.2 Melt Fracture Performance of Metallocene Polyethylene: Capillary rheometer studies

We have already discussed the first technique that was used to prepare blends. According to the first technique, the BN particles in a finely divided state were thoroughly dry-mixed with the resin pellets at appropriate concentrations. Figure 5-1 shows the flow curves of the virgin and 0.5% BN filled (CTF5) m-LLDPE Exact® 3128 obtained by using the capillary rheometer with a capillary die having a diameter, D, of 0.254 mm and a length to diameter ratio, L/D, of 40 at T=163°C. The Bagley correction was applied to the raw data in order to obtain an accurate value for the wall shear stress. It was determined by using an orifice die of L/D=0 having the same die diameter.

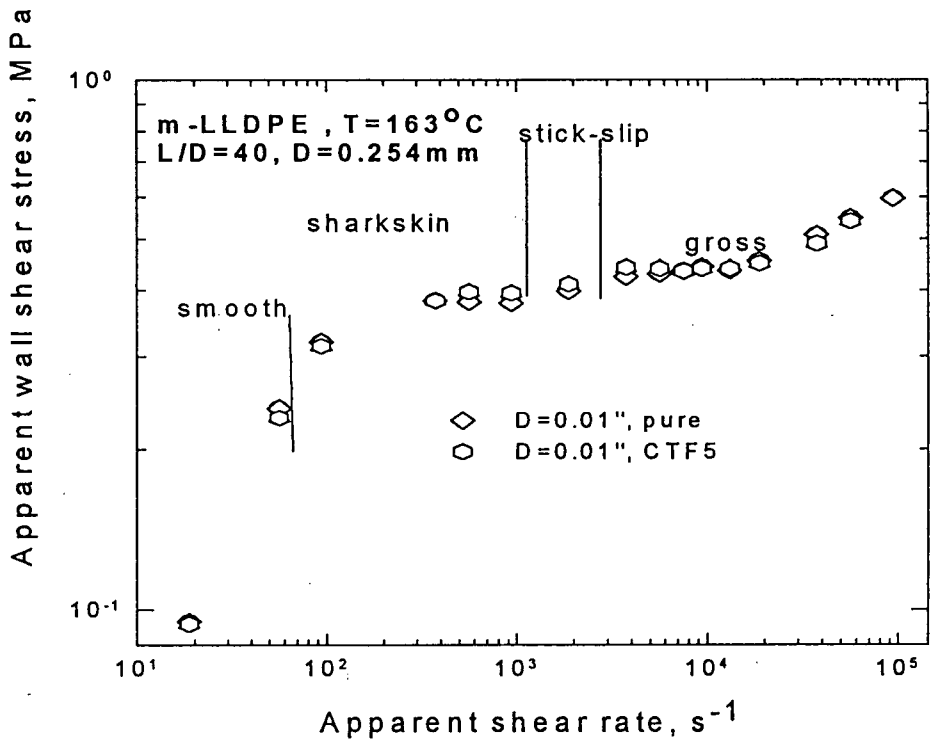

Figure 5-1: Flow curves of the virgin and filled Exact® 3128 obtained by using the capillary rheometer with a capillary die having D=0.254 mm and L/D=40 at T=163°C.

In the case of pure resin, sharkskin first appears at about a shear rate of 45 s^{-1}, followed by stick-slip and finally gross melt fracture at higher shear rate. The addition of 0.5% BN shows no effect on flow curve of the resin. The appearance of the CTF5 filled extrudates is almost the same as those of the pure resin one.

Figure 5-2 depicts the flow curve of m-LLDPE Exact 3128 (pure resin) obtained by using the Nokia Maillefer crosshead having 3.00 mm diameter and 1.52 mm tip at 163 °C. The formulas for calculating the wall shear stress and apparent shear rate were Equations 2-11a and 2-11b. The onset of surface melt fracture for the virgin resin is about 42 s^{-1} that agrees well with the value of 45 s^{-1} obtained from a circular die. The stick slip region does not appear in this case of the crosshead die. The surface melt fracture is followed by the gross melt fracture occur at about 500 s^{-1}.

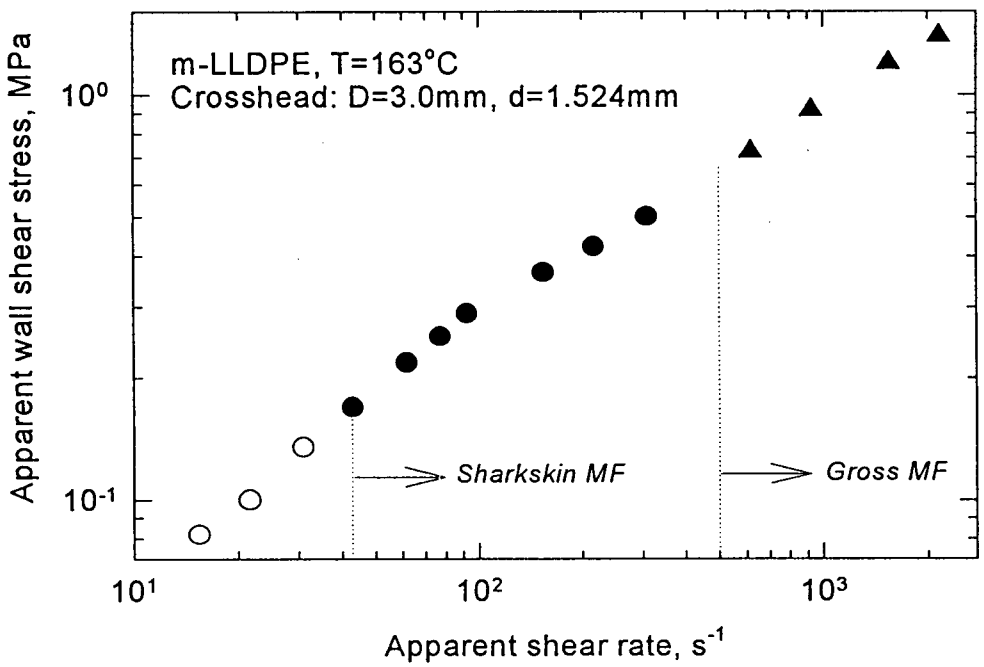

Figure 5-2: The flow curve of PE Exact® 3128 by using the capillary rheometer with Nokia Maillefer crosshead having 3.00 mm die and 1.52 mm tip at 163 °C.

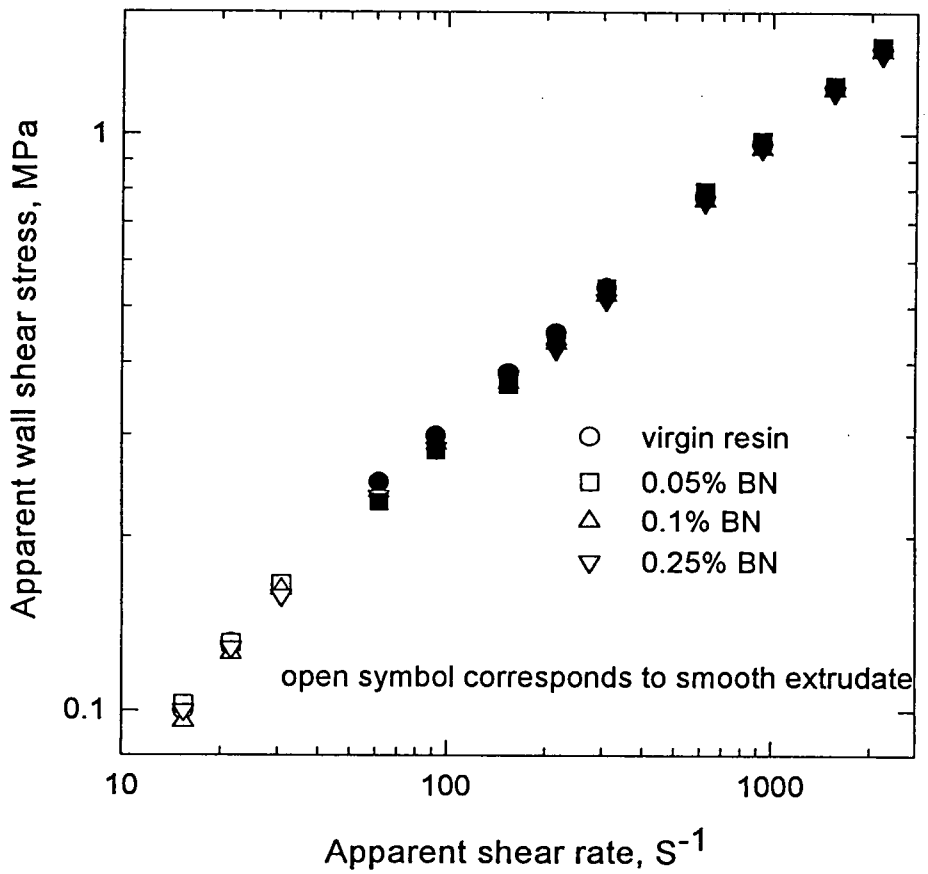

Figure 5-3: The flow curve of PE Exact® 3128 with and without boron nitride (CTF5) obtained with the Nokia Maillefer 4/6 crosshead attached at 163°C. Blends were prepared by dry-mix method. It shows that BN has little effect on melt fracture.

Figure 5-3 shows the flow curve of m-LLDPE Exact® 3128 with and without boron nitride (CTF5) at 163 °C using the crosshead die attached to the capillary rheometer. Blends were prepared by the dry-mix method. The flow curve of pure resin almost coincides with the other three ones that correspond to different BN concentrations. The

maximum shear rate to yield melt fracture at 163 °C upon the appearance of the extrudate are 62, 62, 77 and 92 s^{-1} for the BN concentrations of 0, 0.05, 0.1 and 0.25 weight % respectively.

Experiments at different temperatures were also performed in order to study the effect of temperature on the appearance of the extrudate. Table 5-1 summarizes the results of three sets of experiments at various temperatures obtained for BN type CTF5. The best results were obtained at the maximum BN concentration of 0.25% and the temperature of 204°C. However, this critical rate is far below the maximal shear rates yielding a smooth extrudate that was reported previously (Rosenbaum et al., 1998). Similar results were obtained with BN type CTUF and CTL40. In general, one may conclude that the addition of BN in the dry powder form into the resin has little effect on the melt fracture behavior of resins regardless of the BN type and concentration. However, this could be partially explained by the low degree of dispersion of BN particles that can be achieved by this technique of mixing (dry-mixing).

Table 5-1: The effect of BN on the melt fracture of m-LLDPE (Exact® 3128) at three temperatures obtained for BN type CTF5 added to resin in a dry-mixed form.

T, °C	BN concentration mass %	Max. shear rate, s^{-1}
163	0	42
	0.05	42
	0.1	77
	0.25	93
180	0	62
	0.05	93
	0.1	93
	0.25	93
204	0	93
	0.05	93
	0.1	113
	0.25	124

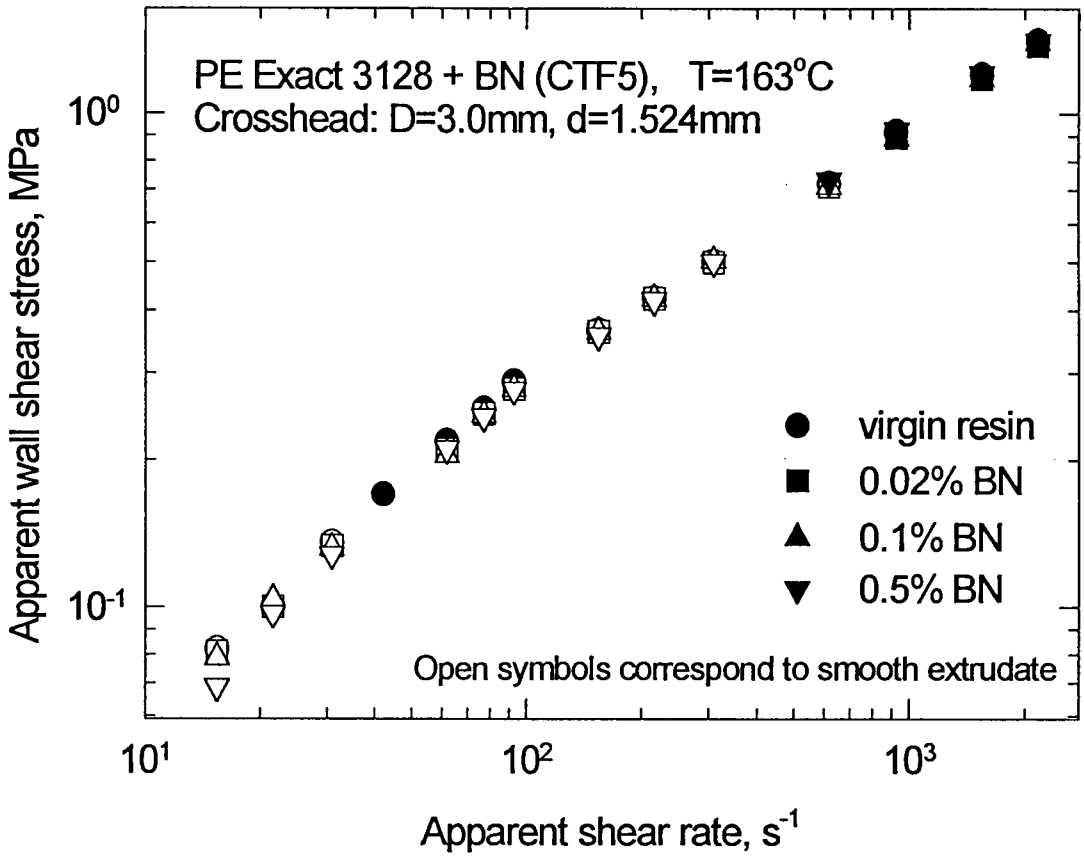

Figure 5-4: The flow curves of virgin and filled m-LLDPE Exact® 3128 with BN (type CTF5) at concentrations of 0.02%, 0.1%, and 0.5% obtained at 163°C by using the crosshead die (second mixing technique). It can be seen that BN has a significant effect on the melt fracture.

Figure 5-4 compares the flow curves obtained for the pure m-LLDPE Exact® 3128 and filled resins with BN (type CTF5) concentrations of 0.02%, 0.1%, and 0.5% at 163°C by using the crosshead die. The blends were prepared by using the second technique. The maximal shear rate at which the extrudates were smooth exceeded 926 s^{-1}. This is well above the critical rate for the onset of gross melt fracture of the virgin resin, which is about 500 s^{-1} (see Figure 5-2). Experiments have shown that the maximal shear rate yielding a smooth extrudate is also sensitive to the BN concentration. The optimal performance was

obtained at low BN contents, particularly 0.02% and 0.1%. Further increase in the additive concentration resulted in decrease in the maximal shear rate for the onset of flow instabilities. The maximal shear rate of 926 s^{-1} was obtained for BN (CTF5) concentrations of 0.02% and 0.1%, while the concentration of 0.5% resulted in the maximum shear rate of 617 s^{-1}. This means that there seems to exist some critical concentration resulting in optimum performance. This depends on the type of the resin and additive. Figure 5-5 depicts extrudate samples obtained at different BN (CTF5) concentrations at the shear rate of 617 s^{-1}. It can be seen that at this shear rate, virgin resin extrudate exhibits severe gross melt fracture, while 200 and 1000 ppm of BN eliminate completely the gross melt fracture. On the other hand, 5000 ppm of BN does not seem to eliminate gross melt fracture, although it appears to alter the extrudate appearance to a certain degree.

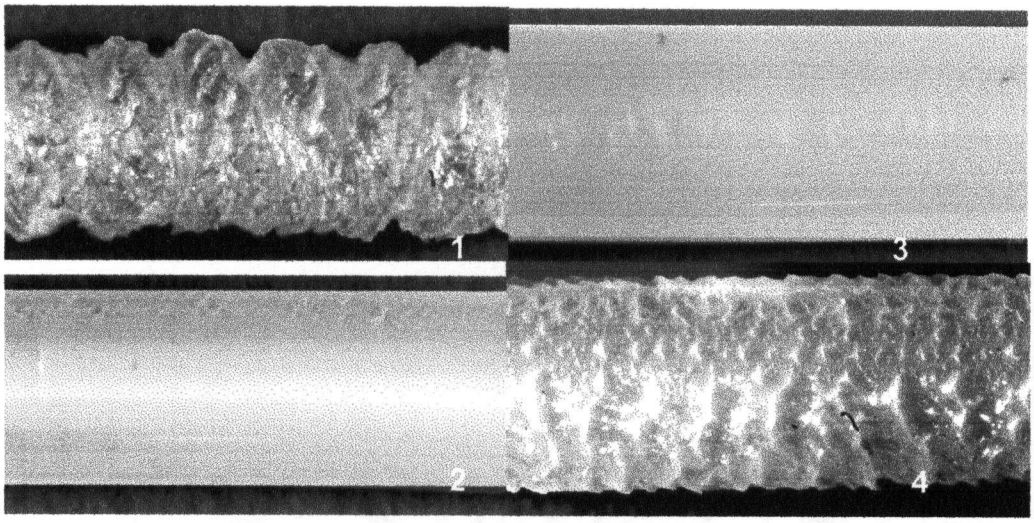

Figure 5-5. The extrudate samples to illustrate the effect of BN (CTF5) on the extrusion of m-LLDPE Exact® 3128 obtained at 617 s^{-1} and 163°C: 1) pure resin; 2) 0.02% BN; 3) 0.1% BN; 4) 0.5% of BN (CTF5)

Table 5-2 summarizes the effect of the BN type (CTUF, CTL40 and CTF5) and concentration on the maximal shear rate yielding a smooth extrudate in the extrusion of m-

LLDPE Exact® 3128 (Nokia Maillefer crosshead attached to the rheometer, D=3.0mm, d=1.52mm).

Table 5-2:Effect of the BN type (CTUF, CTL40 and CTF5) and concentration on the maximal shear rate yielding a smooth extrudate in extrusion of m-LLDPE Exact® 3128 (Nokia Maillefer crosshead attached to the rheometer, D=3.0mm, d=1.52mm) at 163°C. The resin and BN are initially pre-extruded by the second technique to attain good BN dispersion into the resin.

BN type	BN concentration, mass %	Max. shear rate, s^{-1}
Pure PE	0	42
CTUF	0.02	155
	0.1	155
	0.5	155
CTL40	0.02	62
	0.1	93
	0.5	77
CTF5	0.02	926
	0.1	926
	0.5	617

From the results of Table 5-2, it can be seen that the BN CTF5 appears to be the best BN compared to that of CTUF and CTL40. One may naturally ask why this is the case. In order to answer this question, let's review the morphological characteristics of these three different BN powders. CTF5 has an average particle size of 5-10 μm, CTL40 which is essentially an agglomerated version of CTF5 has an average particle size of more than 40 μm, and CTUF has an average particle size of 5-10 μm, but contains a fair amount of B_2O_3 (about 2%) compared to CTF5. This modifies its surface energy so that becomes higher to those of CTF5 and CTL40. As was shown in figure 4-5, the dispersion of the CTF5 is superior compared to that of CTL40 in the pure resin. Thus, one may conclude

that smaller average particle size may result into a better dispersion of BN into m-LLDPE and this results into a better performance in terms of eliminating surface and gross melt fracture.

The average particle size of CTUF is similar to CTF5's. The only difference is that CTUF contain about 2 % of B_2O_3. This shows that surface energy plays an important role here. The presence of B2O3 may cause stronger polymer adsorption and the creation of a stronger structure that is not desirable to improve melt fracture performance.

Further studies on the effect of type and concentration of BN were also carried out. Five additional types of BN were evaluated by using the capillary rheometer equipped with the Nokia Maillefer 4/6 crosshead mentioned above. Various BN concentrations and temperatures were used. The method used to introduce BN into m-LLDPE is by using twin screw extruder (third technique described in section 4.3). The various blends of BN were prepared with the metallocene catalyzed polyethylene m-LLDPE Exact® 3128. The particle size and agglomerated properties of the various BN powders are listed in Table 4-3.

Figure 5-6 shows the flow curve for the m-LLDPE Exact with and without BN431 filled by using the capillary rheometer with a capillary die having L/D=40 and D=1.27 mm. The flow curve for BN431 filled resin is lower than that compared to the pure one. The addition of 0.1% of BN431 does not have any significant effect on the appearance of the extrudate except that the stick-slip oscillating region does not appear in the presence of BN431.

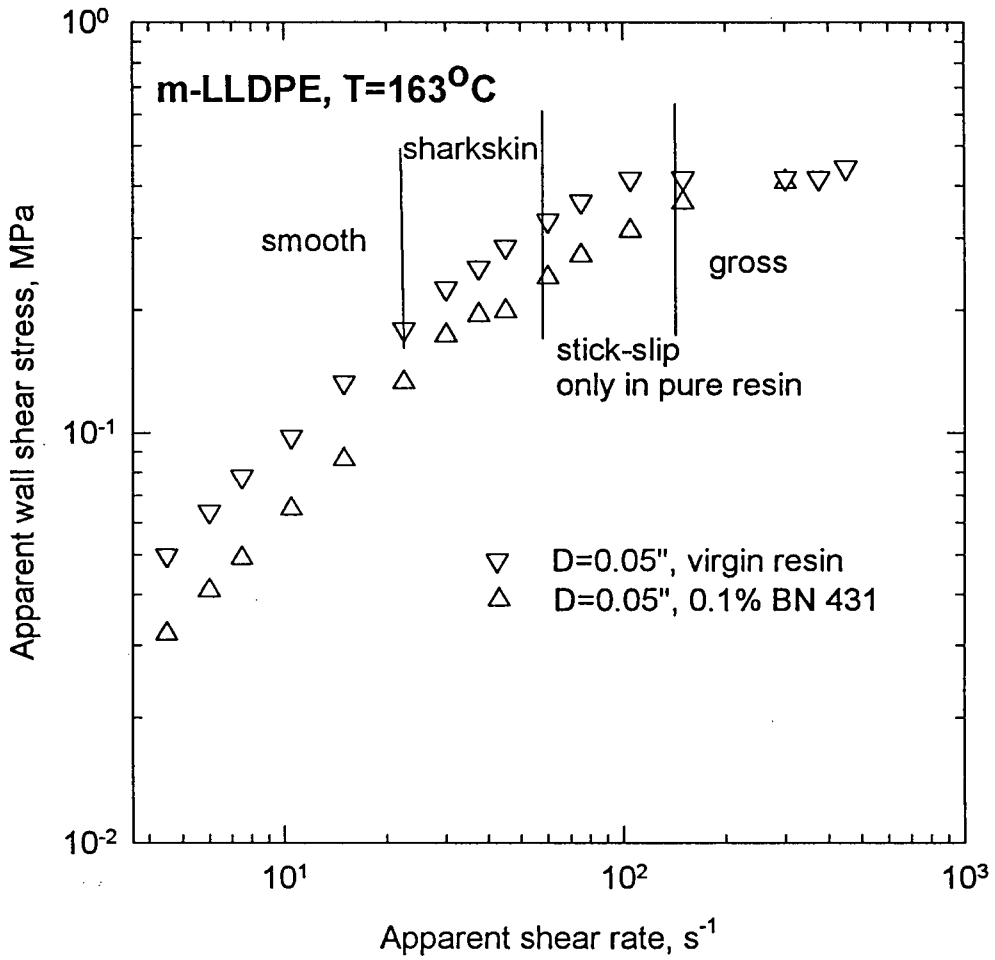

Figure 5-6: The flow curve for the m-LLDPE Exact® 3128 with and without BN431 obtained by using the capillary rheometer at 163°C by using second technique.

Figure 5-7 and 5-8 show a transient capillary experiment in the oscillating regime for the virgin resin and BN 431 filled resin at the apparent shear rate of 100 s^{-1}.

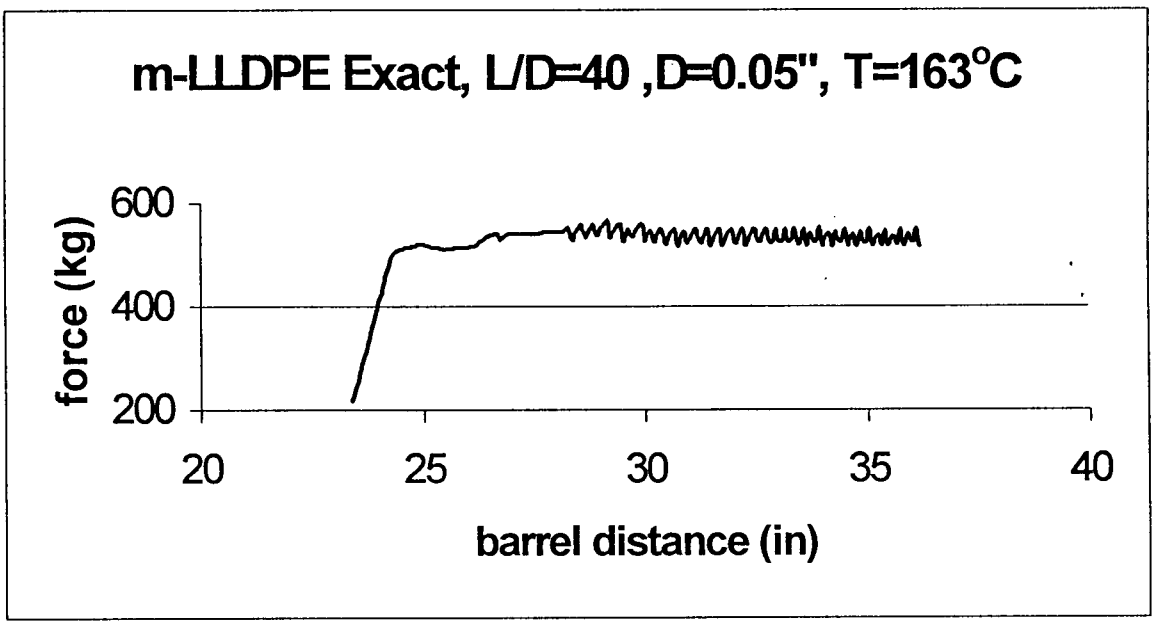

Figure 5-7: Transient capillary experiments for m-LLDPE Exact® 3128 at the apparent shear rate of 100 s^{-1}. Pressure drop oscillations are obtained at this shear rate.

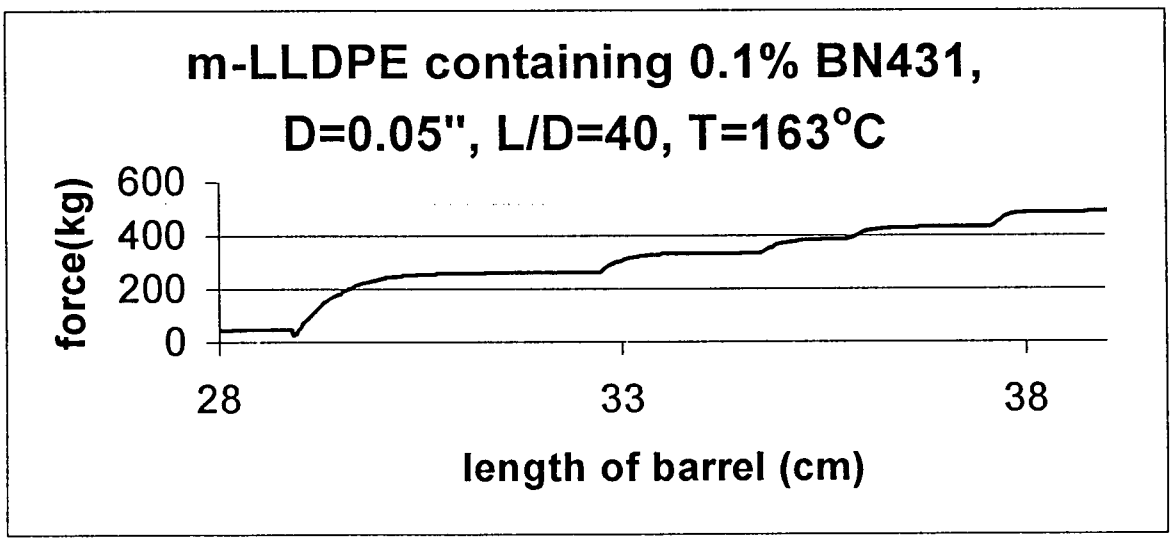

Figure 5-8: Transient capillary experiments for 0.1% BN filled m-LLDPE Exact® 3128 at various shear rates. Note that the force at 430 kg representing the shear rate of 100 s^{-1}. It is surprising the absence of oscillations at the shear rate of 100s^{-1}, mainly due to the presence of BN.

It can be clearly seen from figure 5-7 that the force (pressure drop) fluctuates between 530 kg and 550 kg for the pure resin, at the shear rate of 100 s^{-1}. However, from figure 5-8 it can be seen that there is no oscillation in the presence of BN431 into the resin at the same shear rate of 100 s^{-1}.

Other types of BN were also studied by using the crosshead die at various concentrations and temperatures. The results for maximum shear rates yielding smooth extrudates in extrusion of m-LLDPE Exact® 3128 at 163°C for two concentrations of BN 427-431 (200ppm and 1000ppm) are summarized in figure 5-9.

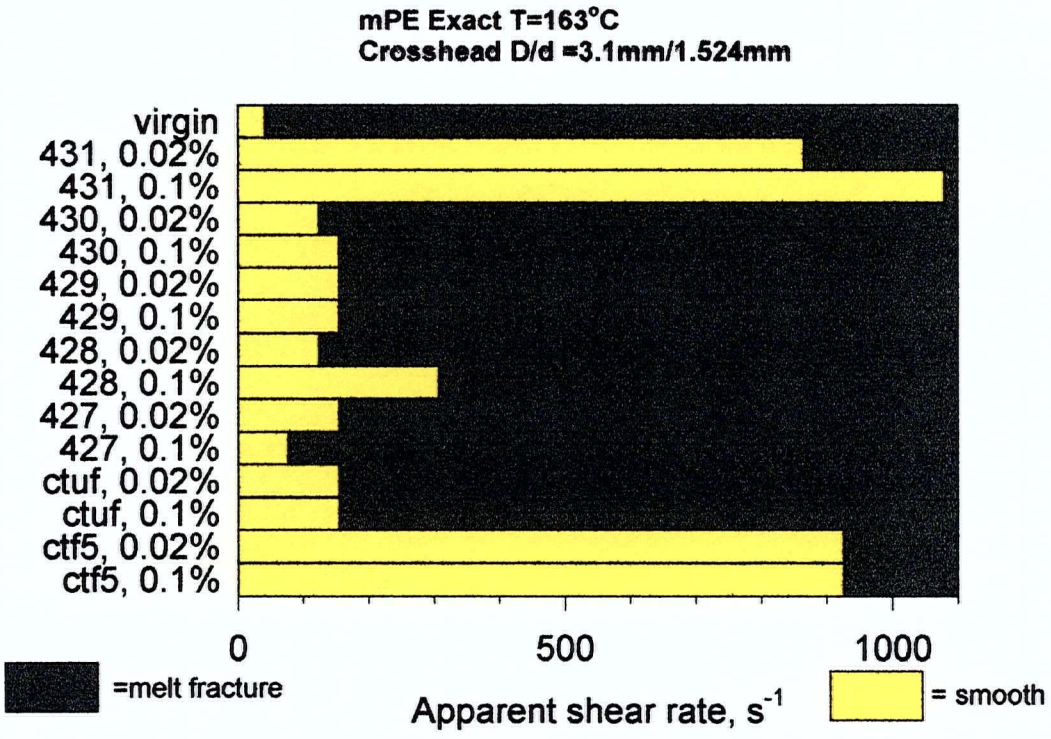

Figure 5-9: The effect of various boron nitride types on the maximum shear rate yielding a smooth extrudate in extrusion of m-LLDPE Exact® 3128 at 163°C for two concentrations of BN (200 ppm and 1000 ppm)

From figure 5-9, it can be seen that BN431 and CTF5 exhibit the best performance in terms of maximizing the critical shear rate for the onset of melt fracture. There are some common characteristics for these two boron nitrides. The particle sizes are small (5-10 μm) as well as they have no agglomerated particles. CTUF, BN427 and BN429 also have small particle sizes but some of their particles are agglomerated. Therefore, we can conclude that small average particle size of the BN and free of any agglomerated particles into the BN powder are the main requirements for maximizing the critical shear rate for the onset of melt fracture.

Figure 5-10 shows the melt fracture results for virgin PE resin, BN 428, 430 and CTF5 at two different temperatures 163 °C and 204°C. It can be seen that the critical shear rates for the onset of melt fracture increase with temperature in most cases.

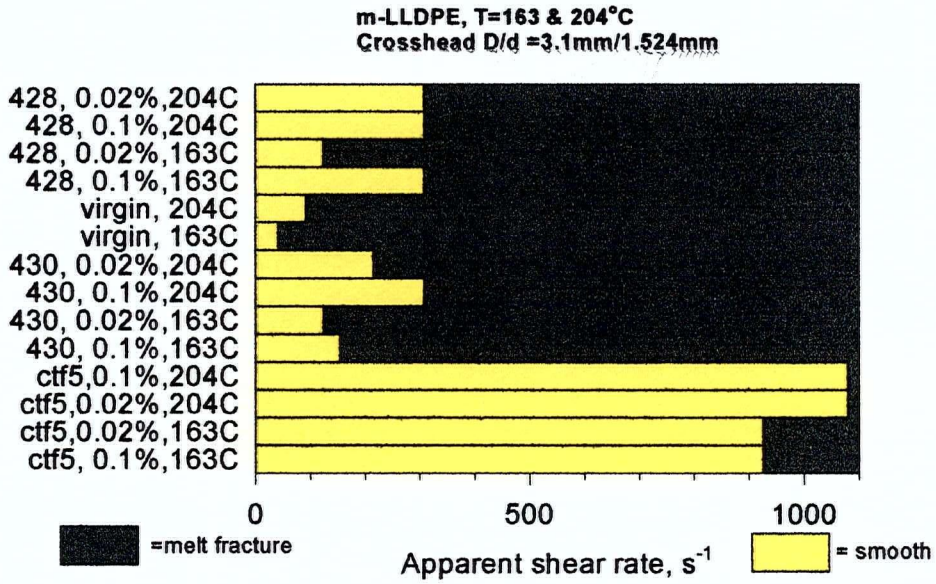

Figure 5-10: The effect of temperature on the melt fracture performance of BN 428, 430 and CTF5 filled m-LLDPE resin at two different temperatures of 163°C and 204°C.

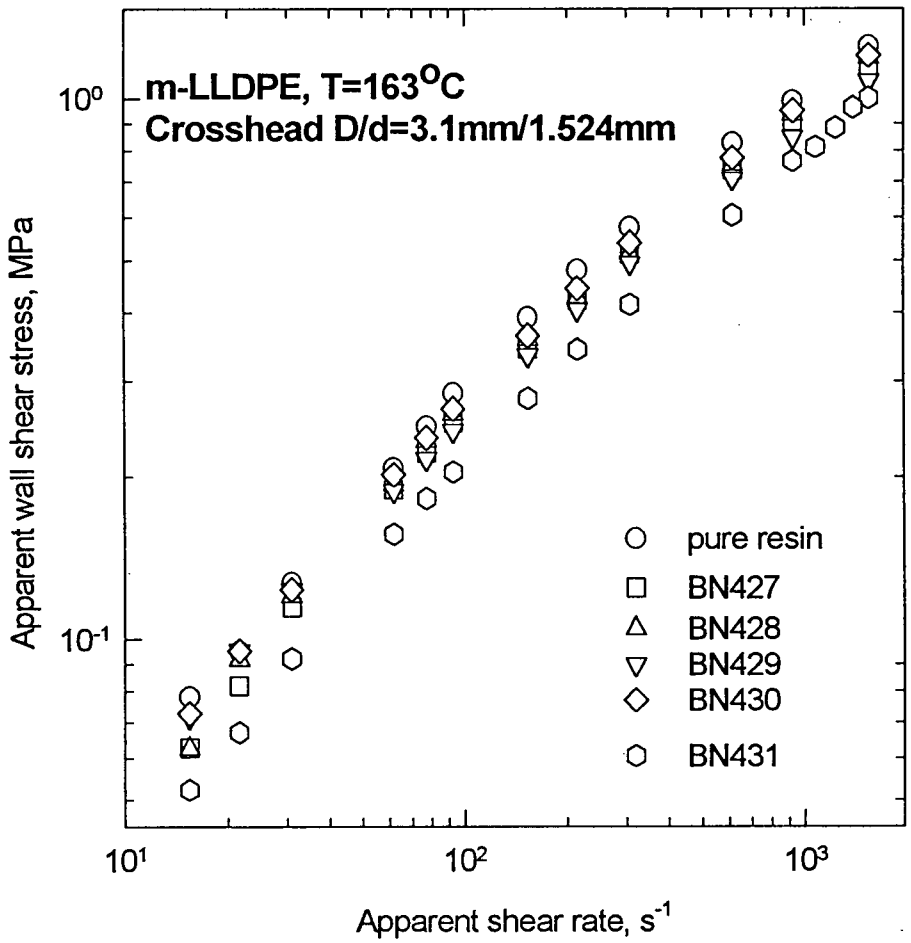

Figure 5-11: The flow curve of pure resin Exact® 3128 and of Exact® 3128 resin containing BN427 to BN431 (0.1 weight % in all cases) using the crosshead die at 163 °C.

Figure 5-11 shows the flow curve for the pure m-LLDPE resin and BN427 to BN431 filled resins (0.1 weight % in all cases) by using the crosshead die at 163 °C. The flow curve for all the filled resins are about the same except for that of BN431 filled one.

The flow curve for BN431 is lower than all the others. Moreover, from figure 5-9, it can be seen that 0.1% BN431 filled resin has the best performance over others. From these data, one may suggest that BN431 not only reduces the driving pressure of extrusion but also postpones the onset of melt fracture to much higher shear rate. As will be shown below, this reduction in pressure is due to the occurrence of polymer slip.

Summarizing this part of the study, one may conclude that for optimum performance of BN the following requirements apply: (1) the BN additive should consist of fine particles (average size of about 5-10 μm), (2) it should be thoroughly dispersed in the resin, and (3) it must be used at its optimal concentration depending on the type of the polymer and the extrusion temperature, and (4) it must not contain B_2O_3 which possibly increase its surface energy and as a result polymer adhesion on the surface of BN might become a factor. The reproducibility of the data for this apparatus is high. Experimental error as reproducibility is checked to be within 5%.

5.3 The Effect of Boron Nitride on the rheological behavior of Teflon FEP 4100 and m-LLDPE: parallel-plate rheometer and sliding- plate rheometer studies

In order to explain the effect of BN on the processability on PE Exact® 3128 during the extrusion in a wire coating process, the following possible mechanisms should be considered.

- Change of the rheological behavior: parallel plate rheometer
- Effect of die geometry: various contraction angles of orifice die
- Wall slip: capillary and sliding plate rheometer

5.3.1 Change of the rheological behavior

To study possible effects of the BN addition to the resin on its rheology, linear oscillatory shear experiments were carried out for the metallocene PE (Exact® 3128) and Teflon® FEP 4100 with and without BN using a Rheometrics System IV parallel-plate rheometer.

5.3.1.1 Metallocene LLDPE Exact® 3128

Frequency sweep experiments for m-LLDPE Exact® 3128 were carried out at 163°C for different levels of BN type. Only CTF5 and BN431 were considered in this study since they gave the best performance in terms of melt fracture performance (see section 5.2). Figure 5-12 shows dynamic mechanical data for virgin m-LLDPE and m-LLDPE filled with three different levels of BN (type CTF5). Surprisingly, no difference was found in the linear viscoelastic behavior of the virgin and CTF5 filled resins. Similar

results were obtained with the CTUF and CTL40 type of BN. This set of data agrees well with those in figure 5-4. The rheological behavior does not change by the addition of CTF5 up to concentrations of 0.5 wt%.

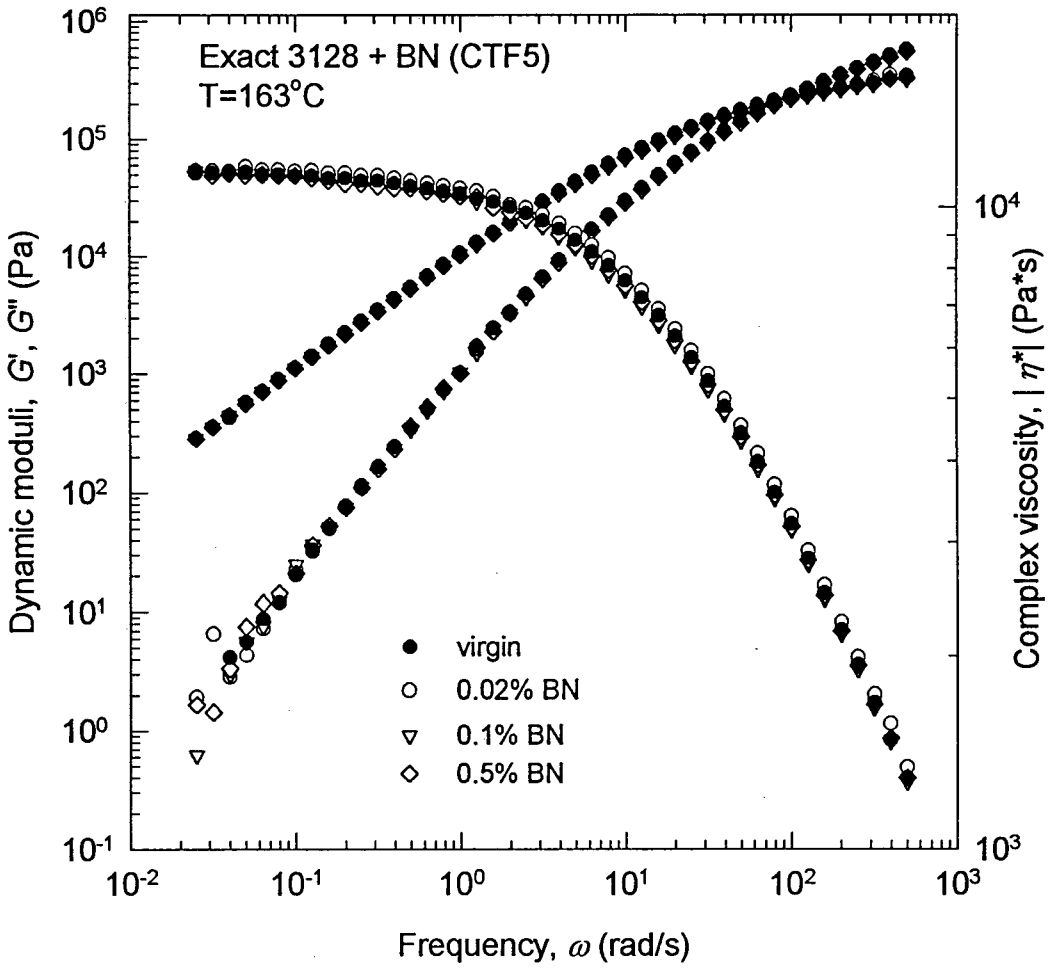

Figure 5-12. Linear viscoelastic data of m-LLDPE Exact® 3128 at 163°C with and without BN (type CTF5).

Since BN 431 performs best in eliminating the melt fracture (see figure 5-9) and the driving pressure in extrusion is lower than that of all other BN (see figure 5-11), its effect on the rheological behavior of m-LLDPE was investigated at 163 °C and plotted in figure 5-13.

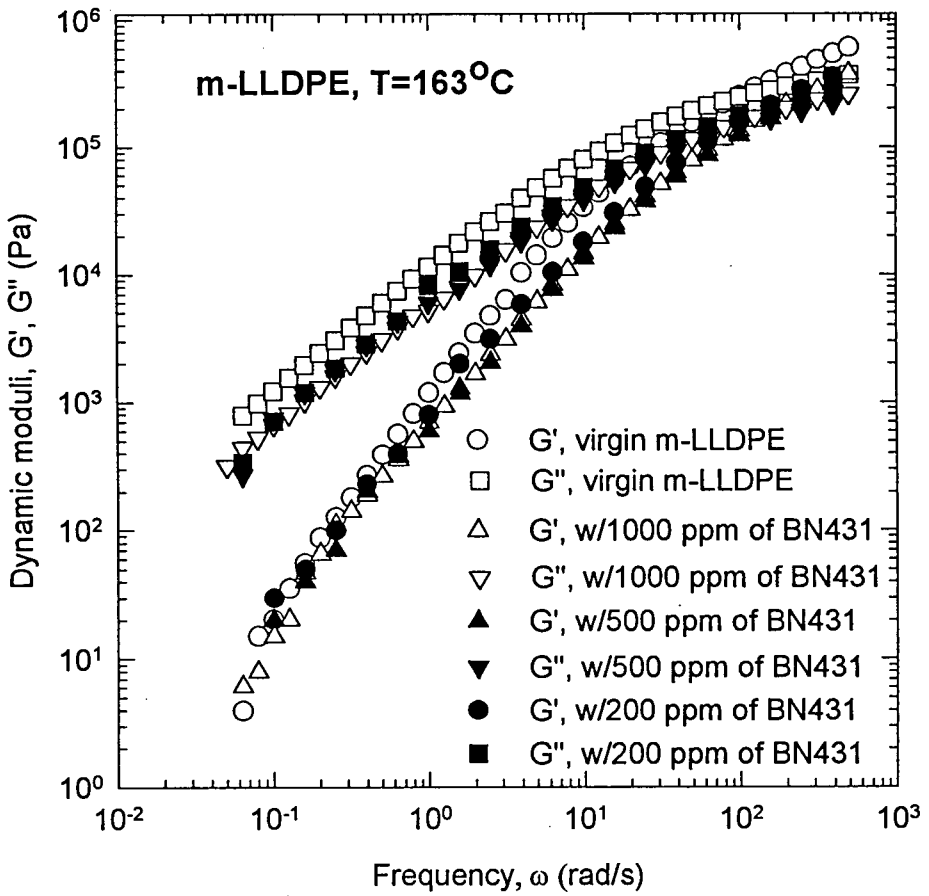

Figure 5-13: Linear viscoelastic data (G', G'') of m-LLDPE Exact® 3128 at 163°C with and without BN (type 431).

It can be clearly noticed that both the storage and loss moduli, G' and G'', of BN431 filled resin are lower than that of the virgin one. This observation agrees well with that shown in figure 5-11 where BN431 had a similar effect on the flow curve of the m-LLDPE Exact® 3128. It is also noted that higher BN concentrations (500ppm and 1000ppm filled resin) resulted into lower moduli values. The same effect can also be observed for the flow curve of virgin and BN431 filled resin plotted in figure 5-14. The question that has to be answered now is whether or not this reduction in the measured linear viscoelastic properties is a reduction in the rheological properties of the bulk of the material or a result of slippage of the resin at the wall. Sliding plate rheometer studies were carried out to answer this question. The results are presented in a later section.

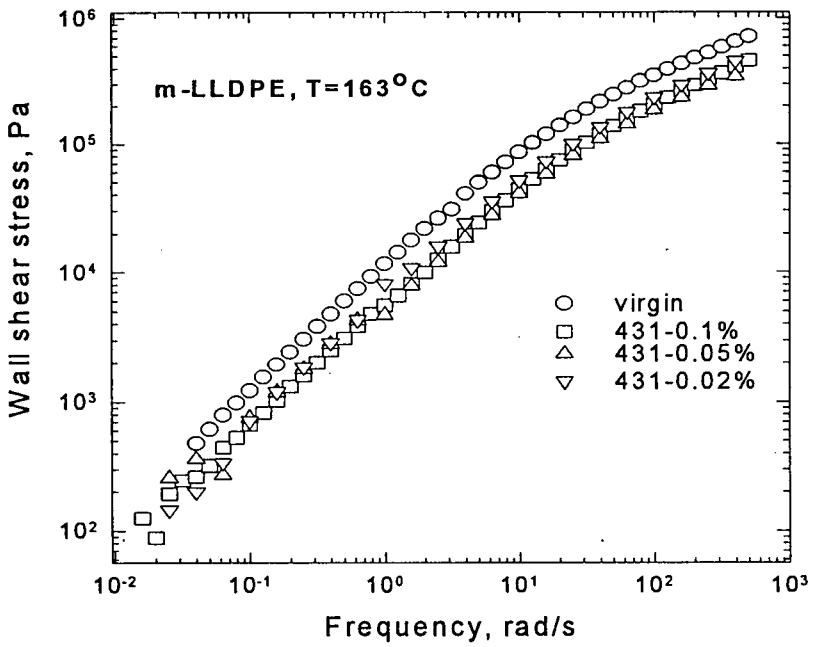

Figure 5-14: The wall shear stress vs frequency for the virgin m-LLDPE and m-LLDPE with BN431 with different levels concentration by using the parallel plate rheometer at 163 °C.

5.3.1.2 Teflon FEP® 4100

Teflon FEP® 4100 was also studied using parallel plate rheometer in order to determine the effect of BN on the rheology of fluoropolymer. Three different concentrations of BN (CTF5), namely 0.025%, 0.05%, and 0.17% along with the pure resin were used. Frequency sweeps were carried out at various concentrations and temperatures. Figure 5-15 depicts the dynamic moduli and complex viscosity of Teflon FEP® 4100 at the temperature of 300°C.

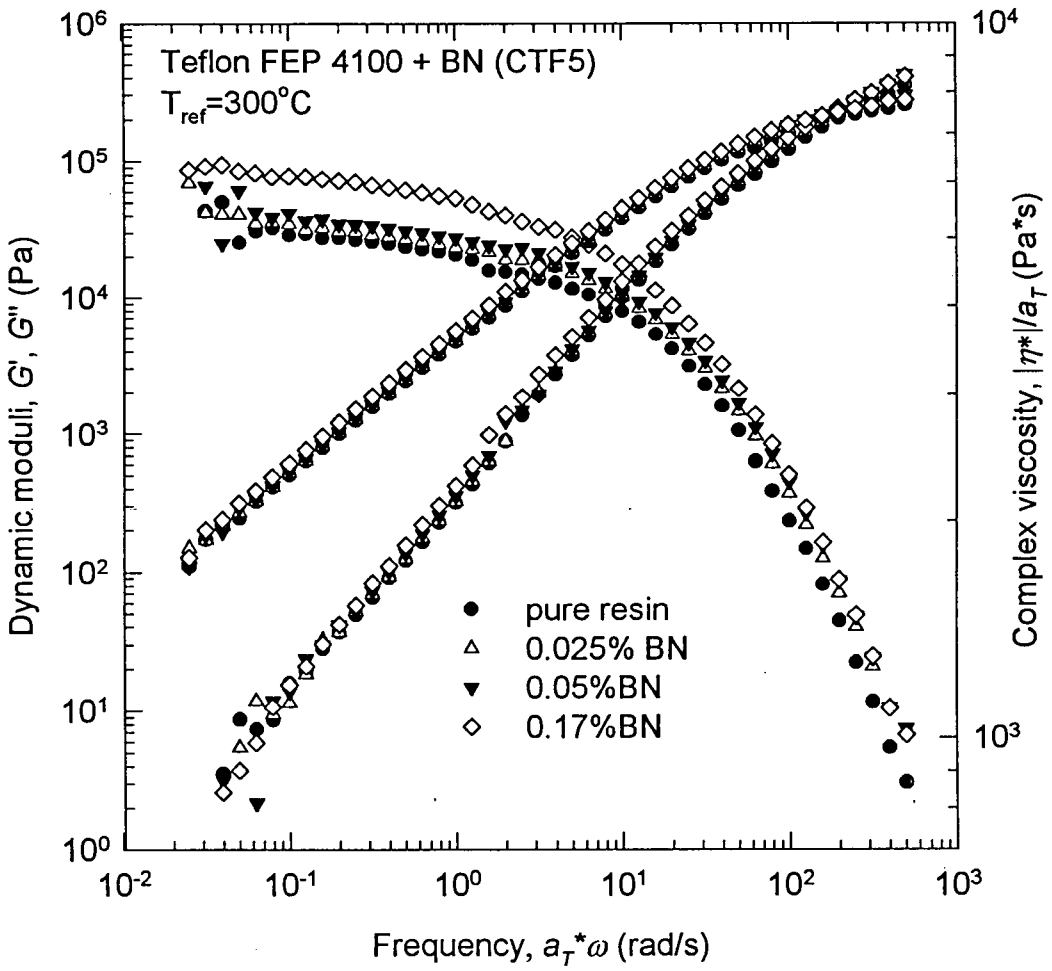

Figure 5-15: Linear viscoelastic data for Teflon FEP 4100 at the reference temperature of 300°C with and without BN (type CTF5).

The incorporation of BN (CTF5) increases all the material functions to a certain degree particularly at small frequencies. This can be attributed to the presence of BN particles that seem to have an effect on the rheology of Teflon FEP®. All three material functions, G', G'', and η^*, increase with the increase in the BN concentration. Therefore the effect of BN (CTF5) on the rheological behavior of Teflon FEP® 4100 was different to that of m-LLDPE Exact® 3128. As discussed before BN had no effect on the rheological behavior of m-LLDPE Exact® 3128.

Figures 5-16 to 5-18 plot the master curves of dynamic moduli of Teflon FEP® 4100 with various levels of BN at 300 °C. In all cases, good time-temperature superposition is obtained.

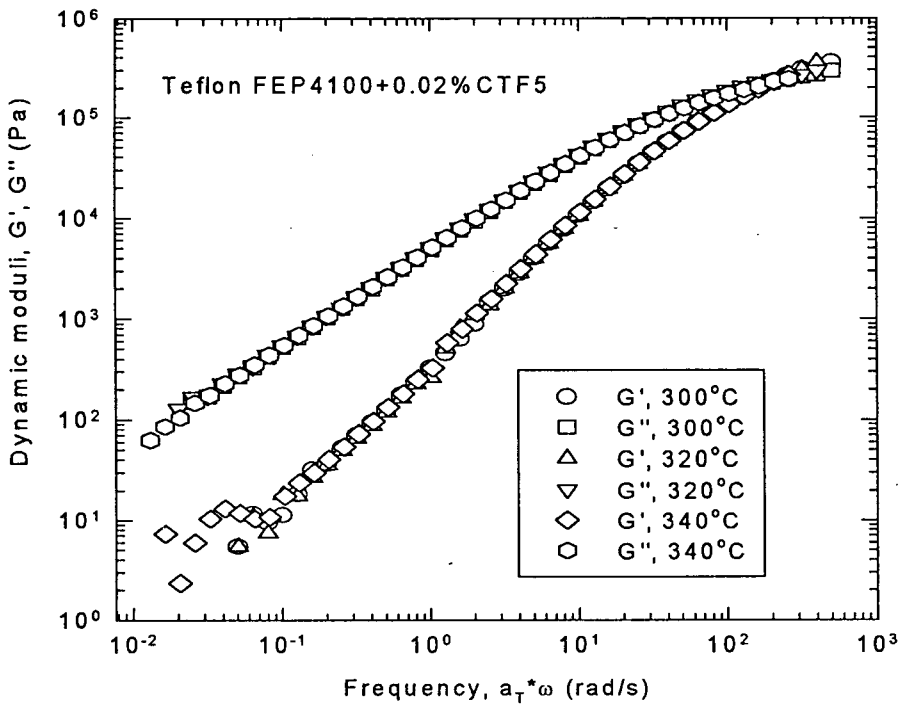

Figure 5-16: The dynamic moduli, G'&G'', of 0.02% CTF5 added Teflon FEP®4100 at reference temperature 300°C.

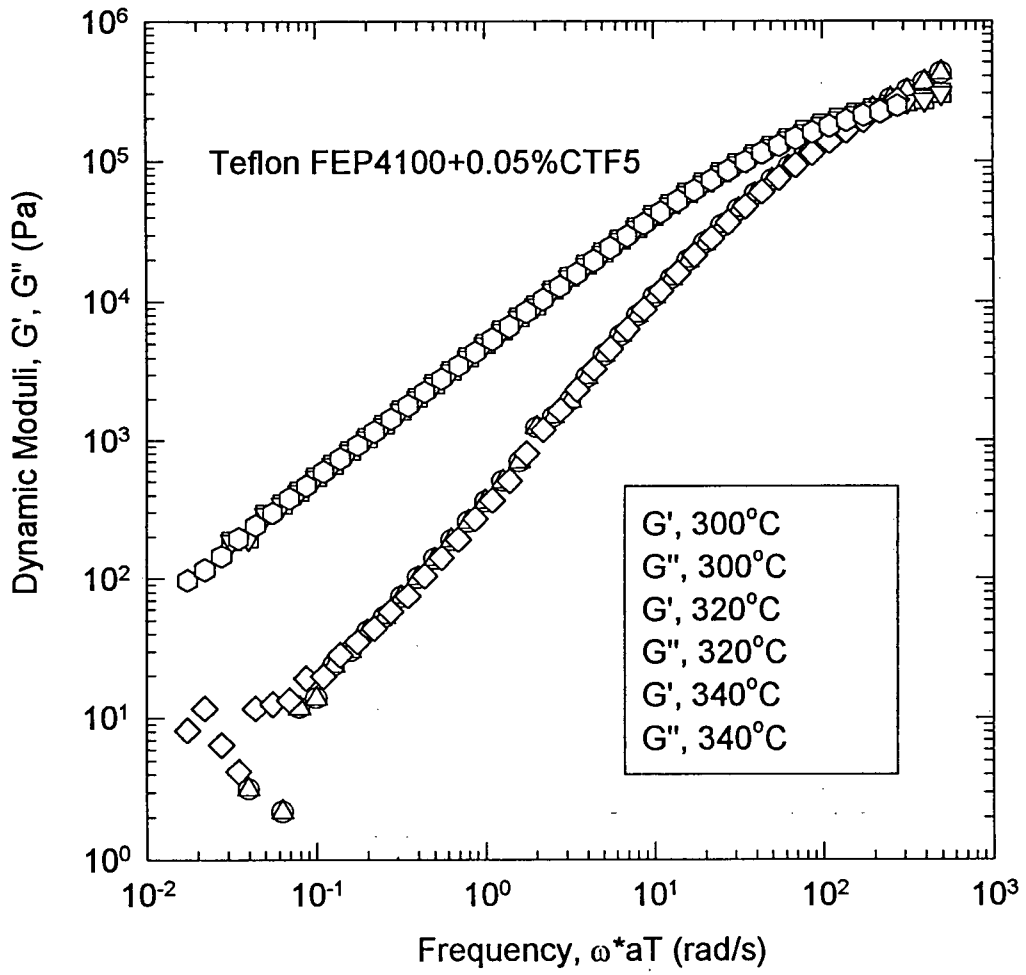

Figure 5-17: The dynamic moduli, G'&G'', of 0.05% CTF5 added Teflon FEP®4100 at reference temperature 300°C.

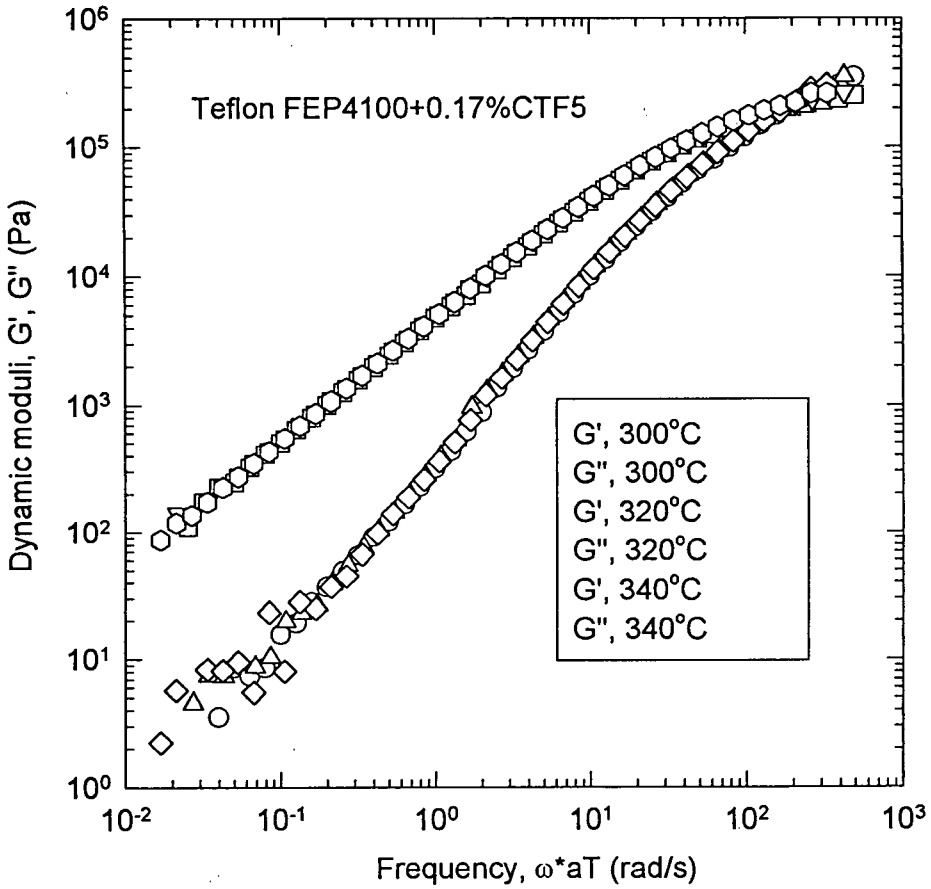

Figure 5-18: The dynamic moduli, G'&G'', of 0.17% CTF5 added Teflon FEP®4100 at reference temperature 300°C.

The shift factors, a_T, to superpose the linear viscoelastic data were also determined at each temperature together with the zero shear viscosity, η_o.

Figures 5-19 to 5-21 summarize the results for the zero shear viscosity at various temperatures.

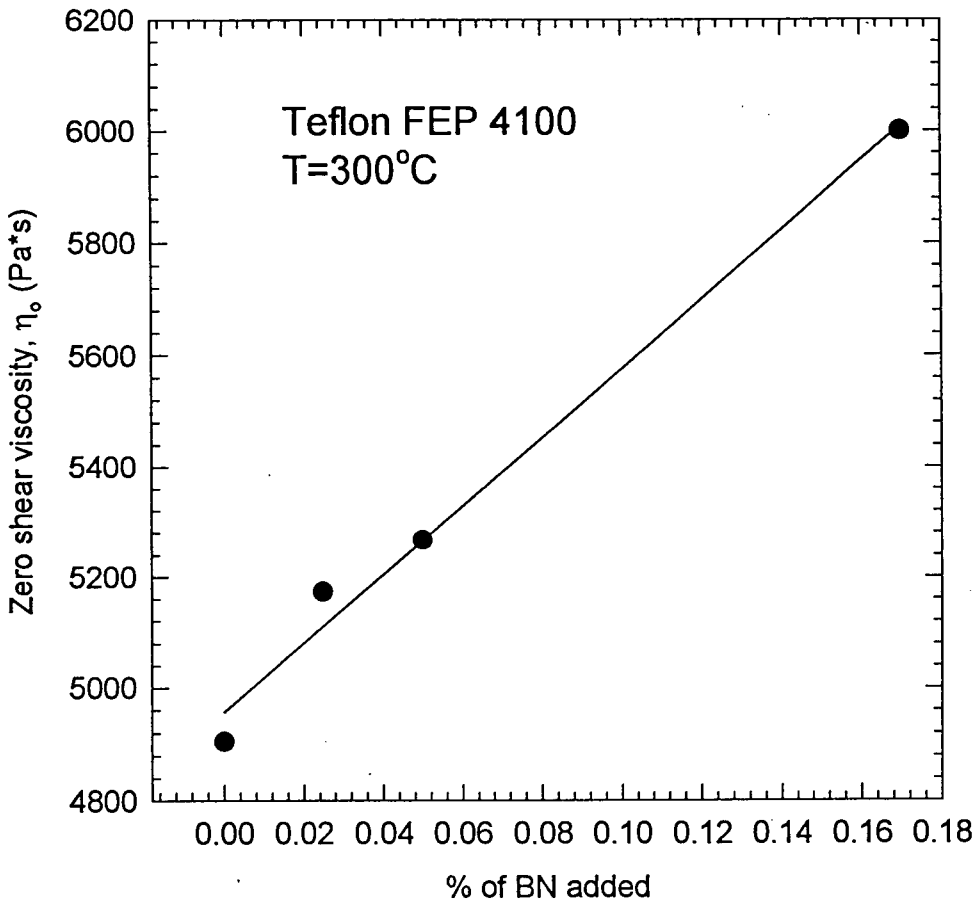

Figure 5-19: The effect of BN concentration on the zero shear viscosity of Teflon FEP® 4100 at 300°C.

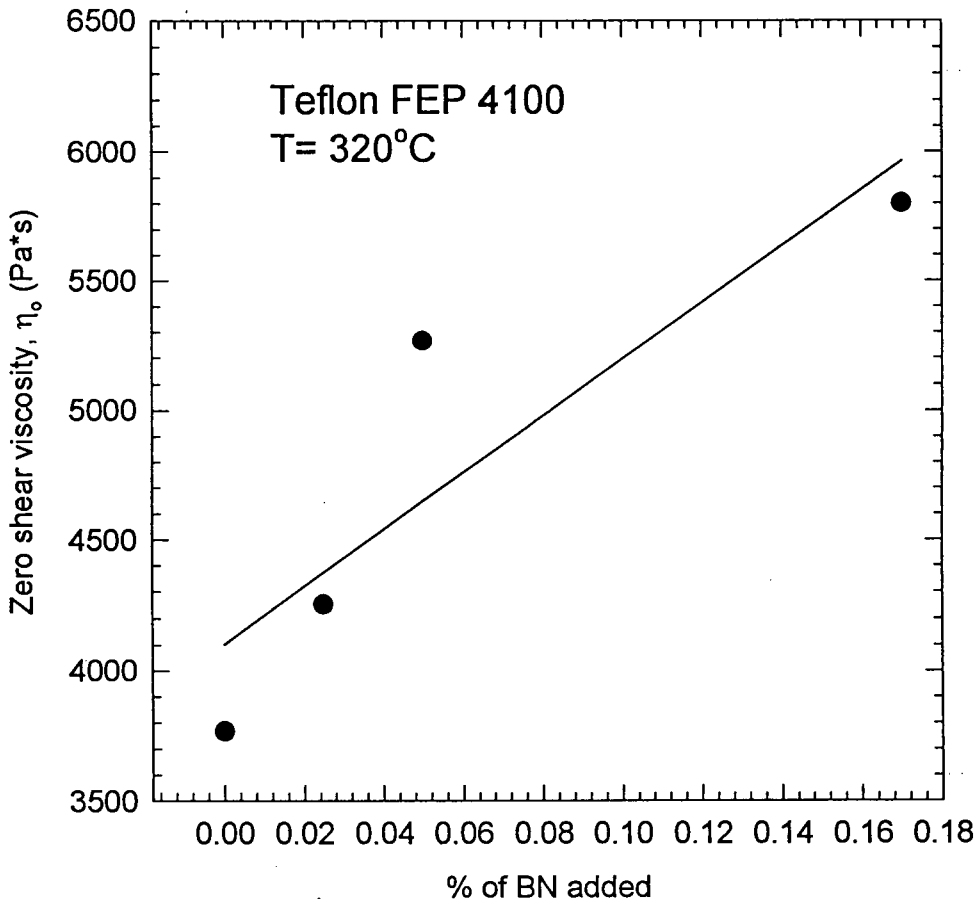

Figure 5-20: The effect of BN concentration on the zero shear viscosity of Teflon FEP® 4100 at 320°C.

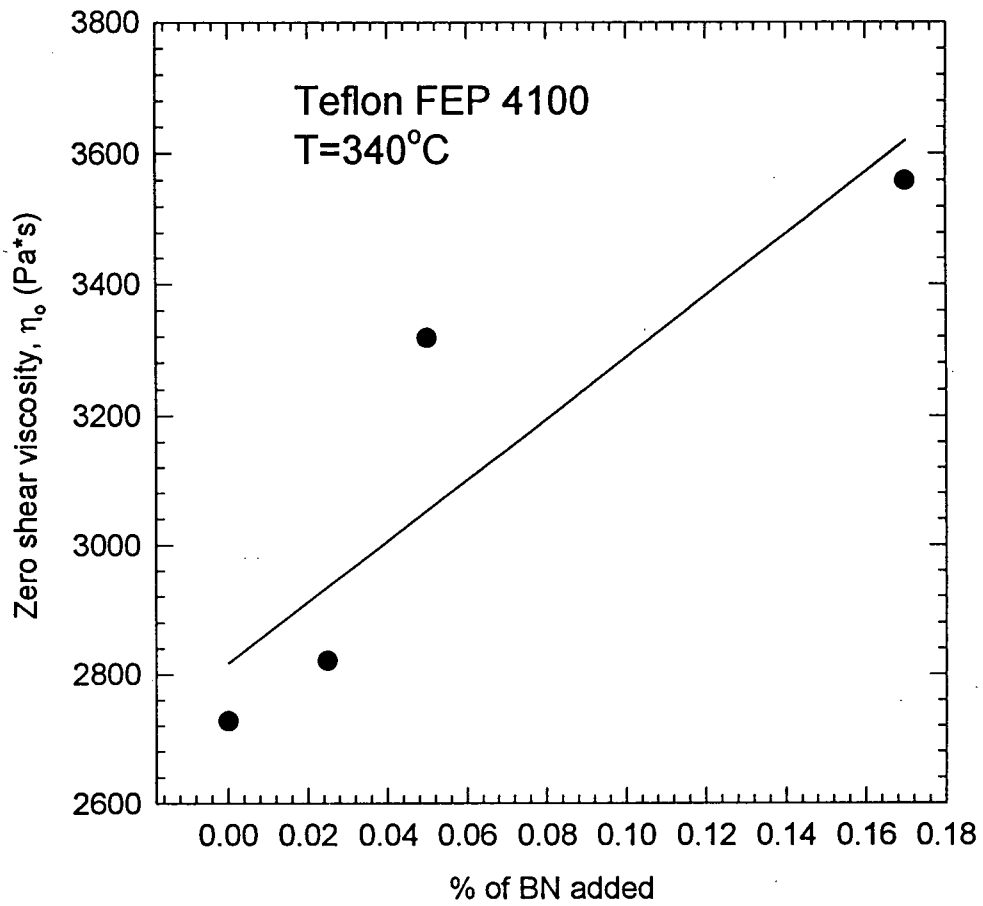

Figure 5-21: The effect of BN concentration on the zero shear viscosity of Teflon FEP® 4100 at 340°C.

It can be seen from figure 5-19, 5-20 and 5-21 that the zero shear viscosity increases with the increase of BN concentration. On the other hand increase of temperature results into decrease of the zero shear viscosity.

Based on the determined shift factor, the activation energies for flow, E_a, were calculated for the various BN concentrations based on an Arrhenius type equation (Eq. 2-25):

$$a_T = \exp\left[\frac{E_a}{R}\left(\frac{1}{T} - \frac{1}{T_{ref}}\right)\right] \qquad \text{(Eq 2-25)}$$

where R is the gas constant and T_{ref} is the reference temperature. Figure 5-22 depicts the relationship between the activation energy for flow and the BN concentration. It clearly shows that the activation energy decreases with increase of the BN concentration.

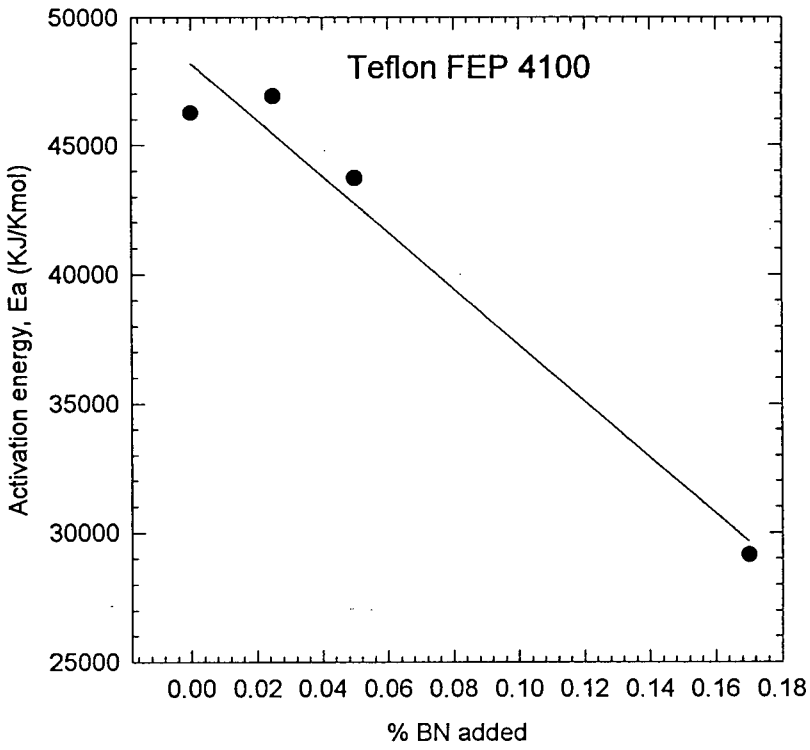

Figure 5-22: The relationship between the activation energy for flow, Ea, and the BN (CTF5) concentration in Teflon FEP 4100.

This finding means that the viscosity becomes less temperature dependent with increase of BN (CTF5) concentration in Teflon FEP® 4100. The reproducibility of the data

for this apparatus is high. Experimental error as reproducibility was checked to be within 2%.

5.3.2 Effect of the die geometry on the BN performance

It has be seen that the effect of BN is more pronounced in the crosshead die rather than the regular capillary die. This implies that the die geometry must play a very important role in this phenomenon. We can see from figure 2-7 that the crosshead provides a much smoother streamlined polymer flow. The polymer entering the die through port 11 flows along the conically converging annular channel defined by surfaces 12 and 22 to enter the die inlet smoothly. It is known that gross melt fracture is originated from the die entrance. This is why the streamlined flow at the entrance part of the die is so important to the melt fracture. In order to model the effect of the streamlined flow on melt fracture, various entrance angle of orifice dies (L/D=0) were used in the capillary rheometer. The entrance angles for this study were 8 °, 15 °, 30 °, 60°, 90° and 150°. Figures 5-23 to 5-24 depict the end pressure as a function of apparent shear rate of m-LLDPE Exact® 3128 with and without CTF5 for six orifice dies having various entrance angles. As can be seen, in spite of the significant differences of the flow curve for each entrance angle, the entrance angle has almost no effect on the extrudate appearance. For all dies, the surface melt fracture starts at around 70 s^{-1}. This means that the streamlined inlet region is a necessary but not a sufficient condition for the effect of BN. In fact, this effect is a combination of annular geometry of the crosshead die and the slowly converging entrance flow that provide the best condition for delaying the onset of melt fracture. Finally it is noted that BN has no effect on the pressure in orifice dies. In other words, the data plotted in figures 5-23 and 5-24 are identical.

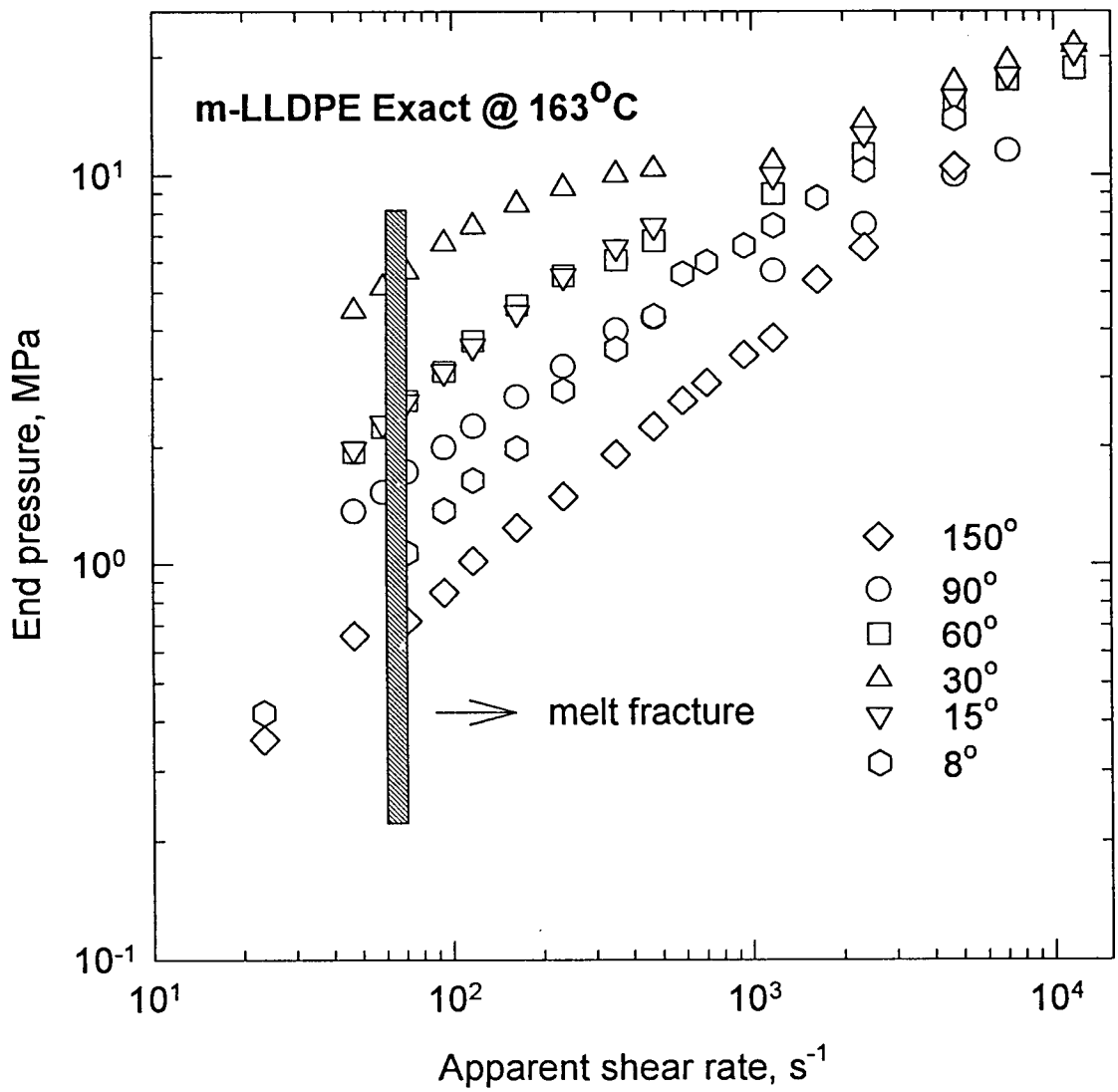

Figure 5-23: The end pressure as a function of apparent shear rate of m-LLDPE Exact® for six orifice dies having various entrance angles.

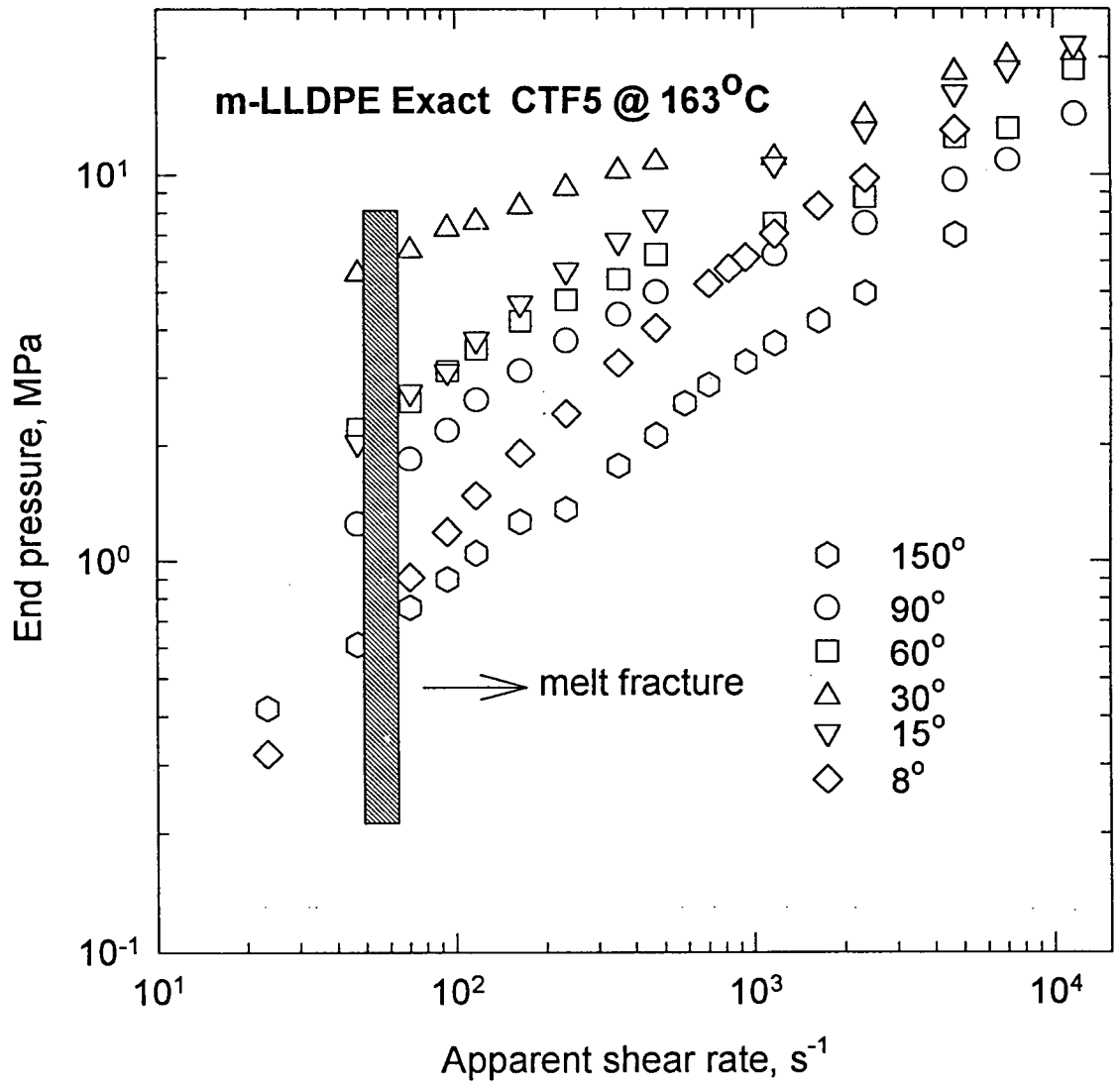

Figure 5-24: The end pressure as a function of apparent shear rate of 0.05% CTF5 filled m-LLDPE Exact® for six orifice dies having various entrance angles.

One surprising effect that can be observed from figures 5-23 and 5-24 is that the end pressure does not change monotonically with entrance angle. This can be seen clearly in figure 5-25 where the end pressure is plotted as a function of entrance angle for several

values of the apparent shear rate. It can be seen that at about 30°, we obtain the maximum end pressure. This observation can be very helpful in assessing the relative important of shear and extensional components of the various contraction angles, as well as in assessing the usefulness of contraction flows in determining the elongational viscosity of polymer melts. (Cogswell, 1977).

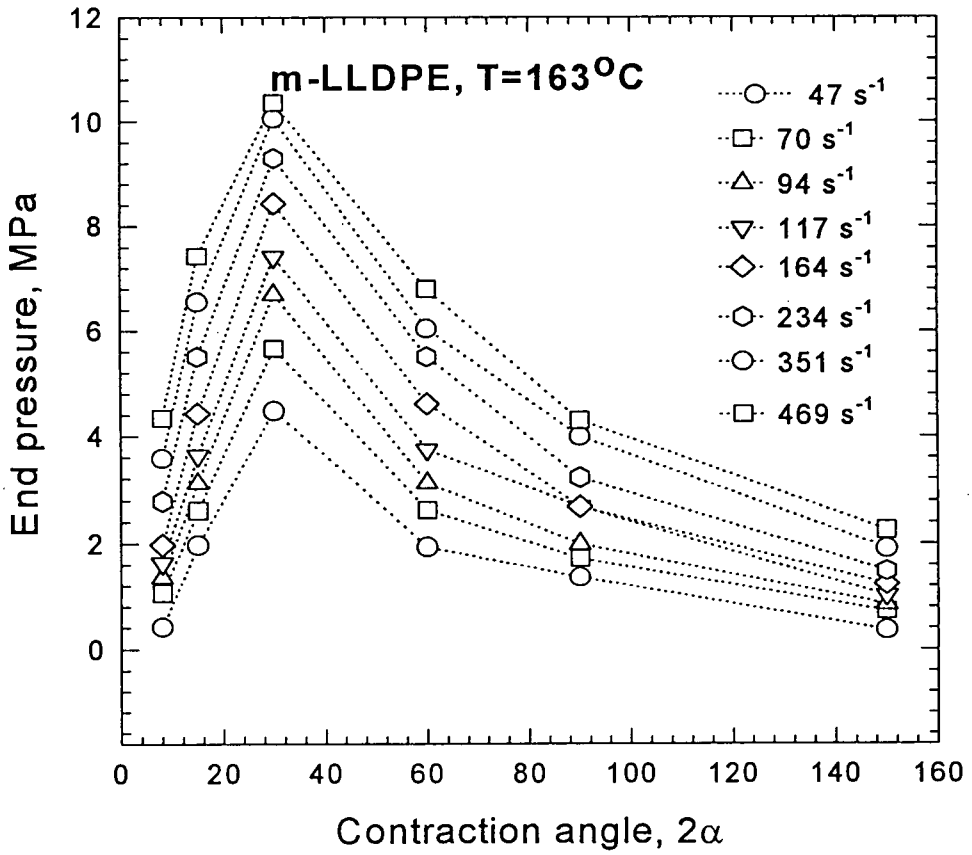

Figure 5-25: The effect of contraction angle on the wall shear stress for m-LLDPE at 163°C.

5.3.3 Wall slip

From the experimental data presented in section 5.2, it was seen that the use of BN 431 into m-LLDPE resulted into reduction of the wall shear stress compared to that of the other powders. This particular BN powder exhibited the best performance in not only eliminating the surface and stick-slip melt fracture, but also postponing the gross melt fracture to a higher apparent shear rate. As discussed before, one may argue that the reduction of the wall shear stress is due to the presence of wall slip. To answer this, capillary rheometer experiments were carried out using various die diameters. The results are summarized in figures 5-26 and 5-27. These figures plot the flow curve of pure m-LLDPE Exact® 3128 with and without addition of BN431 by using the capillary rheometer with dies having various diameters namely 0.254, 0.508 and 1.27mm at 163°C. The length to diameter ratio was 40 for all cases to keep the effect of pressure constant.

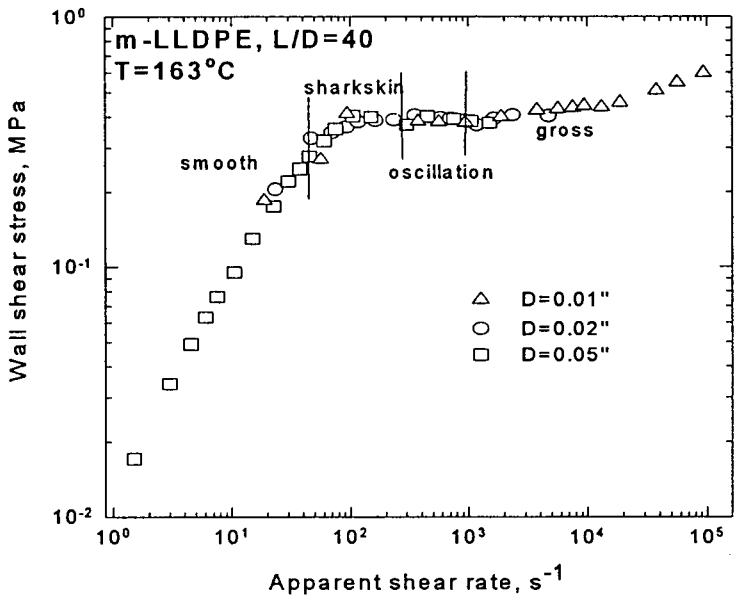

Figure 5-26: The flow curve of pure m-LLDPE Exact® 3128 using capillary dies having various diameters dies (0.254, 0.508 and 1.27mm).

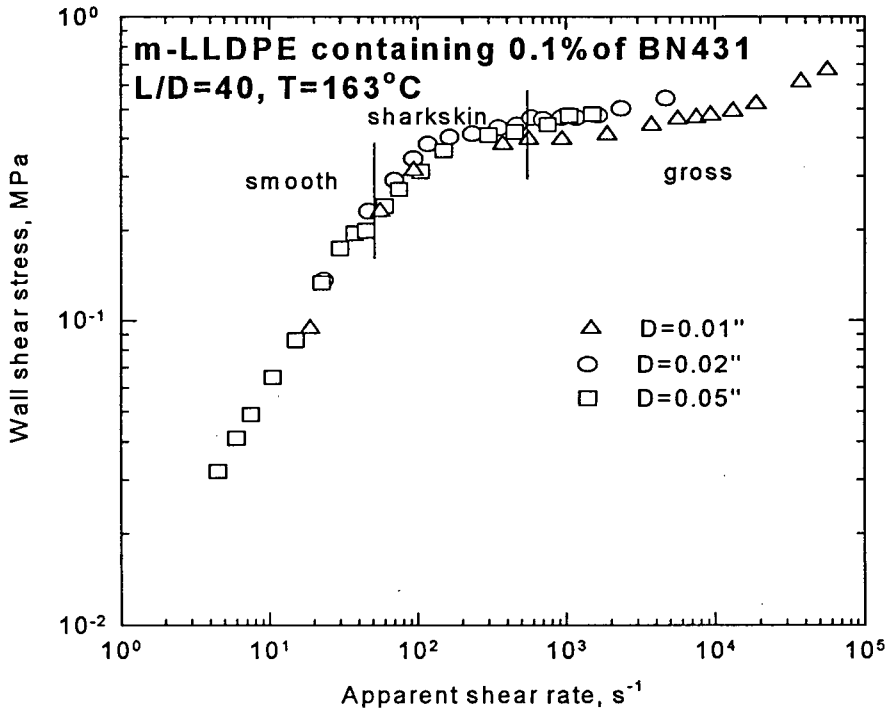

Figure 5-27: The flow curve of m-LLDPE Exact® 3128 with addition of BN431 for capillary dies having various diameters (0.254, 0.508 and 1.27mm).

It can been seen from figure 5-26 that all three flow curves coincide. It means that there is no slip in the case of pure Exact® 3128. However, the flow curves diverge when the wall shear stress exceeds the critical value with addition of BN431 in figure 5-27. This indicates that slip occurs at the die wall. Thus, we can conclude that BN431 does affect the flow profile by causing the polymer to slip along the metal wall. This is shown below more convincingly by carrying out the sliding plate rheometer studies.

Figure 5-28 shows the flow curve of m-LLDPE with the addition of 0.1% BN431 determined by means of the sliding plate rheometer having various gaps spacing. It can be seen that the flow curve becomes gap dependent. Smaller gap spacing shifts the flow curve towards smaller wall shear stress values. This type of gap dependence is consistent

with the occurrence of wall slip. The reproducibility of the data for this apparatus is high. Experimental error as reproducibility is checked to be within 5%.

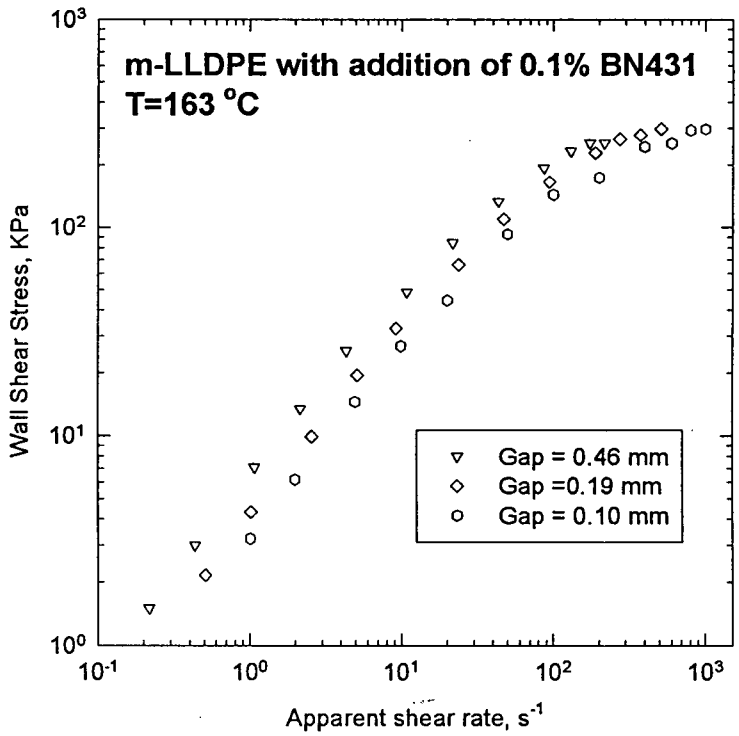

Figure 5-28: The flow curve of pure m-LLDPE Exact® 3128 with addition 0.1% of BN431 determined by the sliding plate rheometer using various gap spacing.

5.4 Flow Visualization on Polypropylene

To identify the mechanism of gross melt fracture elimination by the use of BN as a processing aid, visualization experiments were performed with the experimental set-up presented in section 2.3.4. It is hoped to see that the flow pattern developed in the entrance region to the die is different in the presence of BN. This is demonstrated in this section by using polypropylene as the base resin. Figure 5-29 plots the flow curve of polypropylene with and without BN (CTF5) by using the transparent quartz capillary die. It can be seen that the flow curves corresponding to 0.1% BN added resin result in a small reduction of the wall shear stress at all apparent shear rates used.

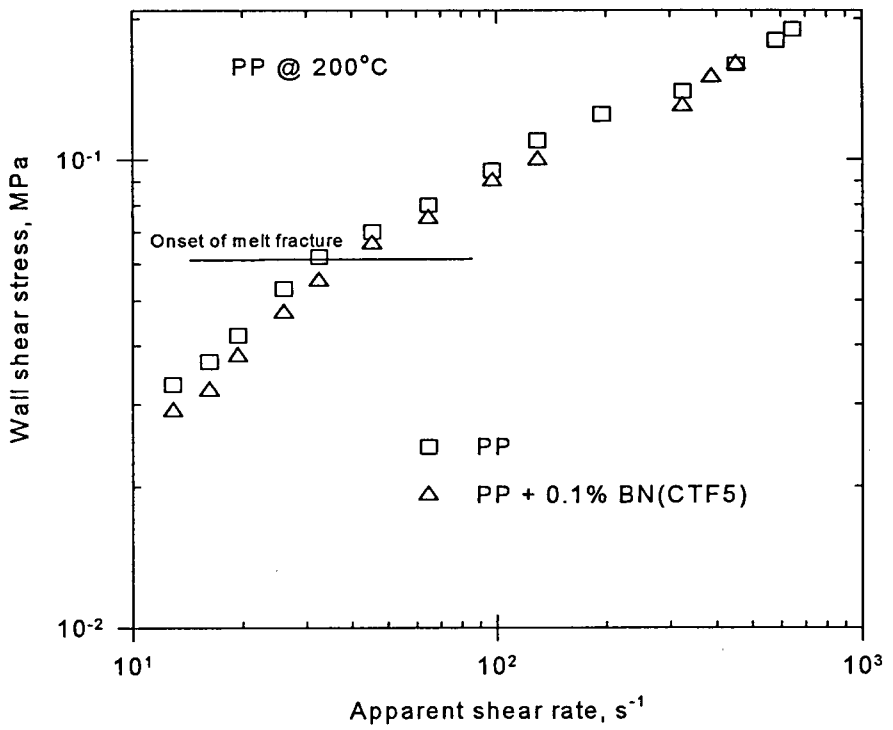

Figure 5-29: The flow curve of polypropylene with and without BN (CTF5) by using the transparent quartz capillary die.

Photographs of the capillary entry region were taken by using the microscope (Nikon SMZ-2T) and Nikon FM-2 35mm photographic camera. The effect of shear rate and additive concentration on the flow pattern development at the entry of the capillary are investigated. Gross melt fracture is known to originate from the die entrance [Bergem, 1976]. The observation of flow pattern may provide additional insight on the effect of additives on the melt fracture phenomena of molten polymers.

Figure 5-30a shows three pictures of the flow of polypropylene at various apparent shear rates (32.4, 324 and 650 s^{-1}) at 200°C. It can clearly be seen that the flow entry angle is higher at the low shear rate, it also has a bigger corner vortex. As the shear rate increases, the flow entry angle become more bend and the corner vortex becomes smaller. Moreover, one can see that there is discontinuous particle motion on the picture at 650 s^{-1}. Gross melt fracture is observed and the streamlines are no longer smooth. It is caused by a discontinue motion of the polymer flow. In fact, the flow in the entry region break into layers, which they seem to move with different velocities. The closer the layer is to the center of the stream, the larger step and more frequent is this discontinuous motion. A schematic diagram to explain this flow pattern development is shown in figure 5-30b. The flow in the entry region appears to be broken into several layers, and each layer moves with its own velocity. At regular time intervals, different in each layer, the motion stops for a brief period. The closer the layer is to the center of the stream, the larger and more frequent are the jumps inside it.

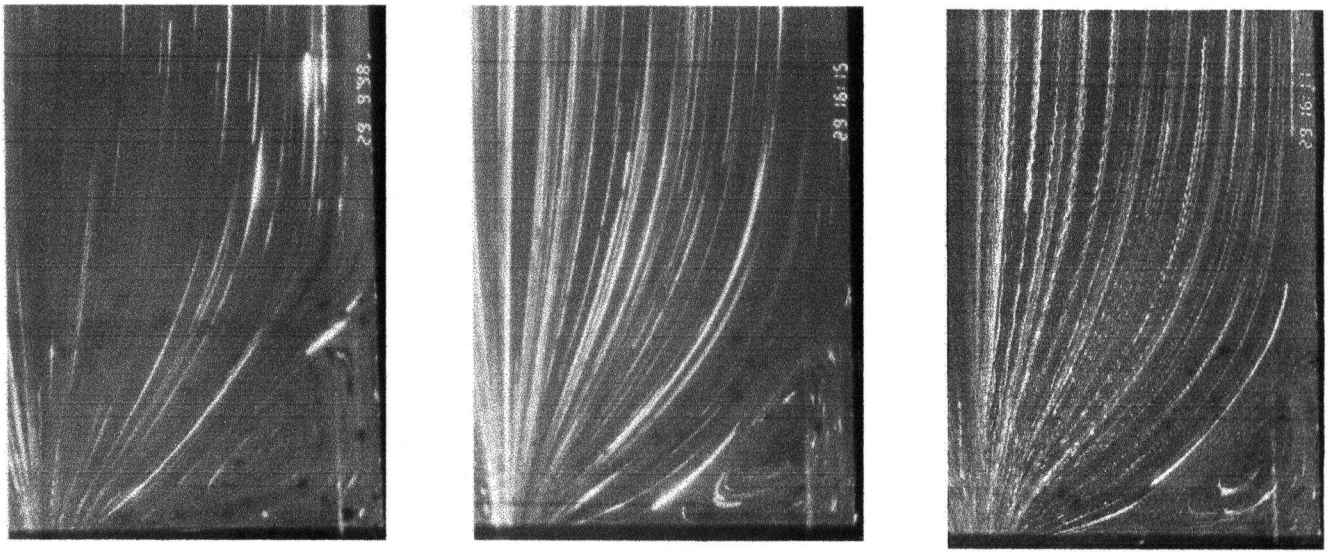

Figure 5-30a: Pictures of the flow of polypropylene at various apparent shear rates (left 32.4 s^{-1}, middle 320 s^{-1} and right 650 s^{-1}) at 200°C.

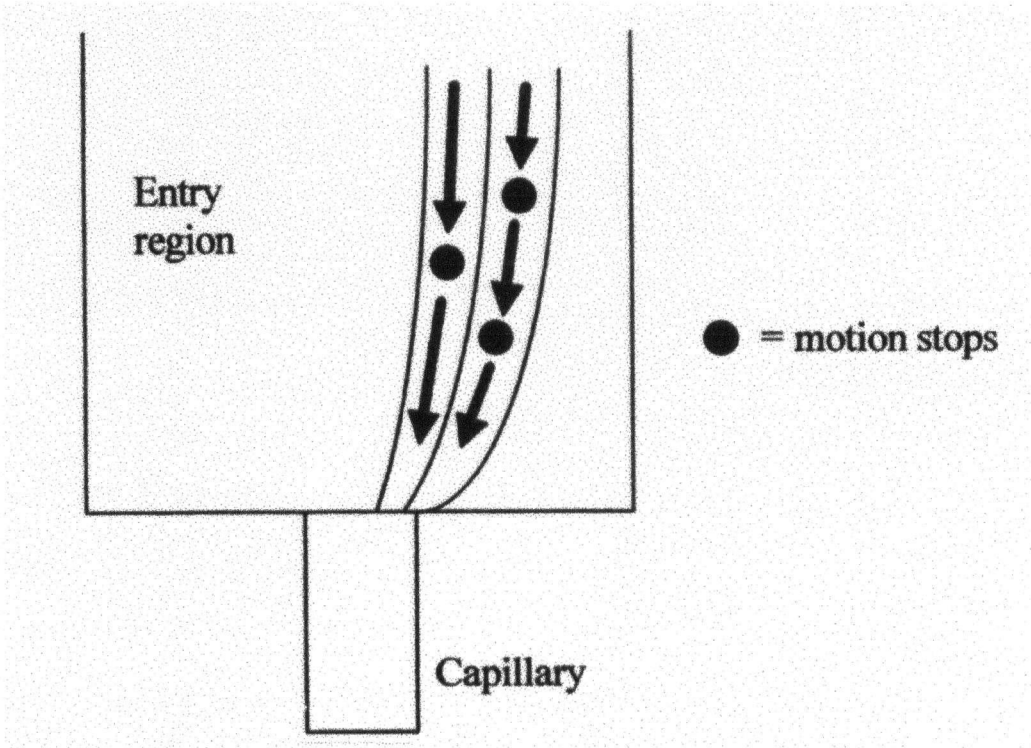

Figure 5-30b: A schematic diagram to explain the flow pattern development at 650s^{-1}.

Figure 5-31 shows the flow of polypropylene with and without the addition of 0.1% BN (CTF5) at the shear rates of 650 s^{-1} at 200°C. It can be seen that the addition of 0.1% BN eliminates the discontinuous streamlines even at the highest shear rate. The streamlines are now smooth and the flow seems to be more organized. This suggests that BN is a good processing aid for eliminating not only the surface melt fracture but also postponing the onset of gross melt fracture to higher shear rates. The mechanism by which the bulk flow is affected by the addition of BN remains to be explained. At least in this section, we have observed the change of the flow pattern development at the entrance to the capillary.

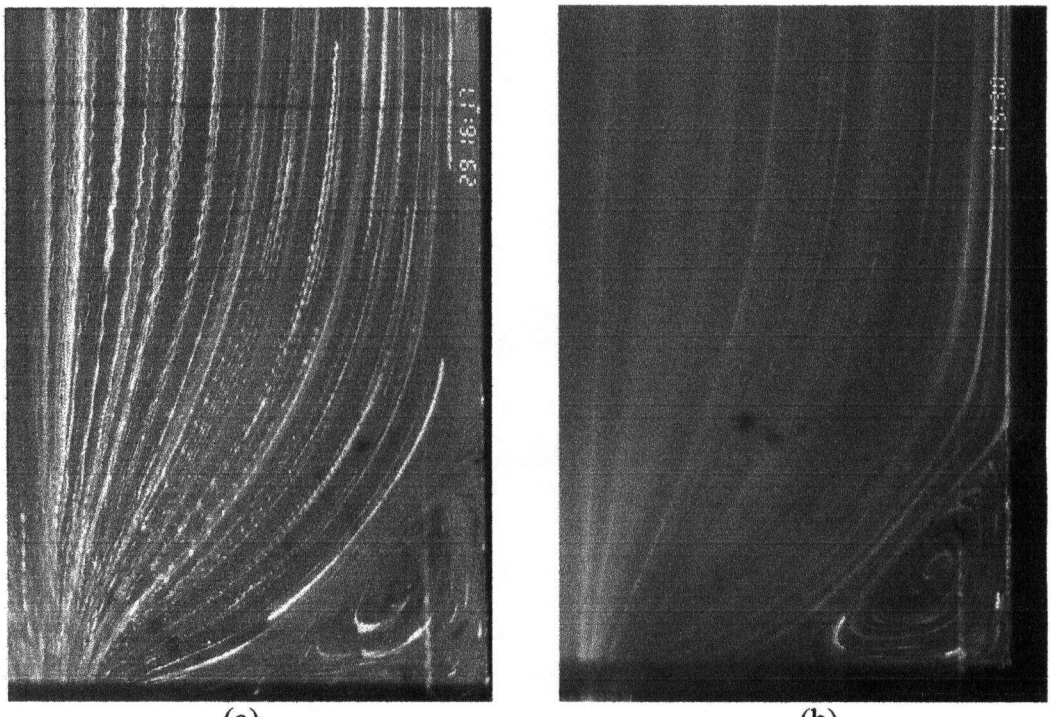

(a) (b)

Figure 5-31: Pictures of the flow of polypropylene with (b) and without (a) the addition of 0.1% BN (CTF5) at the shear rate of 650s^{-1} at 200°C.

Figure 5-32 shows the extrudate of PP at the shear rate of $450s^{-1}$ both with and without BN (CTF5) obtained with the quartz transparent die. The extrudate of PP with 0.1%BN is smooth (left), while the extrudate of pure PP exhibits gross melt fracture (right). This again proves that BN works in eliminating the gross melt fracture of polymers, in this case of polypropylene.

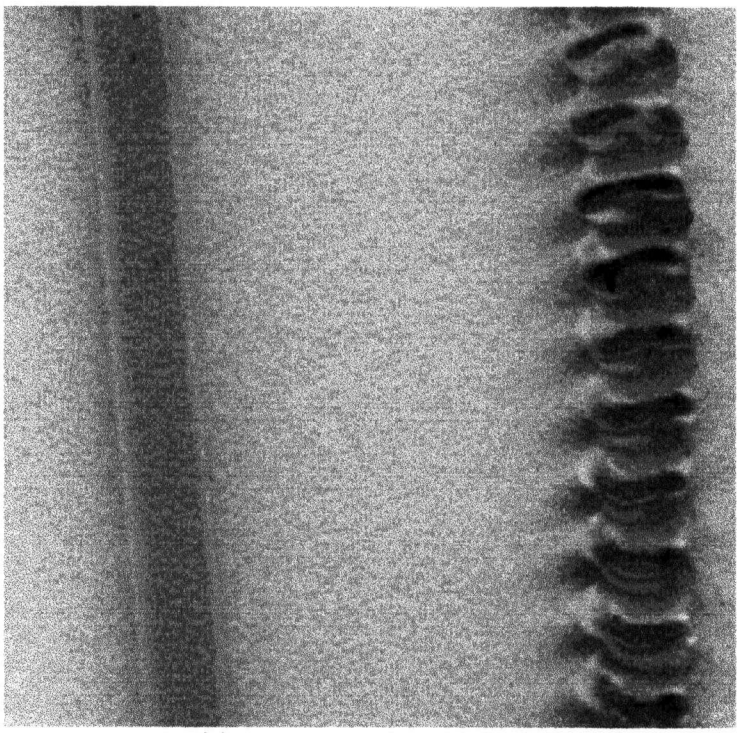

(a) (b)

Figure 5-32: PP extrudate at the shear rate of $450s^{-1}$ with (a) and without boron nitride (b) obtained with the quartz transparent die. The extrudate of PP with 0.1%BN is smooth (a), while the extrudate of pure PP exhibits gross melt fracture (b).

5.5 The Effect of Boron Nitride on the blow moulding process of HDPE

It has been demonstrated that BN is a suitable PA for the extrusion of polyolefins. In this section, we will examine whether or not BN works as a processing aid for the blow moulding process of high-density polyethylene. It is more convincing if a PA is demonstrated that it works in real processes and not just in extrusion using lab-scale equipment. As discussed two HDPE's were tested (see section 4.1). The technnique used to prepare them was the one that makes use of the twin screw extruder. A masterbatch of 5% BN concentrate instead of 10% BN used this time. The chemical and physical properties of two HDPE are listed in section 4-1. The type of BN powder used in these blow moulding studies was CTF5. A twin screw extruder was used to blend two types of HDPE, namely Resin A and Resin B. These are produced by Pétromont company, Montreal, Quebec. Resin A is a high molecular weight high density polyethylene resin with a broad molecular weight distribution produced using Union Carbide's UNIPOL® process. Resin B is a high density polyethylene resin with an intermediate molecular weight distribution and also produced using Union Carbide's UNIPOL® process. This resin is intended primarily for use in intermittent high shear rate blow moulding equipment designed for high speed production of blow moulded containers. As discussed before, a Battenfeld/Fisher 50mm blow moulding machine was empolyed in our blow moulding experiments. The processing details are discussed in section 2.3.5.

5.5.1 Flow Curves of Resins

Figure 5-33 shows the flow curve of Resin A and B by using the crosshead die. It can be seen that addition of BN (CTF5) result in reduction of the wall shear stress by about 5% in both cases.

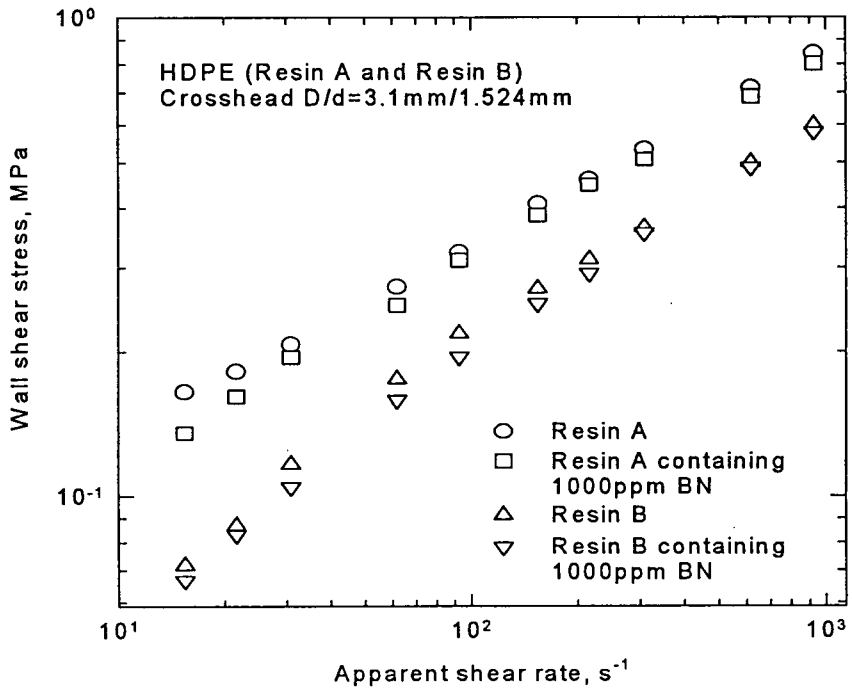

Figure 5-33 : The flow curve of Resin A and B by using the crosshead die. The reduction on wall shear stress by addition of BN is cleanly seen.

Figure 5-34 shows the effect of die gap on the head pressure at the screw speed of 30 rpm for the pure HDPE Resin A and Resin B. The processing temperature were 190 °C and 185°C for Resin A and Resin B respectively. Processing below these temperatures may cause damage of the extrusion screw inside the extruder. It can be seen from figure 5-34 that as the die gap increase, there is less resistant to polymer flow and therefore the head pressure decreases. This is due to the fact that the apparent shear rate decreases with increase of the die gap.

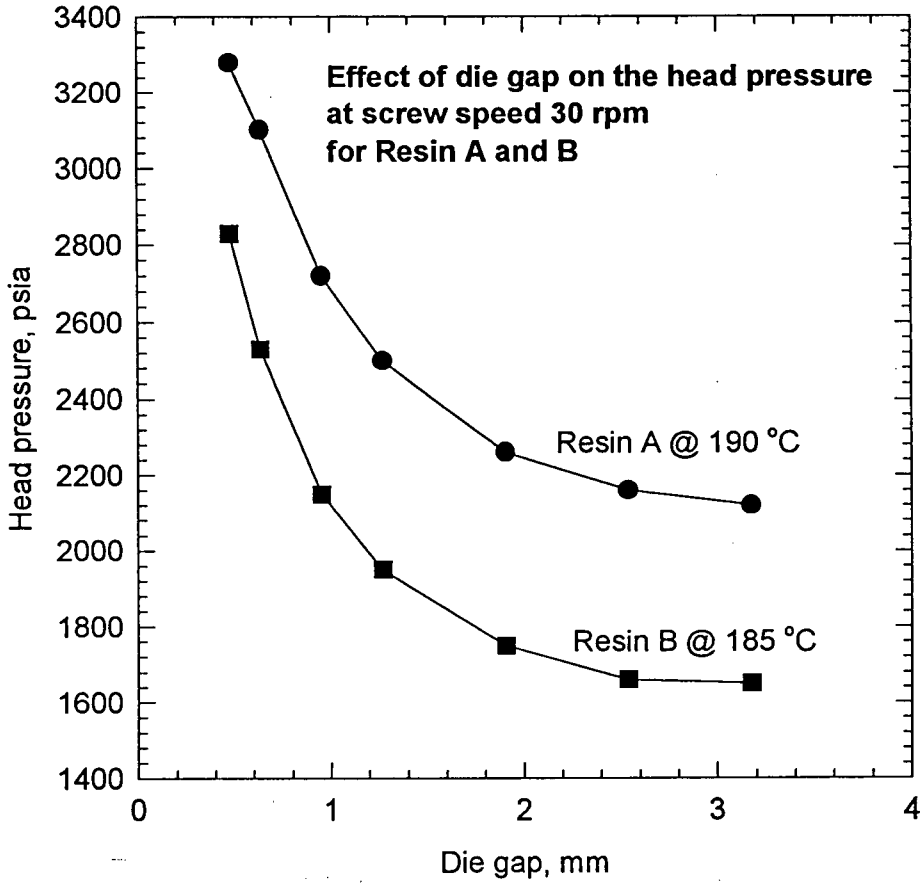

Figure 5-34 : The head pressure varied with the die gap of the pure HDPE Resin A and Resin B at the screw speed of 30 rpm.

Figure 5-35 and 5-36 show the effect of shear rate at the die exit on the head pressure of Resin A and Resin B at the die gap of 0.5mm. It can clearly be seen that BN shifts the flow curve to lower head pressure. In other words, for a given head pressure, higher shear rate (flow rate) can be obtained with the addition of BN. Furthermore, this means that the head pressure can be reduced at certain shear rate with addition of BN for both resins. It can be seen that the reduction in pressure drop with the addition of 1000ppm BN is of the order of 3 to 10 %. The data were collected and plotted as the average of two runs. This reduction is not due to the experimental error as reproducibility was checked to be within 1% (±20psia).

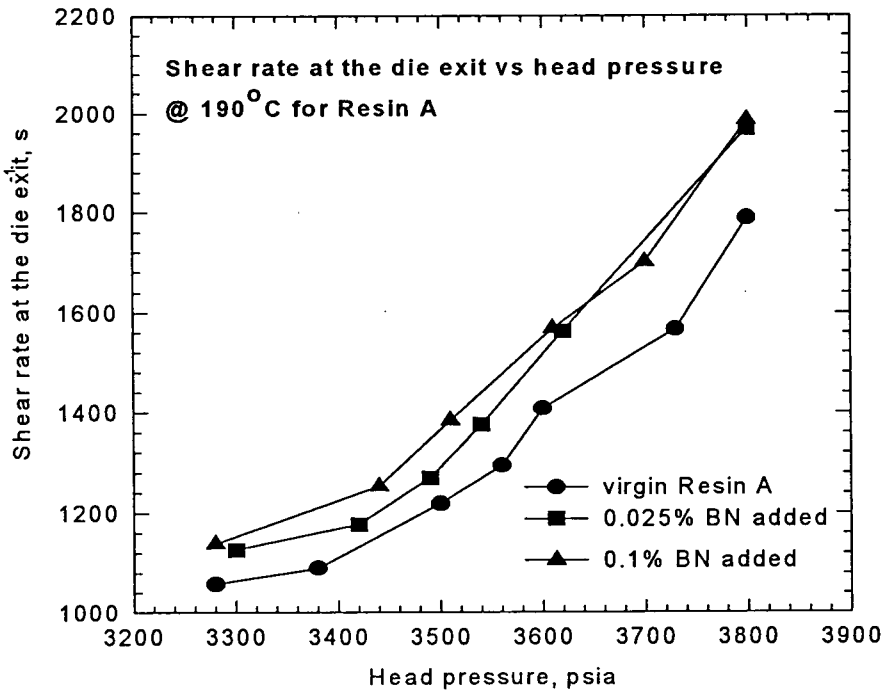

Figure 5-35 : The effect of shear rate at the die exit on the head pressure of Resin A at the die gap of 0.5mm. The screw speed was 30 rpm.

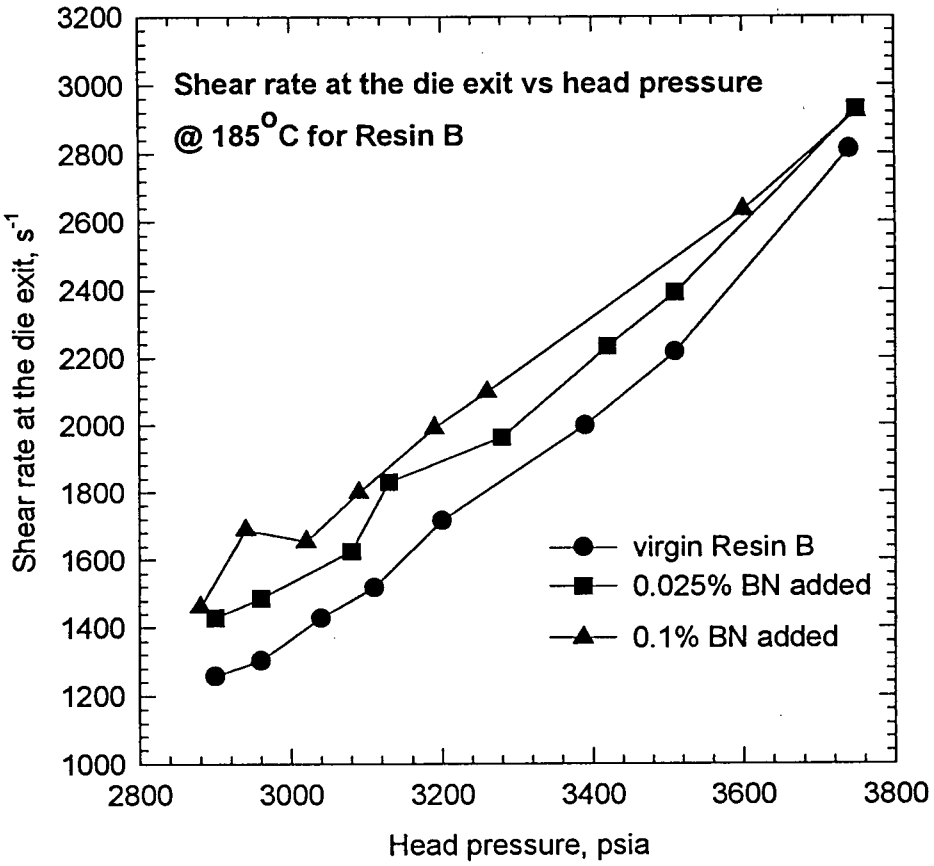

Figure 5-36 : The effect of shear rate at the die exit on the head pressure of Resin B at the die gap of 0.5mm. The screw speed was 30rpm.

5.5.2 Rheological Measurement of Resins A and B

Figure 5-37 and 5-38 plot the storage and loss moduli of Resins A and B at the processing temperatures. It can be seen that the addition of BN has only a negligible

effect on the complex viscosity, η*, for both resins A and B. This is exactly what has been observed for most other BN powders.

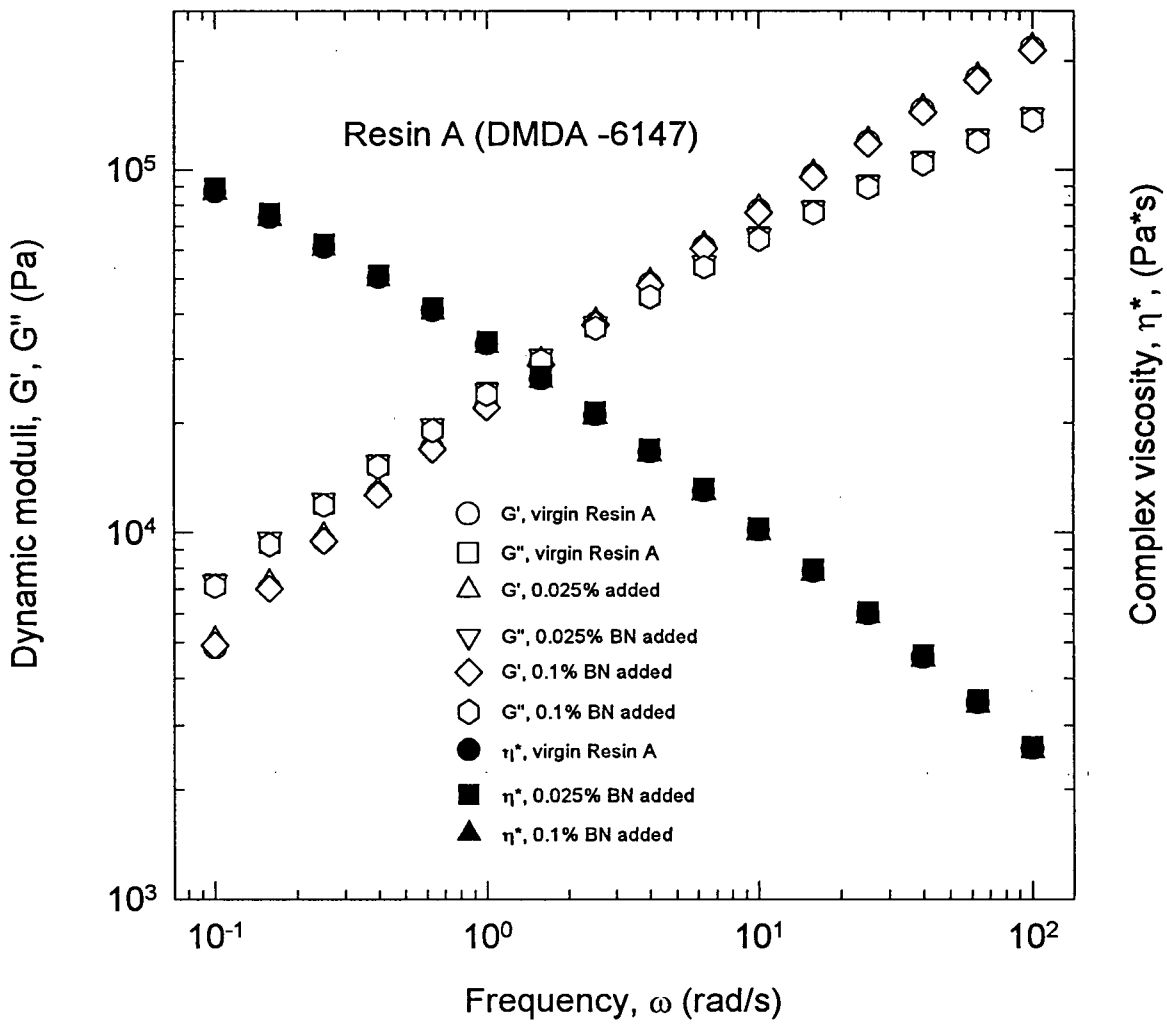

Figure 5-37: The dynamic moduli and complex viscosity, η*, for resin A @190°C.

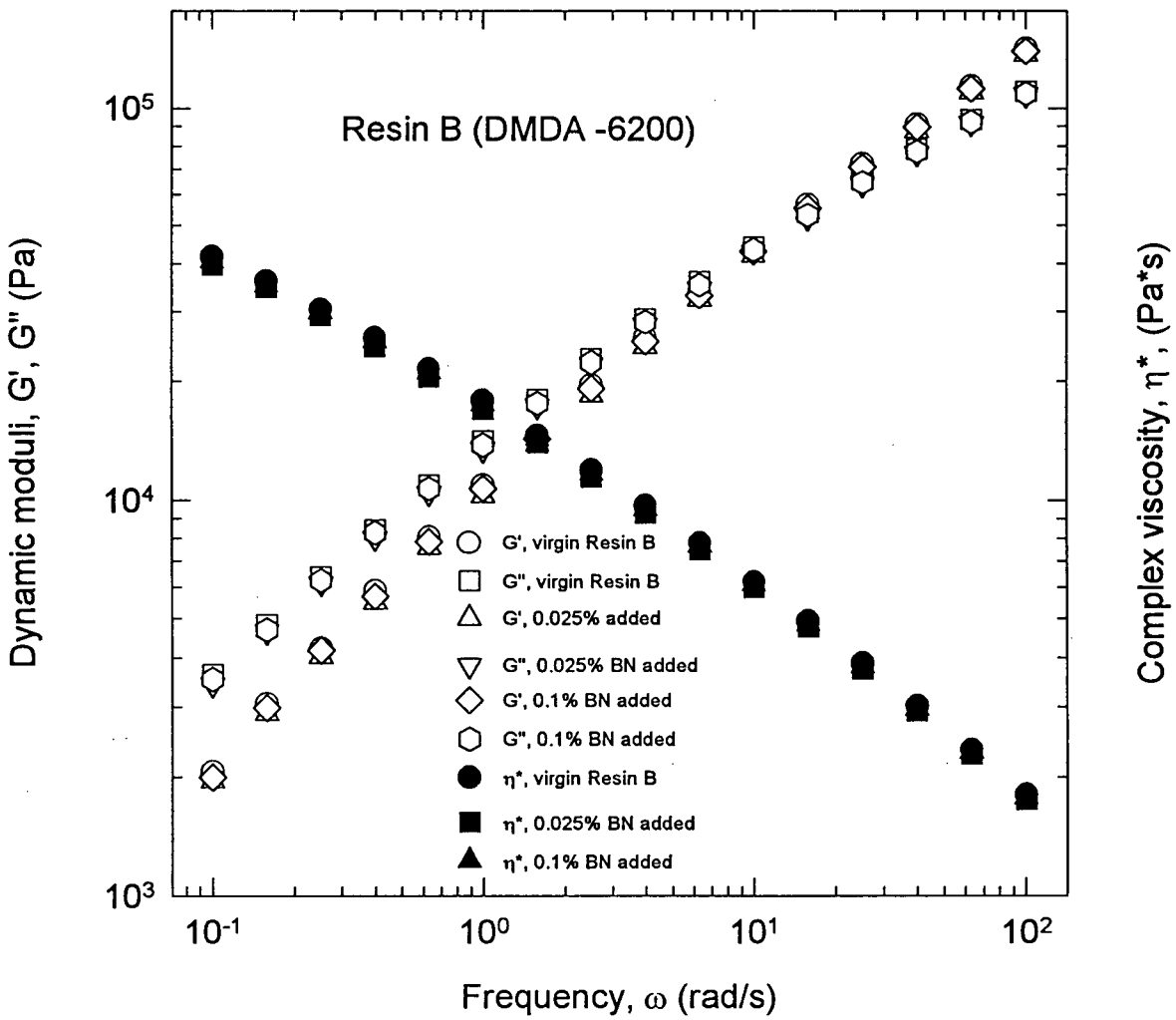

Figure 5-38: The dynamic moduli and complex viscosity, η*, for resin B @185°C.

5.3.3 Transient Extrusion Experiments

Figure 5-39 plots the transient extrusion experiments for resin A with and without BN. The head pressure is plotted as a function of time for pure Resin A and Resin A containing 250 ppm and 1000 ppm of BN. It can be seen that the final steady-state pressure is different for various levels of BN filled resin. The effect of BN on the head pressure is significant and noticeable here. Higher BN concentration reduces the steady-state pressure. What is, however, significant to note is the induction time to attain steady state. While for the case of pure resin A, steady-state is attained fast, it takes about 3 minutes for resin A containing 250 ppm BN and about 8 minutes for resin A containing 1000 ppm of BN. It is apparent that as polymer flows through the die, BN diffuses to the wall and provides some kind of conditioning to the die that allows slippage at the wall. As a result a gradual reduction in the head pressure is observed.

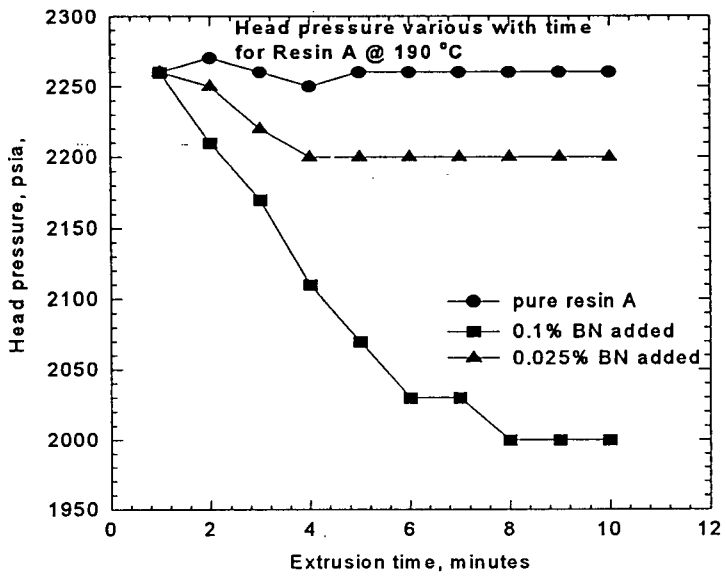

Figure 5-39: The transient extrusion experiment for resin A with and without BN. The screw speed was 30 rpm.

Figure 5-40 plots similar results to figure 5-39 for resin B. The head pressure for 0.025% and 0.1% BN added to resin B are lower than that of the pure resin. The observation at the induction time is also seen here and confirms with the result obtained for Resin A. Visual observation also conducted on the filled resins in order to check the quality of the BN dispersion in the two resin. The result of dispersion is more uniform in Resin B i.e. the parison was uniform in color with Resin B containing 250 and 1000 ppm of BN. However, Resin A containing BN had a white-colored streamlines running along the parison. This indicated that the BN exhibit only medium dispersion in Resin A, mainly due to the high viscosity. This dispersion quality observation related directly to the performance of BN.

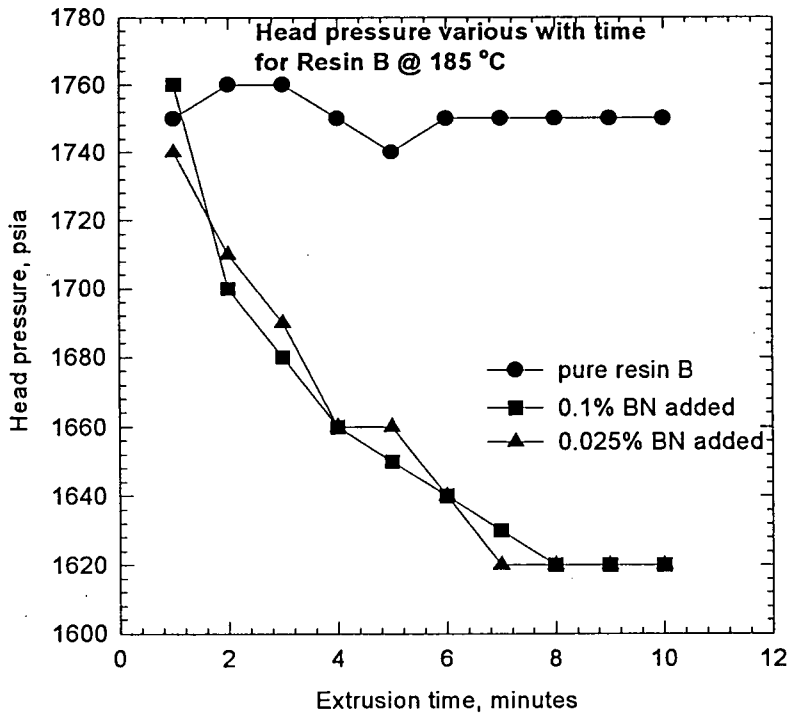

Figure 5-40: The transient experiment for resin B with and without BN. The screw speed was 30rpm.

5.5.4 Visual Observation of the extrudate

In order to examine the appearance of the extrudate surface visually i.e., bottle, pictures are taken and these are shown in figures 5-41 to 5-45. Figure 5-41 shows the surface appearance of a piece of bottle made by using resin A with and without BN. The processing temperature was 190°C, the die gap was 1.6mm and the screw speed was set at 30 rpm. The samples were collected in the regime where pressure is in steady state. The black lines/dots in the picture represent distortions (melt fracture). It can clearly be seen that the surface appearance improves as the concentration of BN increases. Although the performance of BN cannot completely eliminate the melt fracture in this case, it can clearly improve the surface appearance to a certain degree.

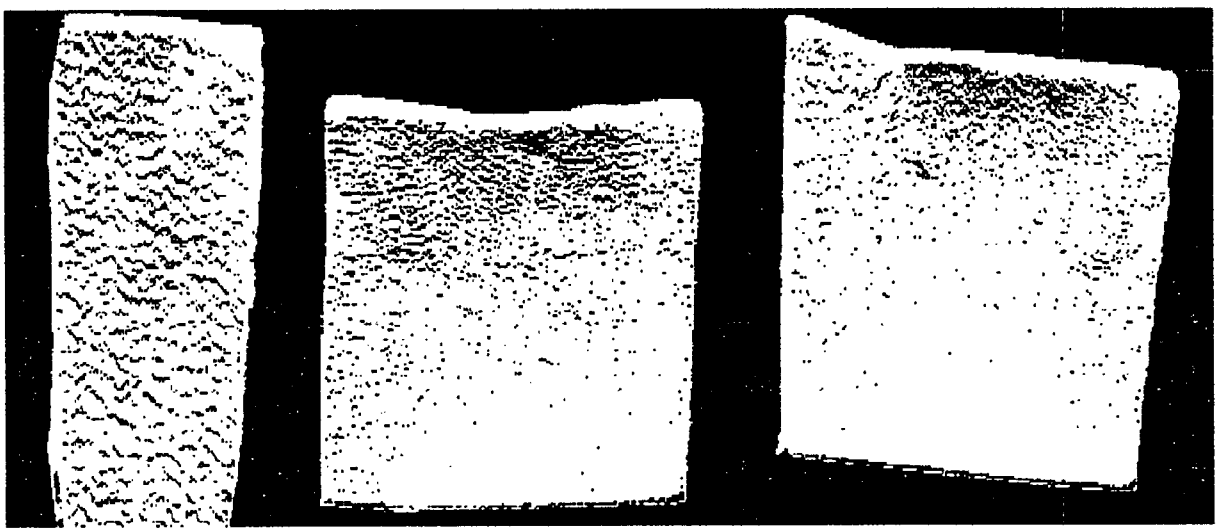

A B C

Figure 5-41: The surface appearance of extrudate (bottle) made by Resin A at the shear rate of $2800s^{-1}$. A) Pure resin A, B) Resin A containing 0.025% BN and C) Resin A containing 0.1% BN.

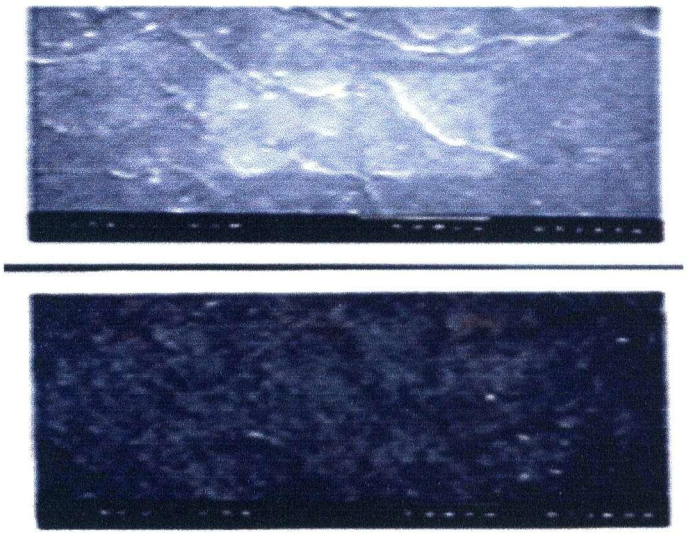

Figure 5-42: SEM pictures showing the surface appearance of the bottle made by using resin A with and without the addition of BN.
A) Pure resin A at the top and B) Resin A containing 0.1% BN at the bottom. It can be seen that the amplitude periodic distortions decrease by the addition of BN into the resin.

SEM pictures are also taken on part of the bottle surface made by using Resin A. Figure 5-42 shows the surface appearance of the bottle made by resin A with and without addition of 0.1% BN. Although BN cannot completely eliminate the melt fracture in this case, it can be seen that the amplitude of the periodic distortions dramatically decreases by the addition of BN into this resin.

Figure 5-43 shows the effect of BN on bottle surface made by resin B. The processing temperature was 185°C at screw speed of 30 rpm and die gap of 1.6mm. The melt index of resin B is almost five times higher than that of resin A. It can be seen that the surface exhibits melt fracture for the pure resin case. However, the surface for the cases of resin containing 0.025% and 0.1% BN remains smooth.

One possible explanation for the differences in the performance of BN for the two HDPE is different in melt index and molecular weight of the resins. Resin A has a low melt index and a much higher molecular weight than Resin B. This might have affected

the dispersion of BN in the more viscous fluid and thus the full effect of BN is not seen in Resin A. More experiments using different screw configuration to obtain a better BN dispersion are required.

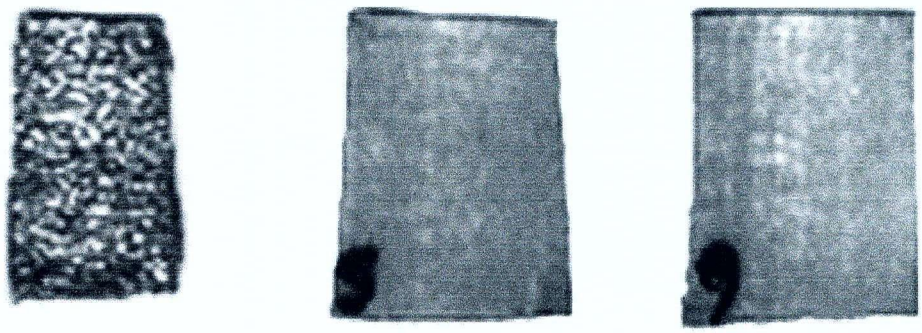

Figure 5-43: Surface appearance of extrudate (part of bottle) made by using Resin B at 2800s^{-1}
A) Pure resin B on the left, B) Resin B containing 0.025% BN on the middle C) Resin B containing 0.1% BN of the right.

The effect of temperature on the extrudate appearance was also examined for Resin A. Experiments were carried out at 190°C and 205 °C. Figure 5-44 shows the temperature effect on the appearance of the bottle surface. It can be seen that a bottle having smooth surface was made at 205 °C, as opposed to the one having melt fractured surface made at 190°C.

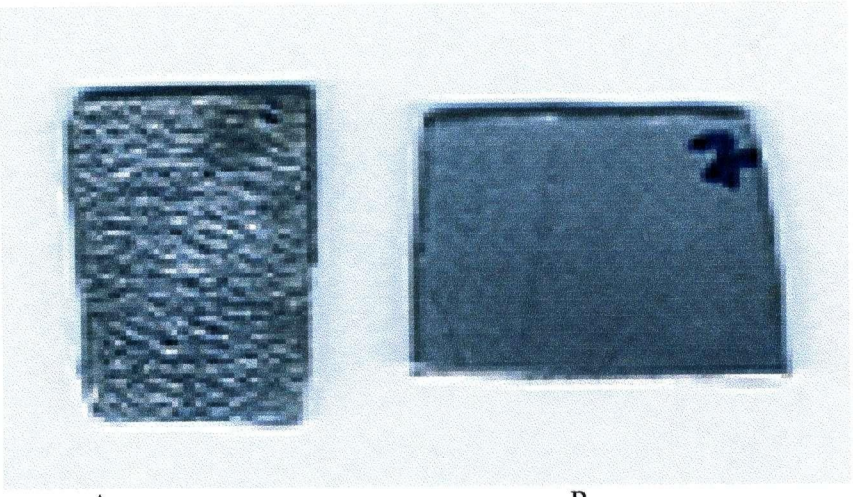

A B

Figure 5-44: The effect of temperature on the bottle surface appearance. The bottle was collected at 190°C (A) exhibits melt fracture while that made at 205°C (B) is free of any defects.

In figure 5-40, it was seen that the pressure decreased with time during a transient extrusion experiment and it became stable only after around 8 minutes for resin containing BN. In order to investigate the effect of the induction time on the surface appearance of the bottle. Samples were collected at two different time instants; i.e., after 1 and 10 minutes from the start-up of the extrusion process. Figure 5-45 shows the surface appearance of the bottle at 1 and 10 minutes respectively. It can clearly be seen that the bottle surface was smooth at the time instant of 10 minutes compared to the sample exhibits melt fracture at 1 minute. This observation implies that BN requires a finite period of time (induction time) in order to migrate to the die wall, promote slip and as a result to eliminate melt fracture.

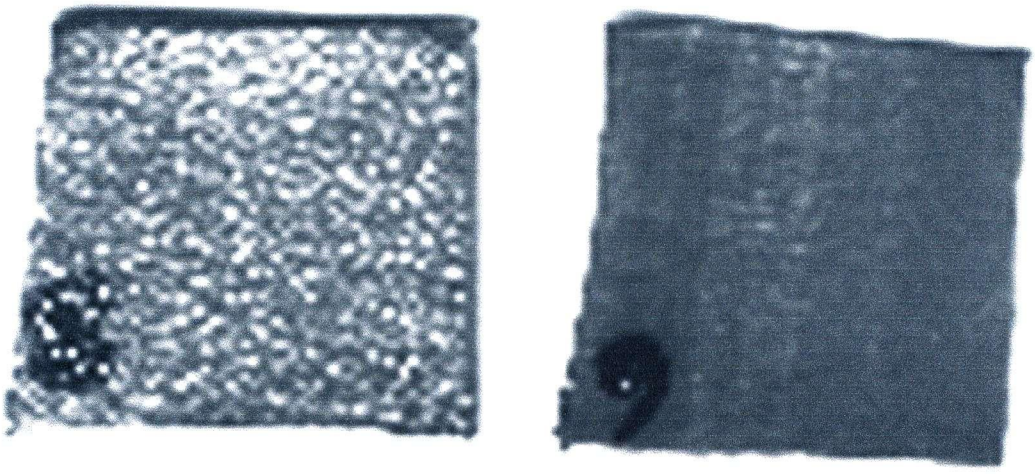

A B

Figure 5-45: The effect of the induction time on the surface appearance of the bottle. The sample (A) collected at time after 1 minute from the start-up of extrusion is fractured compared the smooth one (B), which was collected at 10 minutes after the start-up.
A) Sample collected at time = 1 minute and
B) Time =10 minutes

6 Conclusions

Experiments were carried out in parallel plate and capillary rheometers with a Nokia Maillefer crosshead for m-LLDPE Exact® 3128, Teflon® FEP 4100, HDPE (Resin A and Resin B) and polypropylene polymers. Eight different boron nitride powders were evaluated in terms of their effect on the rheology of polymer, ability to eliminate the sharkskin and postpone the gross melt fracture to higher shear rates. Boron nitride was found to act as an effective processing aid in the extrusion of both fluoropolymers and polyolefins. For the first time, a processing aid was shown not only to eliminate sharkskin and stick-slip (oscillating) melt fracture, but also to postpone gross melt fracture to significantly higher shear rates. The critical conditions and the influence of operating parameters such as the temperature, BN type and concentration were determined.

It is found that BN type CTF5 and BN431 has the best peformance in order to postpone the gross melt fracture. They reduce not only the driving pressure of extrusion but also postpones the onset of melt fracture to much higher shear rate. For optimum performance of BN the following requirements apply: (1) the BN additive should consist of fine particles (average size of about 5-10 μm), (2) it should be thoroughly dispersed in the resin, and (3) it must be used at its optimal concentration depending on the type of the polymer and the extrusion temperature, and (4) it must not contain B_2O_3 which possibly increase its surface energy and as a result polymer adhesion on the surface of BN might become a factor.

Capillary and sliding plate experiments have shown that slip does occur in the presence of BN431 filled resins (section 5.3.3). The change of the entrance flow

structures (section 5.4) may also be one of the possible mechanisms of BN action, postponing the melt fracture to higher shear rate.

Finally, it has been demonstrated that BN works as a processing aid not only in continuous extrusion using lab-scale equipment but also in industrial scale blow moulding process of high-density polyethylene (section 5.5). The performance of BN in blow moulding machine highly depends on the resin type, BN concentration, induction time and processing temperature.

7 Recommendations For Future Work

- Additional experiments should be carried out with other types of boron nitride. Some other processing aid should also be used with boron nitride such as talc, calcium tetraborate, molybdenum sulfide and black carbon. These should be included in the extrusion of polymers at various concentrations to determine its optimal concentration as a function of the processing temperature and type of polymer. Experiments with dies of various geometry are also desirable to see how the die geometry affects the resin processability.
- The flow visualization study should be continued in much more detail, in order to identify the mechanism by which BN and other processing aids affect the extrusion of molten polymers. The visualization technique could also be used independently to measure the slip velocity directly.

References

Atwood, B.T., Schowalter, W.R., *Measurement of slip at the wall during flow of high density polyethylene through a rectangular conduit.* Rheol. Acta, 28, 134-146 (1989).

T.F.Ballenger, I.J. Chen,J.W. Crowder, G.E.Hagler., *Polymer melt flow instabilities in extrusion: investigation of the mechanism and material and geometric variables,* Trans.Soc. Rheol. 15 (1971) 195-215.

Bagley, E.B., *End corrections in the capillary flow of polyethylene.* J. Appl. Phys., 28, 624 (1957).

Bagley, E.B., Schreiber, H.P., *Effect of die entry geometry on polymer melt fracture and extrudate distortion.* Trans. Soc. Rheol., 5, 341 (1961).

O. Bartos, J. Holomek, Unstable flow of amorphous polymers through capillaries. I. *Velocity profiles of polymer having discontinuous flow curve*, Polym. Eng. Sci. 11 (1971) 324-334

Benbow, J.J., Lamb, P., *New aspects of melt fracture.* S.P.E. Trans., 3, 7 (1963).

Bergem, N., *Visualization studies of polymer melt flow anomalies in extrusion.* Proc. 8th Int. Congr. Rheol., Gothenberg, p. 50 (1976).

Binnington, R.J., Troup, G.J., Boger, D.V., *A low-cost laser-speckle photographic technique for velocity measurement in slow flows.* J. Non-Newtonian Fluid Mech., 12, 255-267 (1983).

Bird, R.B., Stewart, W.E., Lightfoot, E.N., *Transport phenomena.* 2nd ed., Wiley, N.Y., 1962.

Bird, R.B., Armstrong, R.C.; Hassager, O., *Dynamics of polymeric liquids, vol. 1: Fluid mechanics.* Wiley, NY, 1987.

Blyler, L.L., Hart, A.C., *Capillary flow instability of ethylene polymer melts.* Polym. Eng. Sci., 10, 193 (1970).

Boudreaux, E.,Jr., Cuculo, J.A., *Polymer flow instability: A review and analysis.* J. Macromol. Sci. - Rev. Macromol. Chem., C 16 (1), 39-77 (1977).

Brochard, F., de Gennes, P.-G., *Shear-dependent slippage at a polymer/solid interface.* Langmuir, 8, 3033-3037 (1992).

Buckmaster, M.D., Henry, D.L., Randa, S.K., *High speed extrusion.* U.S. Pat. No. 5,688,457 (1997).

Cogswell, F.N., *Stretching flow instabilities at the exits of extrusion dies.* J. Non-Newtonian Fluid Mech., 2, 37-47 (1977).

Cogswell, F.N., *Converging flow and stretching flow: a compilation.* J. Non-Newtonian Fluid Mech., 4, 23 (1978).

D. Constantin, LLDPE melt rheology: extensibility and extrusion defects, Polym. Eng. Sci. 24 (1984) 268-274.

Cox, H.W., Macosko, C.W., *Viscous dissipation in die flows.* AIChE J., 20 (4), 785-795 (1974).

Dealy, J.M., *Rheometers for molten plastics.* Reinhold, NY, 1982.

Dealy, J.M., Wissbrun, K.F., *Melt rheology and its role in plastics processing: theory and applications.* Reinhold, NY, 1990.

Denn, M.M., *Surface-induced effects in polymer melt flow.* Proc. XIth Int.Congr.on Rheology, Brussels, Belgium. In: Moldenaers P., Keunings R. (eds.) Theretical and applied rheology. Elsevier Science Publishers, 45-49, 1992.

Denn, M.M., *Issues in viscoelastic fluid mechanics.* Annu. Rev. Fluid Mech., 22, 13-34 (1990).

Denn. M.M., *Polymer flow instabilities: a picaresque tale.* Chem. Eng. Ed., 28, 162-166 (1994).

M.T. Dennison, *Flow instability in polymer melts: a review*, Trans.J. Plast. Inst (1967) 803-808.

Galt, J., Maxwell, B., *Velocity profiles for polyethylene melts.* Modern Plastics, Dec., 115-132 (1964).

Hatzikiriakos, S.G., Dealy, J.M., *Wall slip of molten high density polyethylene. I. Sliding plate rheometer studies.* J. Rheol., 35 (4), 497-523 (1991a).

Hatzikiriakos, S.G., Dealy, J.M., *The effect of interface conditions on wall slip and melt fracture of high density polyethylene.* SPE ANTEC '91 Tech. Papers, 2311-2314 (1991b).

Hatzikiriakos, S.G., Dealy, J.M., *Wall slip of molten high density polyethylene. II. Capillary rheometer studies.* J. Rheol., 36 (4), 703-741 (1992a).

Hatzikiriakos, S.G., Dealy, J.M., *Role of slip and fracture in the oscillating flow of HDPE in a capillary.* J. Rheol., 36 (5), 845-884 (1992b).

Hatzikiriakos, S.G., Dealy, J.M., *Start-up pressure transients in a capillary rheometer.* SPE ANTEC '92 Tech. Papers, 1743-1746 (1992c).

Hatzikiriakos, S.G., *A slip model for linear polymers based on adhesive failure.* Intern. Polymer Processing, VIII 2, 135-142 (1993).

Hatzikiriakos, S.G., Dealy, J.M., *Start-up pressure transient in a capillary rheometer.* Polym. Eng. Sci., 34 (6), 493-499 (1994).

Hatzikiriakos, S.G., *The onset of wall slip and sharkskin melt fracture in capillary flow.* Polym. Eng. Sci., 34 (19), 1441-1449 (1994).

Hatzikiriakos, S.G., Kalogerakis, N., *A dynamic slip velocity model for molten polymers based on a network kinetic theory.* Rheol. Acta, 33, 38-47 (1994).

Hatzikiriakos, S.G., *A multimode interfacial constitutive equation for molten polymers.* J. Rheol., 39 (1), 61-71 (1995).

Hatzikiriakos, S.G., Hong, P.; Ho, W.; Stewart, C.W., *The effect of teflon coatings in polyethylene capillary extrusion.* J. Appl. Polym. Sci., 55, 595-603 (1995).

Hatzikiriakos, S.G., Heffner, G., Vlassopoulos, D., Christodoulou, K., *Rheological characterization of polyethylene terephthalate resins using a multimode Phan-Thien-Tanner constitutive relation.* Rheol. Acta, 36, 568-578 (1997a).

Hatzikiriakos, S.G., Kazatchkov, I.B., Vlassopoulos, D., *Interfacial phenomena in the capillary extrusion of metallocene polyethylenes.* J. Rheol., 41 (6), 1299-1316 (1997b).

Howells, E.R., Benbow, J.J., *Flow defects in polymer melts.* Trans. Plast. Inst., 30, 240-253 (1962).

Kalika, D.S., Denn, M.M., *Wall slip and extrudate distortion in linear low-density polyethylene.* J. Rheol., 31 (8), 815-834 (1987).

E. Karbashewski, A. Rudin, L. Kale, *Effect of polymer structure on the onset of polymer processing defects in LLDPE,* Polm. Eng. Sci. 35 (1995) 1864-1871.

Kazatchkov, I.B., Hatzikiriakos, S.G.; Stewart, C.W., *Extrudate distortion in the capillary/slit extrusion of a molten polypropylene.* Polym. Eng. Sci., 35 (23), 1864-1871 (1995).

Kazatchkov, I.B., Rosenbaum, E.E., Hatzikiriakos, S.G.; Stewart, C.W., *The effect of molecular structure on the rheological behaviour of tetrafluoroethylene/hexafluropropylene copolymers.* ANTEC'96 Tech. Papers, 42, 2120-2124, Indianapolis, May 5-9 (1996).

Kurtz, S.J., *The Dynamics of sharkskin melt fracture: effect of die geometry.* Proc. XIth Int.Congr.on Rheology, Brussels, Belgium. In: Moldenaers P., Keunings R. (eds.) Theretical and applied rheology. Elsevier Science Publishers, 377-379, 1992.

Kurtz, S.J., *Die geometry solutions to sharkskin melt fracture.* Advances in Rheology, ed. B. Mena, A. Garcia-Rejon and C. Rangel Nafaile, UNAM, Mexico City, Vol. 3, 399 (1984).

Lim, F.J., Schowalter, W.R., *Wall slip of narrow molecular weight distribution polybutadienes.* J. Rheol., 33 (8), 1359-1382 (1989).

T.T.S. Lim, *Capillary extrusion of composite materials,* Ann. Tech. Conf. Soc. Plastic. Eng (1970) 13-19.

Lin, Y.-H., *Explanation for slip-stick melt fracture in terms of molecular dynamics in polymer melts.* J. Rheol., 29 (6), 605-637 (1985).

Lupton, J.M., Regester, R.W., *Melt flow of polyethylene at high rates.* Polym. Eng. Sci., 5, 235 (1965).

Meissner, J, *Basic parameters, melt rheology, processing and end-use properties of three similar low density polyethylene samples* . Pure Appl. Chem., 42, 551-612 (1975).

Mooney, M., *Explicit formulas for slip and fluidity.* J. Rheol., 2, 210 (1931).

Moynihan, R.H., Baird, D.G.; Ramanathan, R., *Additional observations on the surface melt fracture behavior of LLDPE.* J. Non-Newtonian Fluid Mech., 36, 255 (1990).

Nason, H.K., *A high temperature - high pressure rheometer for plastics.* J. Appl. Phys., 16, 338 (1945).

Petrie, C.J.S., Denn, M.M., *Instabilities in polymer processing*. AIChE J., 22 (2), 209-236 (1976).

Piau, J.M., El Kissi, N., *The influence of interface and volume properties of polymer melts on their die flow stability*. Proc. XIth Int.Congr.on Rheology, Brussels, Belgium. In: Moldenaers P., Keunings R. (eds.) Theretical and applied rheology. Elsevier Science Publishers, 70-74, 1992.

Piau, J.M., El Kissi, N., Trenblay, B., *Low Reynolds number flow visualization of linear and branched silicones upstream of orifice dies*. J. Non-Newtonian Fluid Mech., 30, 197-232 (1988).

Piau, J.M., El Kissi, N., Trenblay, B., *Influence of upstream instabilities and wall slip on melt fracture and sharkskin phenomena during silicone extrusion through orifice dies*. J. Non-Newtonian Fluid Mech., 34, 145-180 (1990).

Pudjijanto, S., Denn, M.M., *A stable "island" in the slip-stick region of linear low-density polyethylene*. J. Rheol., 38 (6), 1735-1744 (1994).

Ramamurthy, A.V., *Wall slip in viscous fluids and influence of materials of construction*. J. Rheol., 30 (2), 337-357 (1986).

Rauwendaal, C., Fernandez, F., *Experimental study and analysis of a slit die viscometer*. Polym. Eng. Sci., 25, 765 (1985).

Reher, E.-O., Bothmer, D.; Schnabel, R., *Investigations into the wall slippage behaviour of polymer melts from the energy aspect*. Kunststoffe - German Plastics, 78 (11), 40-41 (1988).

Rosenbaum, E.E., Hatzikiriakos, S.G.; Stewart, C.W., *The melt fracture behaviour of Teflon resins in capillary extrusion*. SPE ANTEC '95 Tech. Papers, 41, 1111-1115 (1995).

Rosenbaum, E.E., Hatzikiriakos, S.G.; Stewart, C.W., *Flow implications in the processing of DuPont tetrafluoroethylene/hexafluoropropylene*. Intern. Polymer Processing, X (3), 204-212 (1995).

Rosenbaum, E.E., Hatzikiriakos, S.G., *The effect of viscous heating in capillary rheometry*. SPE ANTEC '96 Tech. Papers, 42, 1080-1084 (1996).

Rosenbaum, E.E., Hatzikiriakos, S.G., *Wall slip in the capillary Flow of molten polymers subject to viscous heating*. AIChE J., 43 (3), 598-608 (1997).

Rosenbaum, E.E., Randa, S.K., Hatzikiriakos, S.G., Stewart, C.W., Henry, D.L., Buckmaster, M.D., *A new processing additive eliminating surface and gross melt fracture in the extrusion of polyolefins and fluoropolymers*. SPE ANTEC '95 Tech. Papers, 44 (1998a).

Rosenbaum, E.E., Hatzikiriakos, S.G.; Stewart, C.W., *Rheological characterization of well-defined tetrafluoroethylene/hexafluoropropylene*. to be published in Rheol. Acta (1998b).

Rudin, A., Worm, A.T.; Blacklock, J.E., *Fluocarbon elastomer processing aid for LLDPE, HDPE and PP resins*. Processing and Property Enhancement Utilizing Modifiers and Additives in Polymers: First Intl. Conf., p.71-81 (1985).

Stewart, C.W., McMinn, R.S.; Stika, K.M., *A model for predicting slip velocity during extrusion with fluoropolymer processing additives*. J. Reinf. Plast. Composites, 12 (6), 633-641 (1993).

Stewart, C.W., *Wall slip in the extrusion of linear polyolefins.* J. Rheol., 37 (3), 499-513 (1993).

Stewart, C.W., . Private communication (1994).

Tordella, J.P., *Unstable flow of molten polymers.* in Rheology, Vol. 5, F. R. Eirich, ed., Academic Press, NY, 57-92, 1969.

Tordella, J.P., *Fracture in the extrusion of amorphous polymers through capillaries.* J. Appl. Phys., 27, 454 (1956).

Tremblay, B., *Sharkskin defects of polymer melts: the role of cohesion and adhesion.* J. Rheol., 35 (6), 985-998 (1991).

Waddon, A.J., Keller, A., *The temperature window of minimum flow resistance in melt flow of polyethylene. Further studies on the effect of strain rate and branching.* J. Polym. Sci., B 30, 923-929 (1992).

Wang, J., Porter, R.S., *On the viscosity-temperature behavior of polymer melts.* Rheol. Acta, 34, 496-503 (1995).

Wang, S.Q., Drda, P.A., Inn, Y.W., *Exploring molecular origins of sharkskin, partial slip, and slope change in flow curves of linear low density polyethylene.* J. Rheol., 40 (5), 875-898 (1996).

White, J.L., *Critique of flow patterns in polymer fluids at the entrance of a die and instabilities leading to extrudate distortion.* Appl. Polymer Symposium, 20, 155-174 (1973).

Notation

a_T	shift factor
b	Rabinowitsch correction
D	capillary diameter, m
D	tip diameter, m
E_a	activation energy for flow, J
e	Bagley end correction or energy
G	shear modulus, Pa
G'	storage modulus, Pa
G''	loss modulus, Pa
G^*	complex modulus, Pa
G_d	amplitude ratio in oscillatory shear
h	gap between plates, m
I	melt polydispersity
K	power-law consistency index, MPa · s^n
L	capillary length or length of sample, m
n	power-law exponent
P	absolute pressure, Pa
P_a	ambient pressure, Pa
P_d	driving pressure, Pa
P_{end}	Bagley correction, Pa
ΔP_{ex}	exit pressure drop, Pa
ΔP_{ent}	entrance pressure drop, Pa
Q	volumetric flow rate, m^3/s
R	capillary radius, m or universal gas constant
T	absolute temperature, K

t	time, s or wall thickness, m
T_g	glass transition temperature, K
T_{ref}	reference temperature, K
u	melt velocity, m/s
u_s	slip velocity, m/s
Δx	plate displacement, m

Greek Letters

α	pressure coefficient of viscosity, Pa^{-1}
δ	mechanical loss angle
$\gamma(t)$	shear strain
$\dot{\gamma}$	shear rate, s^{-1}
$\dot{\gamma}_A$	apparent shear rate, s^{-1}
$\dot{\gamma}_{A,s}$	apparent shear rate, corrected for slip, s^{-1}
$\dot{\gamma}_w$	wall shear rate, s^{-1}
γ_0	strain amplitude in oscillatory shear
η	viscosity, Pa · s
η_0	zero-shear viscosity, Pa · s
η^*	complex viscosity, Pa · s
ρ	density, kg/m^3
σ_c	critical shear stress for the onset of melt fracture, Pa
σ_w	wall shear stress, Pa
σ_0	stress amplitude in oscillatory shear, Pa
ω	frequency, rad/s or specific volume, cm^3/g